

Tailoring the surface properties of nanotube membranes for controlled separations



Flinders
UNIVERSITY
ADELAIDE • AUSTRALIA

Thesis submitted to the School of Chemical and Physical Sciences,
Faculty of Science and Engineering, The Flinders University of South Australia,
in fulfilment of the requirements for the degree of
Doctor of Philosophy
March 2011

Leonora Velleman

Supervisors: Prof. Joseph G. Shapter & A/Prof. Dusan Lasic

ACKNOWLEDGEMENTS

I would like to present my sincere thanks to many people for their support and guidance throughout my PhD. This thesis would not have been possible without the encouragement, guidance and support of my supervisors, Prof Joseph Shapter and A/Prof Dusan Losic, who fostered independent research ideas and were always available to discuss any issues. In particular, I would like to thank my principal supervisor, Prof Joseph Shapter, for always believing in me.

I have had the privilege to work with the smart surface structures group who have given me valuable research advice, support and friendship. I am truly grateful for their time and effort and for all their useful comments and assistance.

I would also like to extend a large amount of thanks to Dr François Guillaume and Dr Jean-Luc Bruneel for their collaboration on my visit to Bordeaux University to use their Raman spectrometer. I am very grateful for their assistance with the Raman measurements and aid in interpreting the spectra. I would also like to thank Dr Gerry Trian and Dr Peter Evans for the preparation of silica coated porous alumina samples.

Finally, I would like to thank all of my family and friends for their support throughout my PhD studies. I could not have done any of this without their support.

DECLARATION

I certify that the work presented in this thesis is, to the best of my knowledge and belief, original unless otherwise acknowledged. The material in this thesis has not been submitted, either in whole or in part, towards another degree at this or any other institution.

Leonora Velleman

LIST OF PUBLICATIONS

The following is a list of peer-reviewed publications arising from the author's Doctor of Philosophy degree. The thesis is based around publications 3 – 8.

1. L. Dumée, L. Velleman, K. Sears, J. Schütz, N. Finn, M. Duke, S. Gray. Control of porosity and pore size of metal reinforced carbon nanotube membranes. *6th conference of the Aseanian Membrane Society & 7th International Membrane Science and Technology Conference AMS6/IMSTEC10*, Sydney, Australia, 2010, submitted.
2. L.Velleman, C.J. Shearer, A.V. Ellis, D. Losic, N.H. Voelcker, J.G. Shapter, Fabrication of self-supporting porous silicon membranes and tuning transport properties by surface functionalisation. *Nanoscale*, 2010, DOI: 10.1039/c0nr00284d.
3. L. Velleman, D. Losic, J.G. Shapter. Gold nanotube membranes; fabrication of controlled pore geometries and tailored surface chemistries. *International Conference on Nanoscience and Nanotechnology ICONN*, Sydney, Australia, 2010, submitted.
4. L.Velleman, G. Triani, P.J. Evans, J.G. Shapter, D. Losic. Structural and chemical modification of porous alumina membranes. *Microporous and Mesoporous Materials* 126 (2009) 87–94.
5. L. Velleman, J.G. Shapter, D. Losic. Gold nanotube membranes functionalised with fluorinated thiols for selective molecular transport. *Journal of Membrane Science*, 328 (2009) 121-126.
6. L. Velleman, J.G. Shapter, D. Losic, Engineered gold nanotube membranes for molecular separations. *International Conference on Nanoscience and Nanotechnology ICONN*, Melbourne, Australia, 2008, art. no. 4639252, pp. 86–89.

7. **L. Velleman**, J.G. Shapter, and D. Losic. Template fabricated gold nanotube membranes: a nucleation and growth study. *15th AINSE Conference on Nuclear and Complementary Techniques of Analysis* 326 - 329 November 2007 Melbourne.
8. **L. Velleman**, G. Traini, P.J. Evans, A. Atanacio, J.G. Shapter, D. Losic. *Atomic layer deposition of SIO_2 on porous alumina membranes: controlling the pore size and transport properties.* Proc. SPIE, Vol. **7267** (2008) 72670S; DOI:10.1117/12.810716

TABLE OF CONTENTS

List of Tables.....	v
List of Figures	vi
List of symbols and abbreviations.....	xi
Chapter 1 Introduction	1
1.1. Overview	2
1.2. Membrane materials and their applications.....	3
1.3. Diffusion through membranes.....	7
1.4. Porous membranes with uniform and ordered architectures	8
1.4.1. Polycarbonate track etched membranes	9
1.4.2. Porous alumina membranes.....	10
1.5. Electroless deposition of gold	11
1.6. Separation studies.....	15
1.6.1. Size based molecular separations	15
1.6.2. Functionalised membranes for enhanced and selective separations	17
1.7. Switchable membranes.....	20
1.8. Thesis outline	23
1.9. References	26
Chapter 2 Experimental Details	37
2.1. Membrane Fabrication	38
2.1.1. Fabrication of porous alumina (PA) membranes	38
2.1.2. Fabrication of gold nanotube membranes	38
2.1.3. Fabrication of silica modified porous alumina membranes via atomic layer deposition	40
2.2. Surface functionalisation of membranes	41
2.2.1. Thiol functionalisation of gold coated membranes	41
2.2.2. Functionalisation of silica modified alumina membranes.....	41
2.3. Characterisation of membranes	42
2.3.1. Scanning and transmission electron microscopy.....	42
2.3.2. Dynamic secondary ion mass spectrometry (SIMS) and ellipsometry characterisation of silica coated PA membranes	43
2.3.3. Electrochemical characterisation of gold nanotube membranes	43

2.3.4.	Contact angle measurements.....	44
2.3.5.	Raman spectroscopy of 3-mercaptopbenzoic acid on gold coated PA membranes	45
2.4.	Investigation of the transport properties of membranes.....	45
2.4.1.	Transport experiments.....	45
2.4.2.	Measurement of dye oil:water partition coefficients	46
2.5.	Synthesis of fluorinated azobenzene for the development of switchable membranes	48
2.5.1.	Synthesis of 4-(4-trifluoromethoxyphenylazo)phenol (1)	48
2.5.2.	Synthesis of 7-[(trifluoromethoxyphenylazo)phenoxy]pentanoic acid (2).....	49
2.6.	References.....	50
Chapter 3 Raman spectroscopy of thiols adsorbed inside the pores of gold-alumina membranes		51
3.1.	Introduction.....	52
3.2.	Experimental details.....	53
3.2.1.	Fabrication of porous alumina membranes.....	53
3.2.2.	Electroless gold deposition	54
3.2.3.	Thiol functionalisation of gold nanotube membranes.....	54
3.2.4.	Raman spectroscopy of MBA on Au-PA membranes	54
3.3.	Results and Discussion	54
3.3.1.	Structural characterisation of gold – alumina (Au-PA) membranes.....	54
3.3.2.	Characterisation of SAMs within the pores of Au-PA membranes by Raman spectroscopy	58
3.4.	Conclusion	63
3.5.	References.....	64
Chapter 4 Comparison of alkanethiol and fluorinated thiols on the transport properties of gold coated polycarbonate membranes.....		66
4.1.	Introduction.....	67
4.2.	Experimental details.....	68
4.2.1.	Electroless gold deposition onto polycarbonate membranes	68
4.2.2.	Investigation of gold nanotube membrane transport properties.....	68
4.3.	Results and discussion	68
4.3.1.	Fabrication and characterisation of gold - polycarbonate membranes	68

4.3.2.	Electrochemical characterisation of thiol modified gold - polycarbonate membranes.....	70
4.3.3.	Transport and selectivity of gold - polycarbonate membranes	72
4.4.	Conclusions	76
4.5.	References	78
Chapter 5	The effects of surface functionality positioning on the transport properties of membranes	81
5.1.	Introduction	82
5.2.	Experimental details	83
5.2.1.	Electroless gold deposition.....	83
5.2.2.	Gold sputtering onto polycarbonate membranes.....	84
5.2.3.	Investigation of membrane transport properties.....	84
5.3.	Results and Discussion.....	84
5.3.1.	Fabrication and characterisation of gold - polycarbonate membranes.....	84
5.3.2.	Surface functionalisation of gold - polycarbonate membranes	88
5.3.3.	Transport properties of gold – polycarbonate membranes	90
5.4.	Conclusion.....	97
5.5.	References	99
Chapter 6	Structural and chemical modification of porous alumina membranes .	101
6.1.	Introduction	102
6.2.	Experimental details	103
6.2.1.	Fabrication and functionalisation of silica modified porous alumina membranes via atomic layer deposition	103
6.2.2.	Investigation of membrane transport properties.....	104
6.3.	Results and Discussion.....	105
6.3.1.	Characterisation of modified porous alumina membranes.....	105
6.3.2.	Transport and selectivity of modified PA membranes	111
6.4.	Conclusions	115
6.5.	References	117
Chapter 7	Forward osmosis through silica modified porous alumina membranes ..	120
7.1.	Introduction	121
7.2.	Experimental details	122

7.2.1.	Fabrication and functionalisation of silica modified porous alumina membranes via atomic layer deposition.....	122
7.2.2.	Water transport experiments	122
7.3.	Results and Discussion	124
7.3.1.	Dye dependence on the water transport through Si-PA membranes	124
7.3.2.	Comparison of water transport through bare PA and Si-PA.....	127
7.3.3.	Effect of salt concentration on the water transport properties	128
7.4.	Conclusions and further work.....	134
7.5.	References.....	136
Chapter 8	Light switchable transport through gold nanotube membranes	138
8.1.	Introduction.....	139
8.2.	Experimental Details.....	141
8.2.1.	Fabrication of porous alumina membranes.....	141
8.2.2.	Electroless gold deposition onto porous alumina membranes	141
8.2.3.	Synthesis of 7-[(trifluoromethoxyphenylazo)phenoxy]pentanoic acid...	141
8.2.4.	Azobenzene functionalisation of gold nanotube membranes	141
8.2.5.	Investigation of membrane transport properties	141
8.3.	Results and Discussion	142
8.3.1.	Characterisation of gold coated alumina membranes	142
8.3.2.	Characterisation of switchable azobenzene thiol on Au-PA membranes	143
8.3.3.	Switchable transport properties of azobenzene modified Au-PA membranes	144
8.4.	Conclusions.....	146
8.5.	References.....	148
Chapter 9	Concluding remarks	151
9.1.	Future directions	154
Appendix	158

LIST OF TABLES

CHAPTER 4

Table 4-1. Transport and selectivity properties of functionalised and bare gold nanotube membranes (errors obtained from three replicate measurements).....	72
---	----

CHAPTER 5

Table 5-1 Advancing contact angle measurements for the unfunctionalised and PFDT functionalised Au-PC membranes.....	90
Table 5-2 Transport and selectivity properties of functionalised and bare gold membranes (errors obtained from three replicate measurements).	91

CHAPTER 6

Table 6-1 Summary of permeation data of hydrophobic (tris(2,2'-bipyridyl)dichlororuthenium(II) hexahydrate, Rubpy) and hydrophilic (rose bengal, RB) through perfluorodecyldimethylchlorosilane (PFDS) functionalised and unfunctionalised ALD silica modified PA membranes (Si-PA). PA membranes with 20 nm pores, modified by 5 ALD cycles were used.	112
--	-----

CHAPTER 7

Table 7-1 List of dye molecules which facilitate and do not facilitate water transport though Si-PA membranes.....	126
Table 7-2 Summary of permeation data of RB (water transport facilitating dye) and Rubpy (non-water transport facilitating dye) through Si-PA membranes.	133

CHAPTER 8

Table 8-1 1 μ L water drop contact angle on azo and decanethiol modifed Au-PA membranes.....	143
Table 8-2 Flux data for EY transport through unfunctionalised and azo-functionalised cis and trans state Au-PA membranes.	145

APPENDIX

Table A-1 Transport and selectivity properties of functionalised and bare gold membranes (errors obtained from three replicate measurements).	158
---	-----

LIST OF FIGURES

Figure 1-1 Schematics of the principal types of membranes [49].	4
Figure 1-2 SEM images of typical polymer (a) and ceramic (b) membranes generally used in commercial applications [67-68].	9
Figure 1-3 SEM image of a 200 nm pore diameter polycarbonate membrane.....	9
Figure 1-4 Fractures of track etched membranes. Etching with (a) 6 M NaOH, (b) 6 M NaOH + 0.01% DBSNa, (c) 6 M NaOH + 0.05% Dowfax. Scale bar: 1 μ m [71].	10
Figure 1-5 SEM image of a porous alumina membrane viewed from the top (a) and cross section (b).	11
Figure 1-6 Schematic of the electroless deposition onto porous templates to obtain gold nanotube membranes.	13
Figure 1-7 Schematic of the electroless deposition process.	13
Figure 1-8 SEM images of Au tubes obtained after dissolution of the PC membrane, (a) deposition time of 1 h, (b) deposition time of 48 h [91].....	14
Figure 1-9 (a) TEM image showing scalloped nature exhibited by nanowires and nanotubes. (b) SEM image exhibiting non-uniform wall thickness near the end of the nanotube [72].	15
Figure 1-10 Schematic of the separation of molecules based on size exclusion.	16
Figure 1-11 Amounts of moles of MV ²⁺ and Ru(bpy) ₃ ²⁻ transported versus time. Membranes contained gold nanotubes with an inner tube diameter of 3.2 nm [2]....	17
Figure 1-12 Schematic of selective separation achievable by modifying the surface properties of the membrane.....	18
Figure 1-13 Flux plots showing toluene and pyridine transport in an i.d. = 2 nm C ₁₆ thiol modified gold nanotube membrane [100].....	20
Figure 1-14 Diffusion of benzenesulfonate anions across a HS(CH ₂) ₁₀ COOH modified gold coated PC membrane: effect of external pH [35].....	20
Figure 1-15 Schematic of the reversible change in membrane properties due to applied external stimuli.....	21
Figure 1-16 Temperature dependent water flux of pristine PC membranes and PNIPAAm modified PC membranes with different monomer concentrations [110].	22
Figure 2-1 Cross sectional schematic of porous alumina fabrication.	39
Figure 2-2 (a) Schematic and photo of the permeation cell set up used in these studies. (b) Photo of the Ocean Optics UV-Vis system.....	47

Figure 2-3 Structures of probe dye molecules used in the transport experiments.	48
Figure 2-4 Scheme of the synthesis of 4-(4-trifluoromethoxyphenylazo)phenol (1) (intermediary) and 7-[(trifluoromethoxyphenylazo)phenoxy]pentanoic acid (2).....	49
Figure 3-1 Schematic of electrolessly gold coated porous alumina membranes and functionalisation of the gold surfaces with 3-mercaptopbenzoic acid.	53
Figure 3-2. SEM images of a) the surface of an Au-PA membrane and b) an area of the membrane where the gold surface layer was cleaved exposing the tips of the gold nanotubes formed within the pores. c) cross section of the Au-PA membrane. d) pore size distribution of Au-PA membranes.	56
Figure 3-3 SEM images of a section of liberated gold nanotubes after dissolution of the porous alumina from the top of the membrane (a) and from the centre of the membrane (b). EDAX analysis of the nanotube array confirming their composition of gold (c).	57
Figure 3-4 Normal Raman spectrum of pure mMBA (a) and SERS spectrum of an mMBA monolayer on gold (b). Normal Raman spectrum of solid mMBA (c) and SERS spectrum of mMBA on an Au-PA membrane (d) over an extended wavenumber range.	59
Figure 3-5 Raman spectra of mMBA when it is attached to the top surface (a) and within the pores (b) of the gold coated membrane.....	60
Figure 3-6 a) Raman spectra of the cross section of an mMBA functionalised Au-PA membrane. b) Plot of the peak height obtained at 1000 cm^{-1} for $4\text{ }\mu\text{m}$ increments across a cross section of an Au-PA membrane. Scans were taken in $4\text{ }\mu\text{m}$ increments starting above the top surface of the membrane. Position $0\text{ }\mu\text{m}$ is the position of the laser at the starting point of the line scan. The line scan finishes below the bottom surface of the membrane.	62
Figure 3-7 Schematic of a cross section of Au-PA exhibiting a bottle neck shaped pore.....	63
Figure 4-1. a) SEM image showing the surface morphologies of gold nanotube membranes prepared using a polycarbonate membrane as the template with a nominal pore diameter of 80nm. Inset: uncoated polycarbonate membrane. b) TEM cross section of 30nm PC membrane plated with gold for 20h. c) Fully dissolved PC membrane resulting in a standing array of gold nanotubes supported by the surface	

gold layer (PC pore diameter: 800 nm). d) Surface etched Au-PC membrane revealing the tips of the gold nanotubes (PC pore diameter: 200 nm).....	69
Figure 4-2. Typical CVs obtained for unmodified, and thiol-modified gold nanotube membranes, PFDT-Au-PC and DT-Au-PC in (a) an electron-transfer experiment performed using a redox probe 1 mM ferricyanide in 0.2 M KCl (scan rate 100 mVs ⁻¹) and (b) a gold reduction experiment performed in 0.1 M sulphuric acid (scan rate 100 mVs ⁻¹).....	71
Figure 4-3 Transport of a hydrophobic (PCN) and hydrophilic (RB) dye through a gold nanotube membrane functionalised with the hydrophobic thiols a) decanethiol and b) perfluorodecanethiol.	75
Figure 4-4 Transport of the hydrophilic dye (RB) through an unfunctionalised membrane and membranes functionalised with decanethiol and perfluorodecanethiol.	76
Figure 5-1 Schematics of the hybrid gold-polycarbonate structures investigated in this study; (a) unmodified PC, (b) Au _(ext+pore) PC, (c) Au _(pore) PC and (d) Au _(ext) PC and corresponding cross sectional images of the membranes after functionalisation, displaying the areas PFDT is adsorbed on.....	83
Figure 5-2 SEM images of the surface of the a) Au _(ext+pore) PC, b) Au _(pore) PC and c) Au _(ext) PC membranes used in this study. Inset: 30 nm unmodified PC membrane. ..	86
Figure 5-3 SEM images of (a) Au _(ext+pore) PC membrane and (b) Au _(pore) PC membrane based on 80 nm pore size polycarbonate membranes. Inset: uncoated polycarbonate membrane.....	87
Figure 5-4 TEM images of the cross section of (a) Au _(ext+pore) PC, (b) Au _(pore) PC and (c) Au _(ext) PC membranes. The dark regions are region of high gold concentrations. Insets: schematics of their corresponding membrane cross-section.	88
Figure 5-5 Transport of hydrophobic (PCN) and hydrophilic (RB) dye through unmodified and PFDT- modified (a) Au _(ext+pore) PC (b) Au _(pore) PC and (c) Au _(ext) PC membrane.....	93
Figure 5-6 Concentration profiles for RB across PFDT modified a) Au _(ext+pore) PC, b) Au _(pore) PC and c) Au _(ext) PC membranes.	96
Figure 6-1 Schematic of the structural and chemical modification of PA membranes which includes (a) bare membrane, (b) atomic layer deposition (ALD) of silica, (c) hydroxylation step by water plasma and (d) functionalisation of silica modified PA	

membranes by perfluorodecyldimethylchlorosilane (PFDS). The top of the pores is presented.....	104
Figure 6-2 The reduction of pore diameters of PA membranes by ALD deposition of silica using different numbers of cycles. SEM images of PA membranes (20 nm pores) before (a) and after silica modification using (b) 3 ALD cycles, (c) 5 ALD cycles and (d) 7 ALD cycles.	106
Figure 6-3 The correlation of the pore diameters and number of ALD cycles (PA membranes with 20 nm pores).	107
Figure 6-4 SEM images of PA membranes with larger pore diameters (100 and 200 nm) before and after ALD silica modifications. (a–c) PA membrane (100 nm pores) before (a) and after ALD deposition using (b) 10 ALD cycles and (c) 20 ALD cycles. (d–f) PA membrane (200 nm pores) before (d) and after ALD deposition using (e) 20 ALD cycles with (f) corresponding to a cross-section image.	108
Figure 6-5 (a) The depth profile of an Si-PA membrane displaying the distribution of Si, obtained by dynamic SIMS analysis using a Cs ⁺ primary ion beam rastered from the top of the Si-PA membrane (20 nm pores, 3 cycles), (b) EDAX analysis graphs from Si-PA prepared by (b) 5 and (c) 10 ALD cycles.	110
Figure 6-6 Images of a water droplet on (a) an unmodified Si-PA membrane (b) a PFDS modified Si-PA membrane (20 nm pores, 5 ALD cycles).....	111
Figure 6-7 Transport of a hydrophobic (Rubpy) and a hydrophilic dye (RB) through (a) unmodified silica PA membranes (Si-PA) and (b) perfluorodecyldimethylchlorosilane (PFDS) modified Si-PA membranes (20 nm pores, 5 ALD cycles).....	113
Figure 7-1 Schematic of the forward osmosis process. The feed cell is filled with water or contaminated water (e.g. seawater). The draw cell is filled with a highly concentrated solution. The water passes through the semi-permeable membrane due to the increased osmotic pressure across the membrane.	121
Figure 7-2 Photographs of a permeation cell with Si-PA, CV and 1 µM KCl at (a) time = 0 and (b) time = 7 h.....	123
Figure 7-3 Amount of water transported through Si-PA membranes after 8h when various charged dyes are used as the permeant.....	124

Figure 7-4 Water volume change in the feed cell due to water transport through Si-PA membranes containing crystal violet (CV) or rose bengal (RB) in the feed cell.	125
Figure 7-5 Amount of water transported for PA and Si modified PA after 400 min when CV or RB is used as the permeant.....	127
Figure 7-6 SEM images of (a) an unmodified PA membrane and (b) a Si-PA membrane.....	128
Figure 7-7 Volume change in the draw (a) and feed (b) cell due to water transport through Si-PA membranes containing crystal violet (CV) in the draw cell and varying KCl concentrations in the solvent.....	130
Figure 7-8 Volume change in the draw (a) and feed (b) cell due to water transport through Si-PA membranes containing rose bengal (RB) in the draw cell and varying KCl concentrations in the solvent.....	131
Figure 7-9 Volume of water transported through Si-PA membranes after 300 min for varying KCl concentrations when crystal violet (a) or rose bengal (b) is in the draw cell.....	132
Figure 7-10 Transport of Rubpy and RB through a Si-PA membrane.	133
Figure 8-1 Schematic of gold coated alumina membrane with adsorbed azobenzene thiol layer and its reversible photisomerisation between the trans and cis states. ...	140
Figure 8-2 SEM images of the suface of a gold nanotube membrane after 16 h of gold deposition (a) and the cross sectional view of the gold nanotube membrane (b).	142
Figure 8-3 Transport of the hydrophilic dye (EY) across the azobenzene modified membrane when switched between the trans (highly hydrophobic) and cis (less hydrophobic) states.	144
Figure 8-4 Schematic representation of the assembly of the azobenzene layer within a pore (top view) in the trans state (a) and the cis state (b).....	145

LIST OF SYMBOLS AND ABBREVIATIONS

ALD	Atomic layer deposition
APTES	Aminopropyltriethoxy silane
Au	Gold
Au-PC	Gold coated polycarbonate
Au-PA	Gold coated porous alumina
$\text{Au}_{(\text{ext-pore})}\text{PC}$	Gold coated polycarbonate on the interfaces and inside pores
$\text{Au}_{(\text{pore})}\text{PC}$	Gold coated polycarbonate only within the pores
$\text{Au}_{(\text{ext})}\text{PC}$	Gold coated polycarbonate only on the interface
BG	Bromocresol green
CV	Cyclic voltammetry
CVD	Chemical vapour deposition
DT	1-Decanethiol
EDAX	Energy dispersive analysis X-ray spectroscopy
EDC	1-Ethyl-3-[3-dimethylaminopropyl]carbodiimide hydrochloride
EY	Eosin yellow
FIB	Focussed ion beam
FO	Forward osmosis
FTIR	Fourier transform infrared spectroscopy
LCST	Lower critical solution temperature
MBA	Mercaptobenzoic acid
MV	Methyl viologen
NEXAFS	Near Edge X-ray Absorption Fine Structure
NHS	N-hydroxy succinimide
NS	Nickel sulphate
PA	Porous alumina
PC	Polycarbonate
PCN	Pinacyanol chloride
PDMS	Polydimethylsiloxane
PF	Potassium ferricyanide
PFDS	Perfluorodecyldimethylchlorosilane
PFDT	Perfluorodecanethiol

PNIPAAM	Poly(<i>N</i> -isopropylacrylamide)
RB	Rose bengal
RhB	Rhodamine B
RO	Reverse osmosis
Ruby	tris(2,2'-bipyridyl)dichlororuthenium(II) hexahydrate
SAM	Self assembled monolayer
SEM	Scanning electron microscopy
Si	Silica
Si-PA	Silica coated porous alumina
SIMS	Secondary ion mass spectrometry
SERS	Surface enhanced Raman scattering
TEM	Transmission electron microscopy
TMA	Trimethyl aluminium
UV-Vis	Ultraviolet – Visible
XPS	X-ray photoelectron spectroscopy

ABSTRACT

Membrane-based separation is a rapidly developing technology which offers many advantages over other separation techniques. However, existing membrane technology requires further research into improving efficiencies which involves flux enhancement, improved selectivity, sufficient long term stability and anti-fouling properties. The fabrication of membrane materials capable of performing highly controlled molecular separations can be achieved by developing nanoporous materials with controllable structural, physical and chemical properties. Recently there has been increased interest in the functionalisation of membrane surfaces in order to enhance the stability and transport properties of membranes. However, current research into the characterisation of functional layers within porous materials is lacking. Further insight into how surface modifications may impact the transport properties of porous membranes is essential for the development of membrane materials.

This thesis presents an approach for tailoring porous materials with surface functionalities and controlling pore architecture to provide controlled transport properties. Membranes such as polycarbonate and porous alumina membranes were used in these studies due to their ordered pore architectures. Further structural modification of the membranes was carried out in order to reduce the pore diameter of the membranes. Pore size reduction was achieved using two methods; electroless deposition of gold and atomic layer deposition (ALD) of silica. The pore size of the membranes was altered systematically by adjusting the number of ALD cycles or by adjusting gold deposition time.

The surface properties of the membranes were tailored in order to provide controlled molecular transport. It is important to determine how surface modifications may impact the transport properties of porous membranes in order to devise more efficient separation processes. Desired chemical properties were imparted to the membranes by modifying the membrane surfaces with self assembled monolayers (SAMs). Predominantly, hydrophobic SAMs were used as it presented a simple technique to demonstrate changes to the transport properties of membranes due to

introduced surface functionalities. The transport properties of fluoro-derivatised membranes (1H,1H,2H,2H-perfluorodecanethiol) towards hydrophobic and hydrophilic molecules was compared with a membrane modified with an analogous alkanethiol; 1-decanethiol to demonstrate the influence that a slight variance in surface modification can have on the transport properties of the membrane. The effects of the controlled positioning of functional groups on the transport properties of the membrane were investigated. Several hybrid membrane structures based on polycarbonate membranes were created in which gold was deposited on different areas on the membrane; on one of the membrane interfaces, within the pores of the membrane and completely coating all surfaces of the membrane. Gold-thiol chemistry was exploited in which the thiols only assembled on the gold coated regions of the membrane thus providing controlled positioning of functional regions. Lastly, silica coated PA membranes were functionalised with perfluorodecyldimethylchlorosilane (PFDS) to demonstrate that the transport and selectivity properties of silica composite PA membranes can be varied by functionalisation using silane chemistry.

The investigation of the coverage and reproducibility of SAMs within porous matrices is of utmost importance in the design of filtration membranes and sensing platforms. The surface enhanced Raman scattering (SERS) effect was employed to confirm and characterise the formation of SAMs of 3-mercaptopbenzoic acid (mMBA) on the surfaces of the gold coated alumina membranes.

To explore more sophisticated surface functionalisation, stimuli responsive membranes were produced. The transport properties of the gold nanotube membranes were controlled through the reversible switching of adsorbed fluorinated azobenzene layers. The fluorinated, hydrophobic end group of the azobenzene chain produces a transition between hydrophobic and less hydrophobic surface properties when switching from the *trans* to the *cis* state. The selective mediation of a hydrophilic probe dye across the membrane was investigated.

CHAPTER 1

INTRODUCTION

1.1. OVERVIEW

Membrane-based separation is a rapidly developing technology which offers many advantages over other separation techniques such as distillation, flocculation, extraction and chromatography [1-3]. Membranes have found a multitude of applications in biotechnology [4-5], pharmaceuticals [6-7], wastewater treatment [8] and desalination [9-10]. The advantages of implementing membranes in these applications include the potential to perform low cost, minimal waste and high throughput separations. However, existing membrane technology requires further research into improving efficiencies which involves flux enhancement, improved selectivity, sufficient long term stability and anti-fouling properties. There is currently a great deal of interest in the development of membrane materials capable of performing highly controlled molecular separations. This can be achieved by developing nanoporous materials with controllable structural, physical and chemical properties. Applications for porous materials would be greatly expanded if their design could be finely controlled, particularly through the fabrication of desired pore architectures or the modification of surface chemistry with functional molecules.

The modification of porous materials with a functional coating can be achieved using self assembled monolayers (SAMs). SAMs present a tool for the tailoring and design of membrane materials with desired physical and chemical properties. Functionalisation of membrane surfaces is also desirable to improve biocompatibility for applications that involve interactions with biomolecules such as in protein separation devices, cell adsorption/growth, tissue engineering and drug delivery. The ability to integrate SAMs within nanopores provides significant advantages in membrane technologies as the nanoconfinement of the SAM will lead to greater encounters and selective interactions with the molecules entering the pore [11-12].

In recent years, there has been increased interest in the construction of responsive or switchable membrane materials [13-16]. Such materials have applications in switchable molecular separations, controlled drug release, chemical and bio-sensing, and molecular electronics. These responsive membrane materials can be achieved through the assembly of “smart” SAMs onto the membrane. Smart SAMs have been

fabricated with reversible properties through changes in wettability [17-18], charge [19], adhesion [20], and biocompatibility [21-23].

In addition to tailoring the surface chemistry of membranes, there has been recent focus on the development of new membrane materials and porous structures. Nanotube membranes have been recently introduced by depositing a thin layer of material such as gold, silica, carbon and metal oxides inside the pores of a template membrane [24-28]. Amongst them, the gold nanotube membrane has received considerable interest for applications in molecular separations [2, 29-30] due to the properties of gold such as chemical inertness, thermal stability, conductivity and the ability to tailor surface properties by chemical and biochemical functionalisation [31-37]. Gold nanotube membranes are highly ordered membranes fabricated through the electroless deposition of gold onto a template membrane [29]. They have received much attention due to the ease and simplicity of surface modifications with thiols and the limitless capacity for additional surface modifications through coupling to the thiol anchors [1, 11, 35]. Through the correct pairing of thiols to target molecules, selective or enhanced transport can be achieved.

1.2. MEMBRANE MATERIALS AND THEIR APPLICATIONS

A membrane is a thin sheet of a natural or synthetic material which moderates the transport of chemical species in contact with it. The material can be various thicknesses, with homogeneous or heterogeneous structures, and differing pore sizes. The main categories of membrane structures are shown schematically in Figure 1-1. Studies to date have demonstrated the ability of nanoporous membranes to perform selective transport and separation of molecules including gases [38], metal ions [39], anions, small organic molecules [40], drugs [41], proteins and nucleotides [34, 42-43]. The simplest strategy for molecular filtration is based on separation by molecular size. Other selectivity processes have been performed such as selectivity based on ionic charge [44], electro-osmotic flow [45], electrophoretic [46] and electrokinetic transport [47].

The main interests in membrane science and technology have been fuelled by the need for sustainable and eco-friendly technologies. Membranes offer simplicity, efficiency, high selectivity, low energy consumption, stability and ease of up-scaling. The membrane industry spans numerous diverse fields where US membrane applications alone is a multi-billion dollar market [48]. Industrial applications include water desalination, water treatment, gas separation, gas storage, microfiltration and pervaporation. Medical applications include controlled drug release, artificial organs and tissue regeneration.

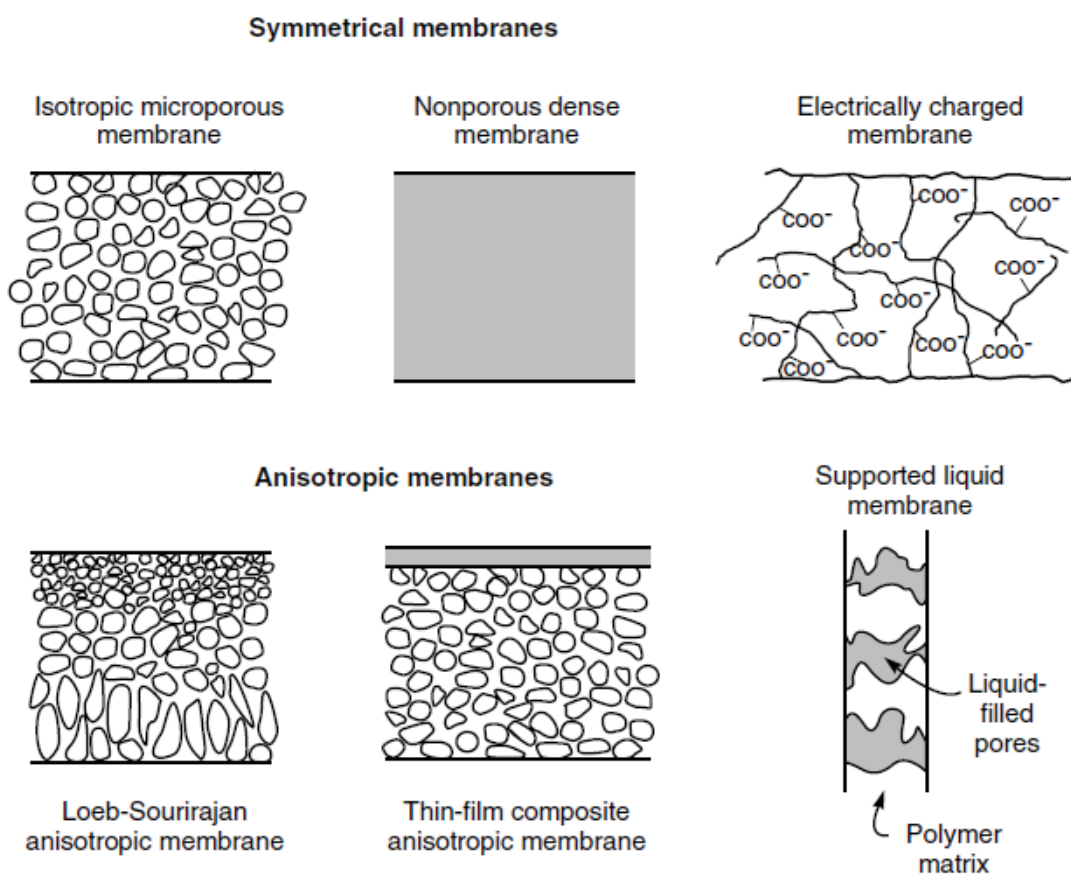


Figure 1-1 Schematics of the principal types of membranes [49].

Membrane technology has become commonplace in water treatment industries. The implementation of membrane systems in water treatment has resulted in decreased running costs leading to a reduction in reclaimed water prices. Reverse osmosis is presently the fastest growing technology in the desalination industry. It is now considered worldwide as the most promising technology for resolving freshwater

scarcity [48]. Reverse osmosis membranes are generally made from polymers and are dense materials which are permeable to water but impermeable to salt, hence enabling the separation of water and salt ions [49].

Membrane based gas separations is a rapidly growing industry with future prospects improving as membrane technology successfully competes against adsorption, absorption and cryogenic technologies. The gas separation industry utilises membranes for the removal of nitrogen and water from air, carbon dioxide from natural gas and the refinement of gasses. The main application for membranes in the gas separation industry is for the separation of nitrogen from air. Nitrogen production represents more than half of the membrane based gas separation industry [48]. However, the largest gas separation industry, by amount of gas treated, is in the refinement of natural gas. While membranes have only attained a small percentage of the natural gas market, membrane implementation in this field is steadily growing. The separation of carbon dioxide from natural gas is of utmost importance for overgrowing concerns for global warming. In particular, the separation of carbon dioxide from industrial fumes is an objective of current research groups worldwide.

Membrane materials are regarded as highly suitable for biomedical applications due to mild operating conditions such as low pressure and temperature thereby preserving the original biological activity. Furthermore for membrane separations additional solvents do not need to be added therefore avoiding possible contamination. Additionally, a variety of membrane materials are available, many of which are biocompatible and highly anti-fouling. Medical applications requiring membranes include the recovery and purification of biologically active molecules [50], hemodialysis [51], artificial organs [5], drug delivery [52], tissue engineering and regenerative medicine [53]. Biologically active compounds such as proteins, DNA, RNA and more recently small bioactive molecules are required to be recovered and refined from highly complex media. Furthermore, membrane materials have recently been employed in controlled drug delivery devices. It is expected that bioactive molecule recovery and drug delivery will excel with the upcoming development of membranes which are responsive to external stimuli such as pH, temperature and UV-Vis irradiation. The most important application of membranes in biomedical applications is in haemodialysis [54], for the treatment of end stage renal disease.

Membranes are also used for blood oxygenation during cardiac surgery and respiratory failure [55]. Furthermore membranes have been used for plasma separation and for cholesterol removal [56]. Emerging applications for membranes in the medical field include artificial organs such as liver, kidney and pancreas and regenerative medicines [48]. As the liver is highly complex and performs multiple functions, artificial livers have thus far only able to perform the detoxification functions of the liver. Therefore promising research has concentrated on the design of bioartificial livers [57]. The fields of tissue engineering and regenerative medicine utilise membrane materials as scaffolding or supporting materials for biological materials. The formation of new tissue can be achieved through using membrane materials as cell supports [58]. Through this technique hybrid materials can be constructed for inducing tissue regeneration in patients and for replacing failing organs.

The membranes employed in the above applications fall into several categories: polymer, inorganic and hybrid organic-inorganic membranes. Membrane applications are mainly dominated by polymer membranes as they are readily commercially available, they offer substantial variety in regards to composition and porosity and are easily fabricated with a large membrane area. Furthermore polymer membranes are generally considered consistent, reliable and cost effective. Considerable research is focussed on tailoring these polymeric materials to suit specific applications through modifying their pore geometries and physical properties. However, polymeric membranes have limitations. Well-defined pore architectures are difficult to achieve and in general they have poor chemical resistance, thermal stability and mechanical strength. Therefore inorganic membrane materials are gaining interest due to their high thermal and chemical stabilities and greater mechanical strength. Particular inorganic membranes such as porous alumina and zeolites consist of highly uniform and ordered pore architectures [59]. Unfortunately inorganic membranes tend to be brittle and more expensive than their polymer counterparts and are therefore generally dismissed in large commercial industries such as water treatment. Recently hybrid organic-inorganic membranes have gained considerable interest [60-61]. They are comprised of either inorganic membranes coated in organic layers or inorganic porous materials embedded into a

polymer matrix. These membranes offer improved performance in regards to selectivity, permeability and stability.

1.3. DIFFUSION THROUGH MEMBRANES

Molecules dissolved in liquids or gases are continually and randomly moving. When there are areas of differing concentrations of molecules in the solvent the molecules will diffuse from areas of high concentration to low concentration. The concept of diffusion was mathematically described by Adolf Fick, a physician who derived Fick's laws of diffusion in 1855 [62]. Fick's laws are often used to describe and model membrane transport properties observed in osmosis, reverse osmosis, gas permeation, drug delivery and cell membrane functions [63]. Fick's first law of diffusion [62] states that the net rate of diffusion is;

$$J = -D \frac{dC}{dx} \quad (1)$$

where the rate of diffusion or flux, J , is proportional to the concentration gradient, dC/dx , and a proportionality constant termed the diffusion coefficient, D . The minus sign indicates that the diffusion is in the direction of higher to lower concentration. The concentration gradient is the driving force behind the diffusion of molecules. The molecules will flow in the direction which will eliminate the concentration difference. If a permeable membrane separates solutions of high and low concentration, the molecules on the high concentration side will diffuse across the membrane to the low concentration side. Diffusion will continue until the concentrations on both sides of the membrane reach equilibrium.

The connection between the flux, J , and the driving force, dC/dx , is the diffusion coefficient, D . Fick described the diffusion coefficient as "the constant depending of the nature of the substances". It is determined by the nature of the diffusing solute and the nature of the membrane or medium through which diffusion takes place. The diffusion coefficient of the solute within the membrane will differ from the diffusion coefficient in the bulk solvent. Thus for transport across a membrane the description of diffusion becomes more complicated and Fick's law must be adapted [64-65]. Generally the concentration of the solute immediately within the membrane will not be the same as the concentration in the solution adjacent to the membrane. The distribution of the solute between the bulk solution and the membrane material is

described by the partition coefficient, K . The partition coefficient is the concentration of the solute immediately within the membrane divided by the concentration in the adjacent solution and hence describes the solute's ability to enter the membrane. The partition and diffusion coefficients are grouped together in a new term, the permeability coefficient, P , which is defined as;

$$P = \frac{KD}{L} \quad (2)$$

where L is the thickness of the membrane. Thus Fick's first law of diffusion becomes;

$$J = P(C_1 - C_2) \quad (3)$$

where C_1 and C_2 are the concentrations of the solutions on either side of the membrane. The partition coefficient is often found to have a more pronounced influence on the permeability or flux than the diffusion coefficient [66]. Therefore the differences in diffusion tend to be less important than differences in the solute's affinity for or solubility in the membrane material. Consequently the permeability coefficients of solutes are highly dependent on their partition coefficients. In other words, the more soluble or attracted a molecule is to a membrane the greater its permeability coefficient.

1.4. POROUS MEMBRANES WITH UNIFORM AND ORDERED ARCHITECTURES

Typically, the membranes used in commercial applications involve materials with a non-uniform sponge-like network of pores (Figure 1-2). These membranes have substantially differing pore sizes throughout the material resulting in a non-ideal platform to investigate fundamentals of transport phenomena. Porous materials which contain pores that run perpendicular to the surface with no lateral crossovers have recently gained interest. Membranes with such structured architectures thereby provide an ideal model for studying how pore size and surface chemistry affect the transport properties of the membrane. Such ideal porous membranes include polymeric track-etched and anodic alumina membranes which are commercially available and are commonly used as tools for filtration.

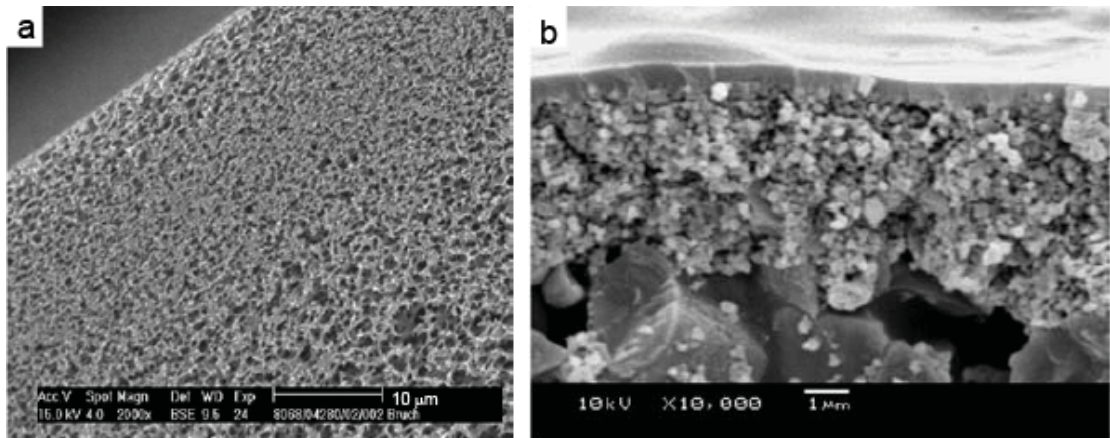


Figure 1-2 SEM images of typical polymer (a) and ceramic (b) membranes generally used in commercial applications [67-68].

1.4.1. Polycarbonate track etched membranes

Polycarbonate track etched membranes are generally considered to be consistent porous membranes containing cylindrical pores of uniform diameter [4, 11]. Due to these characteristics, polycarbonate membranes have been used as ideal platforms to investigate the fundamentals of transport phenomena [5-7, 10, 15]. Generally polycarbonate membranes have low porosity (< 15 %) and a thickness ranging from 6 – 11 μm [69]. Commercially available membranes are produced with pore sizes ranging from 10 nm to \sim 10 mm. Although polycarbonate membranes posses a few idealistic characteristics such as a narrow pore size distribution, the pores are randomly distributed (Figure 1-3).

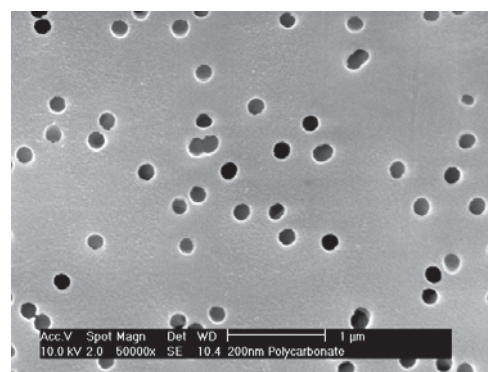


Figure 1-3 SEM image of a 200 nm pore diameter polycarbonate membrane.

Polycarbonate membranes are fabricated using the track etch method which involves bombarding a polycarbonate film with a collimated beam of energetic heavy ions to

create linear damage tracks [70-71]. The damage tracks are then chemically etched to form cylindrical pores. Factors such as etch time and temperature determine the diameter of the pores. Lower temperatures ($\sim 1\text{-}2$ °C) promote even etching of the pores to produce cylindrical pores. With higher temperatures, the etching is rapid and the pores exhibit a cigar-like shape in which the diameter of the pore is tapered towards the top and bottom surface of the membrane (Figure 1-4) [71]. Commercially available track etch membranes are found to exhibit these ‘cigar’ shaped pores [71-73].

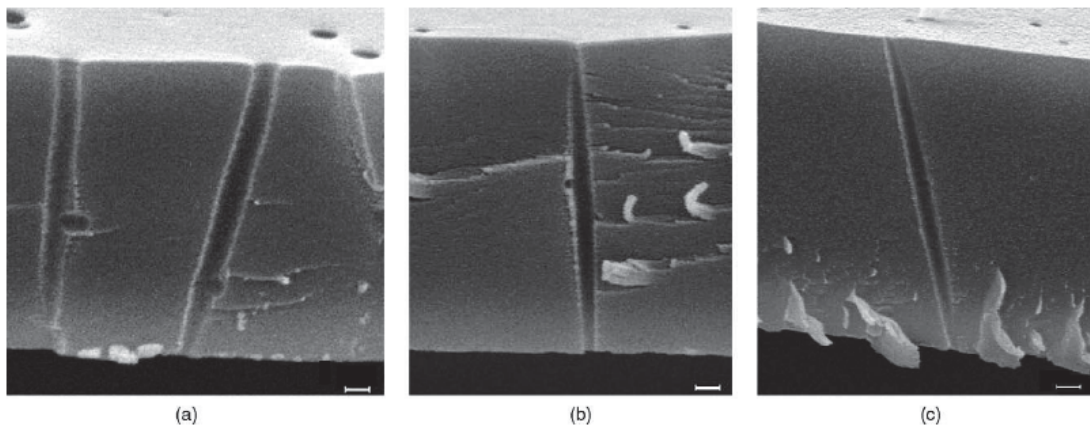


Figure 1-4 Fractures of track etched membranes. Etching with (a) 6 M NaOH, (b) 6 M NaOH + 0.01% DBSNa, (c) 6 M NaOH + 0.05% Dowfax. Scale bar: 1 μm [71].

1.4.2. *Porous alumina membranes*

Porous materials such as porous alumina (PA) membranes possess a higher degree of pore structure and order than polycarbonate membranes. Recently there has been increased interest in the fabrication and characterisation of PA membranes [74-75]. Due to their aligned and uniform cylindrical pores, PA has been extensively used as membranes in separation technologies [40, 76] and as ideal template structures for the fabrication of nanotubes and nanowires [77-79]. The attraction of PA membranes is based on the low cost of fabrication in comparison to other inorganic membranes, thermal stability, order, uniformity and density of nanopores. PA membranes are highly porous materials with porosities as high as 30-50 % [80]. Unlike polycarbonate membranes, there is a regular distribution of the pores. However, in comparison to polymeric membranes PA fabrication is more expensive and tends to be more brittle and fractures easily.

Due to aluminium's high affinity for oxygen, its surface is always covered in an oxide film [81]. This film is composed of alumina (Al_2O_3) which is highly resistant and provides corrosion protection to the aluminium. It is possible to make these layers porous by using an electrochemical process called anodisation. PA forms via self organisation where the length, diameter and density of the pores are precisely controlled by the anodisation conditions. Factors during anodisation such as electrolyte composition, pH and applied voltage govern the structure of the PA formation. Porous alumina exhibits pores with hexagonal order (Figure 1-5), and can be fabricated with pore diameters that range from 20 - 200 nm and membrane thicknesses ranging from several microns to hundreds of microns [82-83].

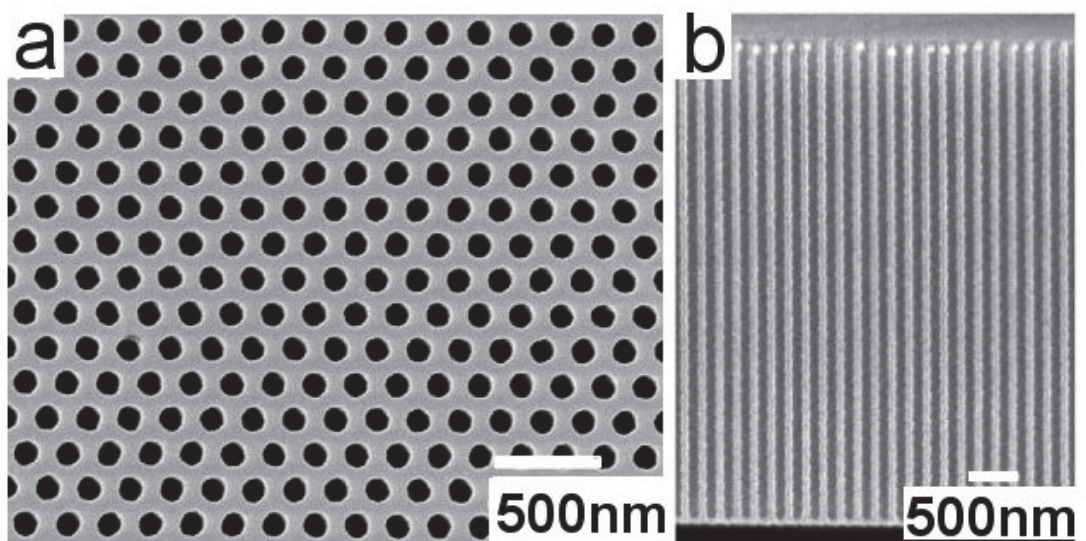


Figure 1-5 SEM image of a porous alumina membrane viewed from the top (a) and cross section (b).

1.5. ELECTROLESS DEPOSITION OF GOLD

Several strategies can be used to modify the structure of porous materials including electrochemical metal deposition, electroless metal deposition, chemical and plasma polymerisation, sol-gel deposition and chemical vapour deposition [84]. Amongst these deposition methods, electroless deposition is advantageous in the coating of porous materials as this technique is not limited to the structure of the material that can be coated. The advantage of electroless deposition is the ease of depositing materials within thick porous membranes. The majority of the other deposition

methods outlined above are only capable of modifying the top surfaces of the membrane. Other methods which are capable of depositing material within membranes involve very complex procedures. Electroless deposition of gold onto template membranes not only precisely controls the pore diameter [2, 29] but additionally provides a suitable platform for further modifications with SAMs such as thiols [31-37]. Through exploiting gold – thiol chemistry, these gold coated membranes can be functionalised with a wide variety of thiols [85].

C.R. Martin pioneered gold nanotube membranes which utilises electroless gold deposition [29]. This technique evenly coats the pore walls of the membrane thus forming hollow gold nanotubes (Figure 1-6). The deposition of the gold depends on several factors, the gold deposition time, temperature, pH and concentration of the gold in the gold deposition bath. As deposition time continues the thickness of the gold increases. Thus by controlling the deposition parameters the inner pore diameter of the gold nanotubes can be decreased down to 1 nm, hence providing a tool for molecular separations.

Briefly, the process used for electroless deposition consists of several steps as outlined in Figure 1-7. Firstly the membrane is sensitised in a tin solution followed by the deposition of catalytic silver nanoparticles. The membrane is then immersed in the gold deposition bath in which gold displaces the silver nanoparticles and further gold is reduced by formaldehyde and so the gold layer becomes thicker with time. Although electroless deposition has predominantly been used to deposit gold onto polycarbonate membranes, this technique is not only limited to polycarbonate surfaces but can be used to plate various materials [77, 86-87].

The formation of electroless gold layers within porous materials has been extensively studied by several groups. It is important to obtain homogeneous electroless deposition in porous materials which is achieved by reducing the rate of gold deposition. Although it appears counterintuitive to coat the surfaces in catalytic silver nanoparticles, these nanoparticles serve another function in which the gold ions are preferentially reduced at the surfaces containing silver nanoparticles thereby only coating those areas with gold. The electroless deposition method deposits nanometre sized gold particles on the pore walls and as deposition time continues these particles

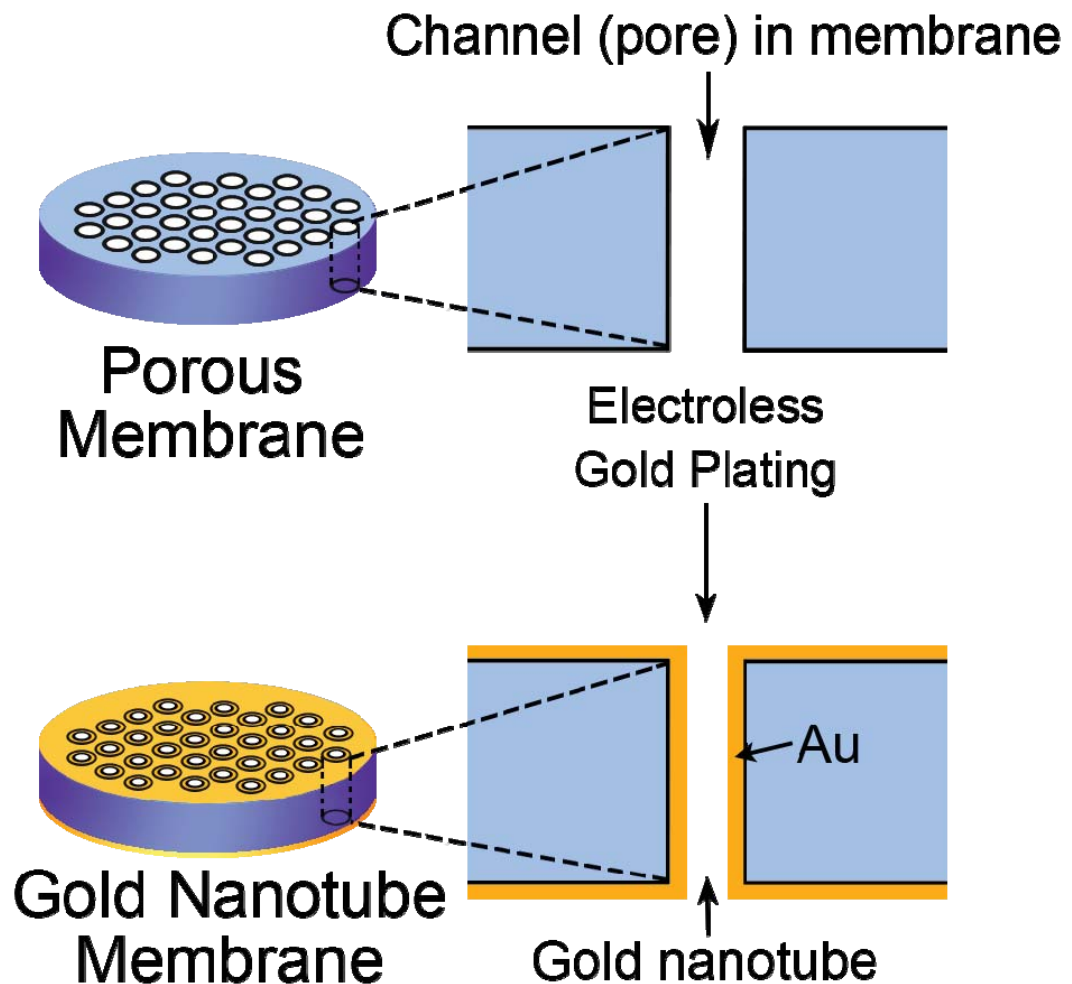


Figure 1-6 Schematic of the electroless deposition onto porous templates to obtain gold nanotube membranes.

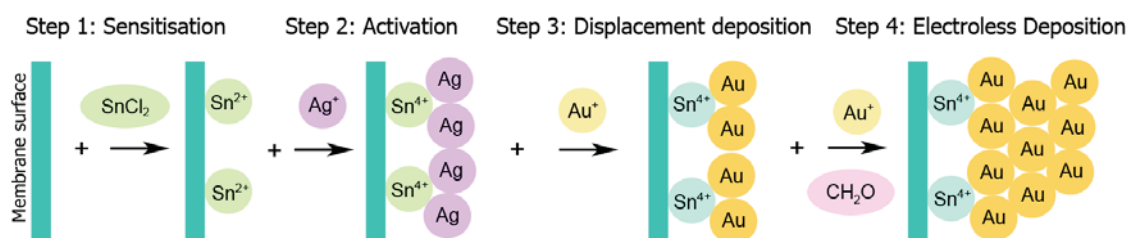
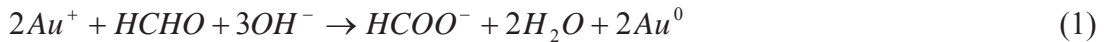


Figure 1-7 Schematic of the electroless deposition process.

grow to form a compact gold layer. The size of these gold particles and their nucleation distance is dependent on several factors including the concentration of gold, pH and temperature of the gold deposition bath. It has been shown that with higher temperatures, the rate of gold deposition increases and thus inhomogeneous gold deposition occurs [72]. Gold deposition is typically carried out at 1 – 4 °C to

ensure a slow deposition rate to allow for fine deposited layers [29]. The reduction of Au^+ ions to elemental Au is depicted by reaction 1:



The pH of the gold deposition bath is found to have a profound effect on the quality of electroless deposition. From reaction 1, it is apparent that at neutral and acidic pH gold deposition cannot take place. It is evident that increasing pH values will accelerate the rate of gold deposition. Previous studies have shown that the ideal pH for the promotion of homogeneous gold films was found to be in a range of pH 8 – 10.

Electroless deposition has been extensively employed for the fabrication of templated nanostructures for use in applications such as in electronics [29], catalysis [88] and sensing [89-90]. As the pores in polycarbonate and alumina membranes are cylindrical, gold nanotubes or nanowires can be formed. Figure 1-8 displays SEM images of gold nanotubes which were formed within a polycarbonate membrane. After gold deposition the polycarbonate template can be dissolved thus liberating the gold nanotubes [29, 73].

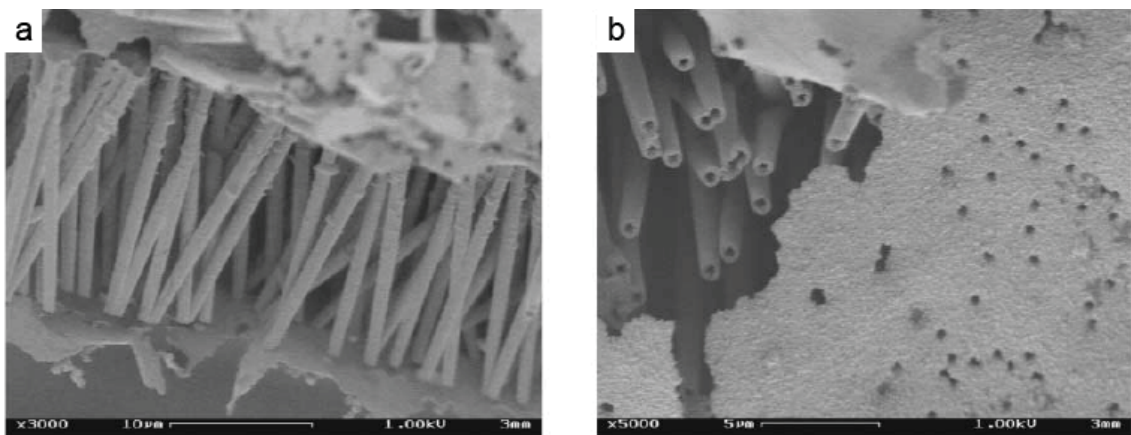


Figure 1-8 SEM images of Au tubes obtained after dissolution of the PC membrane, (a) deposition time of 1 h, (b) deposition time of 48 h [91].

When taking a closer look at liberated gold nanotubes the scalloped nature of the gold tubes due to the ‘cigar’ shaped pores of the polycarbonate is apparent (Figure 1-9). Figure 1-9(b) presents an SEM image of the tip of a gold nanotube illustrating that the gold deposition is favoured at the surfaces of the membrane [72]. This is apparent from the thicker nanotube wall observed at the tip of the nanotube.

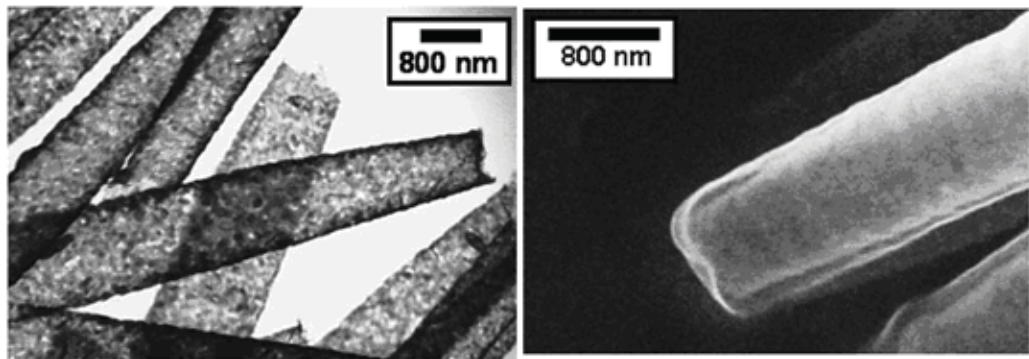


Figure 1-9 (a) TEM image showing scalloped nature exhibited by nanowires and nanotubes. (b) SEM image exhibiting non-uniform wall thickness near the end of the nanotube [72].

In order to apply the electroless gold deposition method to other materials, the electroless deposition method will need to be tailored to suit that particular material. For example, Martin and co-workers achieved electroless gold deposition onto porous alumina by adapting a few of the experimental procedures. Firstly, the membrane needed to be functionalised in order for tin chelation to occur. This was achieved by modifying the alumina with the silane; trimethoxysilylsuccinic anhydride [77]. Secondly, as their porous alumina membranes were ten times thicker than the polycarbonate samples they reduced the gold deposition rate to allow for homogeneous deposition and to inhibit the formation of bottle necked pores. This was achieved by reducing the pH of the gold deposition bath from 10 to 9. Therefore through adapting the electroless deposition procedure a wide variety of materials can be coated with gold.

1.6. SEPARATION STUDIES

1.6.1. *Size based molecular separations*

Membranes can be used to separate molecules based on their size, charge and hydrophobicity. Size based separation is the simplest strategy for molecular separation using membranes. A schematic of the concept of size based separation is presented in Figure 1-10. For membranes to be used as molecular filters, the pore size must be of molecular dimensions. Electroless deposition of gold has provided a

method to decrease the pore size of porous membranes. As stated previously, the pore size of membranes can be reduced to approximately 1 nm using electroless deposition. C. R. Martin's group demonstrated the separation of two molecules of differing size through gold nanotube membranes [2]. Methyl viologen (MV^{2+}) and tris(bipyridine)ruthenium(II) chloride ($Ru(bpy)_3^{2+}$) were separated using a gold nanotube membrane with a pore size of 3.2 nm. The amount of each molecule that was transported across the membrane is depicted in Figure 1-11. MV^{2+} is a small molecule and was easily transported through the membrane. $Ru(bpy)_3^{2+}$ however is a larger molecule and its transport was hindered.

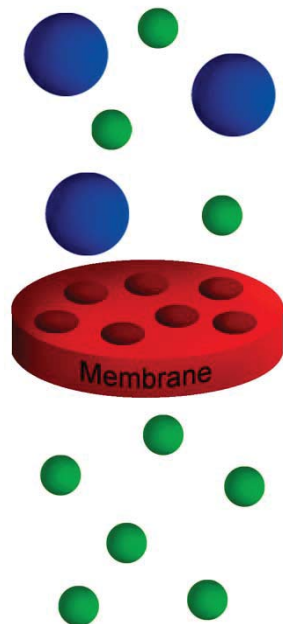


Figure 1-10 Schematic of the separation of molecules based on size exclusion.

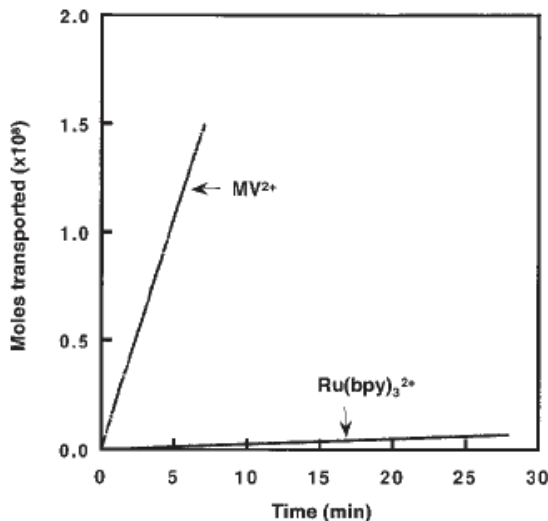


Figure 1-11 Amounts of moles of MV^{2+} and $\text{Ru}(\text{bpy})_3^{2+}$ transported versus time. Membranes contained gold nanotubes with an inner tube diameter of 3.2 nm [2].

1.6.2. Functionalised membranes for enhanced and selective separations

The separation of similarly sized molecules is a complex scenario and requires more sophisticated membrane materials. Surface modification can be applied to membranes in order to separate similarly sized molecules based on their chemical characteristics. Surface modification can result in highly selective separations due to the chemical interaction between the permeate and the molecules on the surface [11, 92-93] and can also be used to produce anti-fouling surfaces [94]. However, the application of surface modification in commercial membranes is not widely considered other than their use as anti-fouling coatings [43, 95-96]. Research into exploiting surface chemistry to enhance transport selectivity and sensing is relatively new but is exceedingly important especially in the biotechnology industry which requires separation of complex biomolecules and controlled delivery of drugs. Consequently, surface modification is an important factor in membrane design as it has the potential to tailor and design membrane materials with desired physical and chemical properties. Through the correct pairing of surface modifications to target molecules, selective or enhanced transport can be achieved (Figure 1-12).

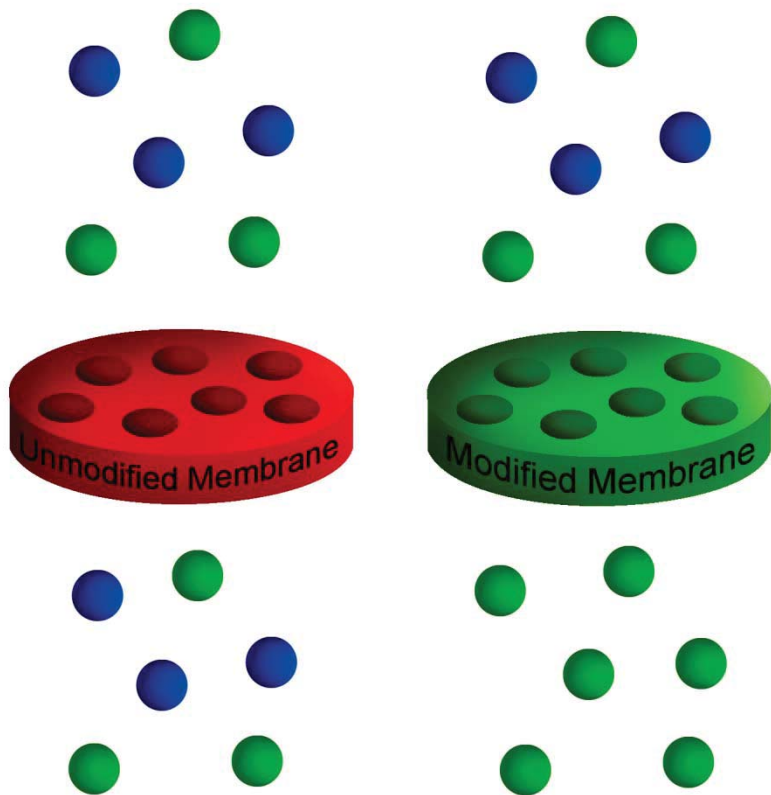


Figure 1-12 Schematic of selective separation achievable by modifying the surface properties of the membrane.

Chemical selectivity is generally introduced into the membrane through the addition of SAMs or polymer coatings. Gold nanotube membranes have been widely used to investigate the effect of surface functionality on the transport properties of membranes mainly due to the ease of chemical functionalisation. Due to the large affinity between thiols and gold, SAMs of thiols can readily be formed on all surfaces of the membrane [85, 97-99]. Thiols are compatible with most organic functional groups thus it is possible to incorporate a variety of terminal functionalities in gold-thiol monolayers, hence introducing tailored chemical sensitivity into the membrane [99]. However, the stability of thiols on gold is limited by the strength of the gold-sulphur bond which is relatively weak. The formation of defects commonly occurs during long term storage and therefore most thiol modified surfaces are only viable for several months [85]. Thiol layers tend to be susceptible towards decomposition via processes such as oxidative degradation, but the main limitation in their stability is due to desorption.

C. R. Martin and co-workers assembled thiols within the pores of gold nanotube membranes in order to modify the chemical environment within the pores [100]. A long chain hydrophobic thiol and a short chained hydrophilic thiol were used to probe the effects on the passage of hydrophobic and hydrophilic molecules across the membranes. It was found that hydrophobic molecules were preferentially transported by membranes functionalised with the long chain thiol while hydrophilic molecules were preferentially transported by the short chain hydrophilic thiol. Assembly of the long chained thiol onto the nanotube membrane resulted in blocked pores into which only hydrophobic species could partition. Therefore this functionalised membrane can be used to separate hydrophobic and hydrophilic molecules. Figure 1-13 illustrates the separation of hydrophobic (toluene) and hydrophilic (pyridine) species across a gold nanotube membrane modified with the hydrophobic long chain alkanethiol.

Stroeve's and Martin's groups have worked extensively on the selective transport of ions across membranes [19, 34-35, 101]. They established that modifying gold nanotube membranes with carboxylic acid terminated thiols leads to selective ion transport dependent on the pH of the surrounding media. Through controlling the pH or applied potential they were able to control the flow rates of solutes across the membrane. For example Stroeve's group produced a gold nanotube membrane that has been modified with a carboxylic acid terminated SAM ($\text{HS}(\text{CH}_2)_{10}\text{COOH}$). At low pH the thiols are protonated and hence the membrane is anionic selective and at high pH the thiols are deprotonated and so the membrane becomes cationic selective [19]. Figure 1-14 presents permeation data for an anion (benzenesulfonate) through the modified membrane. It is seen that low pH allows transport of anionic molecules whereas at high pH the transport is hindered.

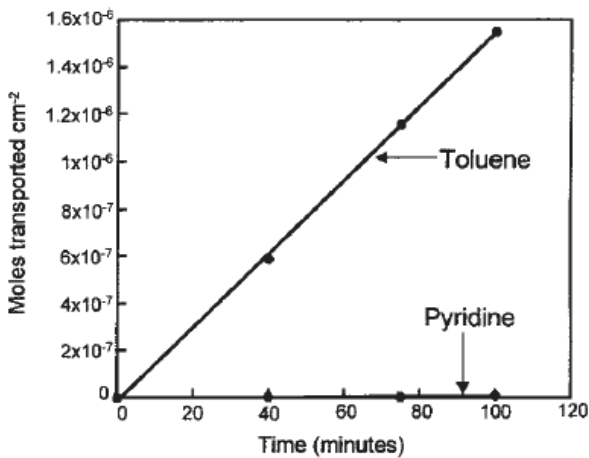


Figure 1-13 Flux plots showing toluene and pyridine transport in an i.d. = 2 nm C₁₆ thiol modified gold nanotube membrane [100].

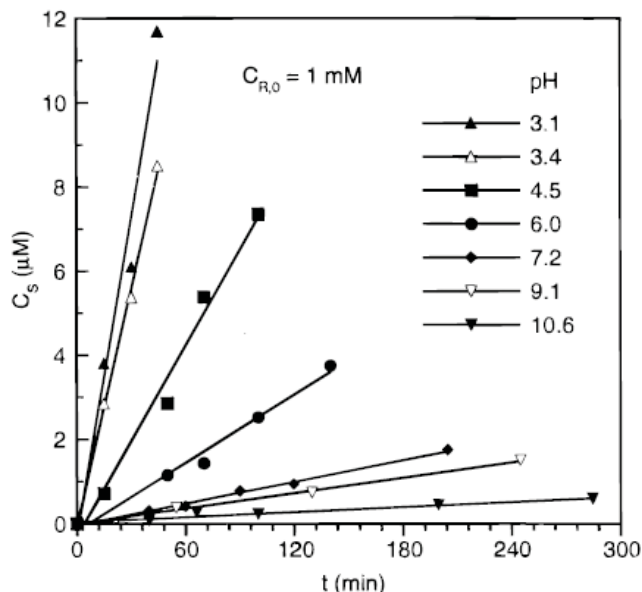


Figure 1-14 Diffusion of benzenesulfonate anions across a HS(CH₂)₁₀COOH modified gold coated PC membrane: effect of external pH [35].

1.7. SWITCHABLE MEMBRANES

In recent years, there has been increased interest in the construction of stimuli responsive or gating membrane materials due to their ability to selectively mediate molecular transport [13-16]. Such membranes exhibit changes in permeability and selectivity due to a response to applied external stimuli such as light [18, 102], temperature [23], electrical potential [32, 103-104], and surrounding media [105-106]. As the properties of the membrane can be controlled on demand, these

responsive membranes have great potential in applications including switchable molecular separations [107], controlled drug delivery systems [41], chemical and bio-sensing [108].

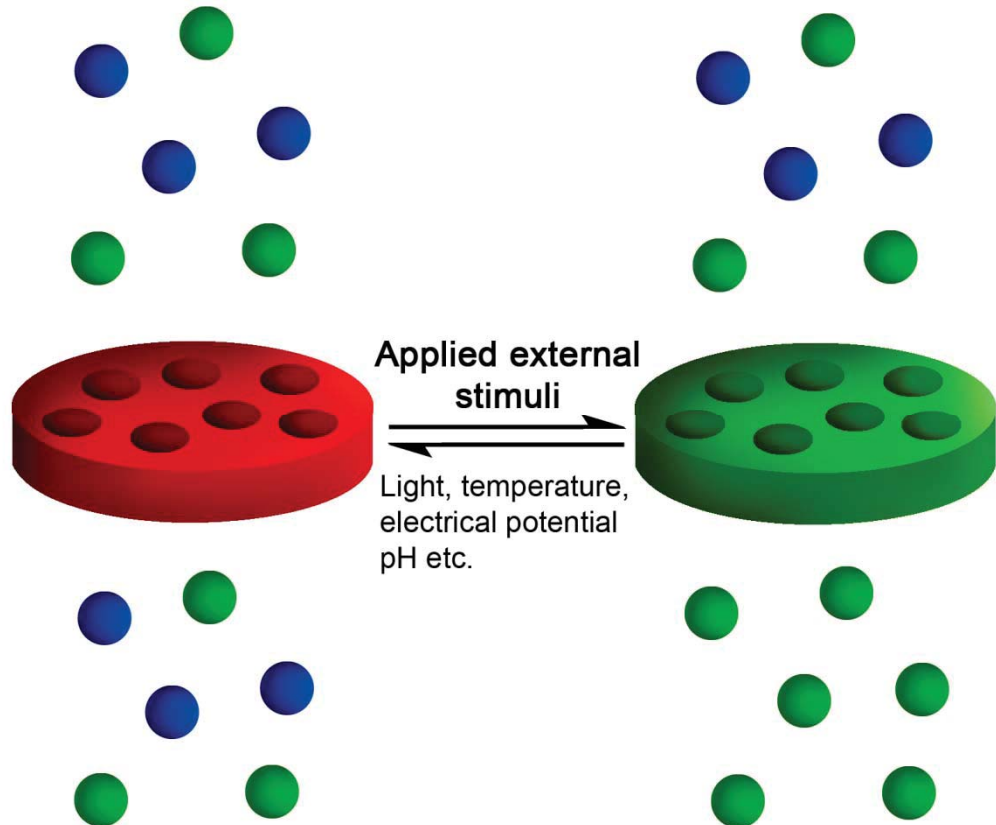


Figure 1-15 Schematic of the reversible change in membrane properties due to applied external stimuli.

Stimuli responsive membranes have been devised which can regulate the size of the pore in order to mimic biological membranes. These membranes are achieved by grafting responsive polymers which can undergo a definitive transformation in their structure or volume directly onto existing porous materials [4]. Amongst the external stimuli outlined, temperature responsive films are the most easily fabricated and controlled, therefore much research has focussed on thermo responsive membranes [107, 109-110]. These thermo responsive films include polymers such as poly(*N*-isopropylacrylamide) (PNIPAAM). At temperatures below the lower critical solution temperature (LCST), which is 32 °C in the case of PNIPAAM, the layer is extended thus blocking the pores and inhibiting the transport of molecules (Figure 1-16). At temperatures higher than the LCST of PNIPAAM the layer is collapsed thus allowing molecules to diffuse across the membrane. Therefore PNIPAAM grafted

onto porous membranes can serve as a gate capable of regulating the transport of solutes across the membrane [107, 110].

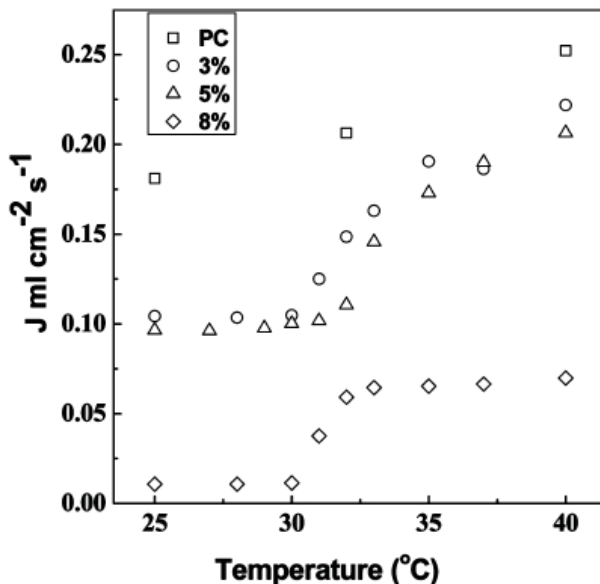


Figure 1-16 Temperature dependent water flux of pristine PC membranes and PNIPAAM modified PC membranes with different monomer concentrations [110].

Electrically responsive membranes can be achieved through modification of membranes with polymers which respond to electrical stimuli such as polypyrrole [41, 111]. Polypyrrole has been widely used to modify porous materials due to its ability to expand and contract upon applied electrical stimulus. The modulation of the pore size is realised by changing the electrochemical state of the polypyrrole layer. Doktycz and co-workers developed a polypyrrole modified vertically aligned carbon nanofiber membrane in which the controlled swelling of the polypyrrole film resulted in a reduction or expansion of the interspacing between the nanofibers thus modulating the size selective transport through the interfiber spacing [112]. Kim and co-workers demonstrated the utilisation of a polypyrrole modified PA membranes for controlled drug release [41]. These membranes exhibited quick response times to the applied stimuli with steady drug flow rates thus providing accurate dosage control.

Self assembled monolayers also present a favourable route for the fabrication of responsive membranes. As outlined in section 1.6.2, Martin and co-workers have demonstrated that modification of the membranes by SAMs containing carboxy-terminal groups produce membranes where the ionic flux can be controlled by the pH

value [19]. However, there are countless stimuli responsive SAMs which have been devised on planar surfaces which are yet to be applied in membrane technology. Through expanding responsive membrane technology, highly sophisticated separations can be achieved.

1.8. THESIS OUTLINE

This thesis presents an approach for tailoring porous materials with surface functionalities to provide controlled transport properties. Emerging research in membrane technology involves the development of new membrane materials capable of performing highly controlled molecular separations. In order to obtain these materials porous membranes will need to be fabricated with controllable structures and surface chemistry. Consequently the studies in this thesis implement membrane materials with ordered pore architectures such as polycarbonate and porous alumina membranes. Sophisticated tailored surfaces are especially important in biomedical applications where the manipulation of biomaterial – membrane interactions requires utmost control. The development of intelligent membranes capable of responding to external stimuli and specific molecular interactions and recognition are crucial in the biomedical industry. However, membrane technology in this area is undeveloped and requires further exploration into the construction of sophisticated membrane modifications. Therefore the main objective of this thesis is to explore the effects of immobilising various surface functional layers onto membrane materials. This is achieved through the fabrication, modification and characterisation of nanotechnology based membrane materials.

Chapter 3 presents the characterisation and confirmation of SAM assembly within gold coated alumina membranes. Identification of the coverage and reproducibility of SAMs within porous matrices is of utmost importance in the design of filtration membranes and sensing platforms. Whilst enormous effort has been made to investigate and characterise SAMs on planar surfaces, the characterisation of SAMs within restricted spaces such as pores is poorly understood and difficult to probe. The surface enhanced Raman scattering (SERS) effect was employed in order to confirm and characterise the deposition of 4-mercaptopbenzoic acid (MBA) within gold coated

alumina membranes. The SERS effect allows very low concentrations or even single molecules to be detected when they are adsorbed onto roughened metal surfaces such as gold, silver and copper. Mapping techniques were used to characterise the distribution of MBA assembly within the pores.

Chapter 4 describes the modification of gold coated polycarbonate membranes with the highly hydrophobic thiol (perfluorodecanethiol, PFDT), to impart chemical sensitivity towards hydrophobic and hydrophilic molecules. Thiol chemistry is seldom used in commercial devices due to concerns over their durability and stability. SAMs of fluorinated thiols present a promising alternative. SAMs made from fluorinated thiols produce an extremely low surface energy and highly hydrophobic surface which are found to be robust and relatively defect free. To determine the effectiveness and stability of membranes modified with fluorinated SAMs, comparative studies were carried out using a non-fluorinated alkanethiol of comparable chain length (decanethiol, DT). The selectivity of these membranes towards hydrophobic and hydrophilic organic molecules was explored.

Chapter 5 investigates several hybrid membrane structures based on polycarbonate membranes where gold is deposited on different areas on the membrane; on one of the membrane interfaces, within the pores of the membrane and completely coating all surfaces of the membrane. Gold-thiol chemistry was exploited in which the thiols only assembled on the gold coated regions of the membrane thus providing controlled positioning of functional regions. The highly hydrophobic thiol, PFDT, was used to modify the membranes. The effects of the controlled positioning of functional groups on the transport properties of the membrane were investigated by analysing the transport of hydrophilic and hydrophobic dyes across the membranes. Such studies are important to give insight into how surface modifications may impact the transport properties of porous membranes in order to devise more efficient separation processes.

Chapter 6 presents the atomic layer deposition (ALD) of silica onto porous alumina (PA) membranes with the aim of fine-tuning pore diameters. Chemical functionalisation of silica coated PA membranes with perfluorodecyldimethylchlorosilane (PFDS) imparted hydrophobic chemical

selectivity to the silica modified PA membranes. The transport properties and selectivity of PFDS modified silica-PA membranes towards hydrophobic and hydrophilic organic molecules was explored.

Chapter 7 characterises the selective onset of forward osmosis across silica modified alumina membranes. In this study we observe the onset of forward osmosis only when particular solutes are used in the draw solution. A set of dyes of differing size, charge and hydrophobicity were used as draw solutes in order to investigate the effects of draw solution solute on the water transport ability. The possible mechanisms behind this discriminatory water transport were explored.

Chapter 8 presents a switchable separation process developed using stimuli responsive surface modifications. The transport properties of gold coated PA membranes were controlled through the reversible switching of adsorbed fluorinated azobenzene layers. A conformational change occurs in the azobenzene unit when illuminated with UV or visible light. Depending on the wavelength of irradiation, the molecule can switch between its *trans* and *cis* state. A transition to the *cis* state essentially buries the end functionality of the assembled molecule. The azobenzene used in this study contains a hydrophobic fluorinated end group and hence produces a transition between hydrophobic and less hydrophobic surface properties when photoisomerisation from the *trans* to the *cis* state occurs. The photoresponsive characteristics of these azobenzene modified membranes were examined through the switchable transport of a hydrophilic probe dye across the membrane.

Chapter 9 presents concluding remarks and the future direction for novel membrane development based on the approaches explored in this thesis.

1.9. REFERENCES

1. Jirage, K.B., Hulteen, J.C., and Martin, C.R., *Effect of thiol chemisorption on the transport properties of gold nanotubule membranes.* Analytical Chemistry, 1999. **71**(21): p. 4913-4918.
2. Jirage, K.B., Hulteen, J.C., Martin, C.R., *Nanotubule-Based Molecular-Filtration Membranes.* Science, 1997. **278**: p. 655-658.
3. Han, J.Y., Fu, J.P., and Schoch, R.B., *Molecular sieving using nanofilters: Past, present and future.* Lab on a Chip, 2008. **8**(1): p. 23-33.
4. Kleps, I., Miu, M., Simion, M., Ignat, T., Bragaru, A., Craciunoiu, F., and Danila, M., *Study of the Micro- and Nanostructured Silicon for Biosensing and Medical Applications.* Journal of Biomedical Nanotechnology, 2009. **5**(3): p. 300-309.
5. Adiga, S.P., Curtiss, L.A., Elam, J.W., Pellin, M.J., Shih, C.C., Shih, C.M., Lin, S.J., Su, Y.Y., Gittard, S.A., Zhang, J., and Narayan, R.J., *Nanoporous materials for biomedical devices.* Jom, 2008. **60**(3): p. 26-32.
6. Losic, D. and Simovic, S., *Self-ordered nanopore and nanotube platforms for drug delivery applications.* Expert Opinion on Drug Delivery, 2009. **6**(12): p. 1363-1381.
7. Hillebrenner, H., Buyukserin, F., Stewart, J.D., and Martin, C.R., *Template synthesized nanotubes for biomedical delivery applications.* Nanomedicine, 2006. **1**(1): p. 39-50.
8. Vandevivere, P.C., Bianchi, R., and Verstraete, W., *Treatment and reuse of wastewater from the textile wet-processing industry: Review of emerging technologies.* Journal of Chemical Technology and Biotechnology, 1998. **72**(4): p. 289-302.
9. Duke, M.C., Mee, S., and da Costa, J.C.D., *Performance of porous inorganic membranes in non-osmotic desalination.* Water Research, 2007. **41**(17): p. 3998-4004.
10. Shannon, M.A., Bohn, P.W., Elimelech, M., Georgiadis, J.G., Marinas, B.J., and Mayes, A.M., *Science and technology for water purification in the coming decades.* Nature, 2008. **452**(7185): p. 301-310.

11. Velleman, L., Shapter, J.G., and Losic, D., *Gold nanotube membranes functionalised with fluorinated thiols for selective molecular transport*. Journal of Membrane Science, 2008. **328**: p. 121-126.
12. Velleman, L., Shearer, C.J., Ellis, A.V., Losic, D., Voelcker, N.H., and Shapter, J.G., *Fabrication of self-supporting porous silicon membranes and tuning transport properties by surface functionalization*. Nanoscale, 2010. **2**(9): p. 1756-1761.
13. Yang, B. and Yang, W.T., *Novel pore-covering membrane as a full open/close valve*. Journal of Membrane Science, 2005. **258**(1-2): p. 133-139.
14. Martin, C.R., Nishizawa, M., Jirage, K., Kang, M.S., and Lee, S.B., *Controlling ion-transport selectivity in gold nanotubule membranes*. Advanced Materials, 2001. **13**(18): p. 1351-1362.
15. Nishizawa, M., Menon, V.P., and Martin, C.R., *Metal Nanotubule Membranes with Electrochemically Switchable Ion-Transport Selectivity*. Science, 1995. **268**: p. 700-702.
16. Casasus, R., Marcos, M.D., Martinez-Manez, R., Ros-Lis, J.V., Soto, J., Villaescusa, L.A., Amoros, P., Beltran, D., Guillem, C., and Latorre, J., *Toward the development of ionically controlled nanoscopic molecular gates*. Journal of the American Chemical Society, 2004. **126**(28): p. 8612-8613.
17. Critchley, K., Jeyadevan, J.P., Fukushima, H., Ishida, M., Shimoda, T., Bushby, R.J., and Evans, S.D., *A mild photoactivated hydrophilic/hydrophobic switch*. Langmuir, 2005. **21**(10): p. 4554-4561.
18. Lim, H.S., Han, J.T., Kwak, D., Jin, M.H., and Cho, K., *Photoreversibly switchable superhydrophobic surface with erasable and rewritable pattern*. Journal of the American Chemical Society, 2006. **128**(45): p. 14458-14459.
19. Lee, S.B. and Martin, C.R., *pH-switchable, ion-permselective gold nanotubule membrane based on chemisorbed cysteine*. Analytical Chemistry, 2001. **73**(4): p. 768-775.
20. Liu, D.B., Xie, Y.Y., Shao, H.W., and Jiang, X.Y., *Using Azobenzene-Embedded Self-Assembled Monolayers To Photochemically Control Cell Adhesion Reversibly*. Angewandte Chemie-International Edition, 2009. **48**(24): p. 4406-4408.

21. Liu, Y., Mu, L., Liu, B.H., Zhang, S., Yang, P.Y., and Kong, J.L., *Controlled protein assembly on a switchable surface*. Chemical Communications, 2004(10): p. 1194-1195.
22. Mu, L., Liu, Y., Zhang, S., Liu, B.H., and Kong, J., *Selective assembly of specifically charged proteins on an electrochemically switched surface*. New Journal of Chemistry, 2005. **29**(6): p. 847-852.
23. Zareie, H.M., Boyer, C., Bulmus, V., Nateghi, E., and Davis, T.P., *Temperature-responsive self-assembled monolayers of oligo(ethylene glycol): Control of biomolecular recognition*. Acs Nano, 2008. **2**(4): p. 757-765.
24. Schneider, J.J. and Engstler, J., *Carbon and polymer filaments in nanoporous alumina*. European Journal of Inorganic Chemistry, 2006(9): p. 1723-1736.
25. Yamaguchi, A., Uejo, F., Yoda, T., Uchida, T., Tanamura, Y., Yamashita, T., and Teramae, N., *Self-assembly of a silica–surfactant nanocomposite in a porous alumina membrane*. nature materials, 2004. **3**: p. 337-341.
26. Steinhart, M., Wehrspohn, R.B., Gosele, U., and Wendorff, J.H., *Nanotubes by Template Wetting: A Modular Assembly System*. Angewandte Chemie-International Edition, 2004. **43**: p. 1334 – 1344.
27. Martin, C.R. and Kohli, P., *The emerging field of nanotube biotechnology*. Nature Reviews Drug Discovery, 2003. **2**(1): p. 29-37.
28. De Leo, M., Pereira, F.C., Moretto, L.M., Scopece, P., Polizzi, S., and Ugo, P., *Towards a better understanding of gold electroless deposition in track-etched templates*. Chemistry of Materials, 2007. **19**(24): p. 5955-5964.
29. Menon, V.P., and Martin, C.R., *Fabrication and Evaluation of Nanoelectrode Ensembles*. Analytical Chemistry, 1995. **67**: p. 1920- 1928.
30. Wirtz, M., Parker, M., Kobayashi, Y., and Martin, C.R., *Template-synthesized nanotubes for chemical separations and analysis*. Chemistry-a European Journal, 2002. **8**(16): p. 3573-3578.
31. Gyurcsanyi, R.E., Vigassy, T., and Pretsch, E., *Biorecognition-modulated ion fluxes through functionalized gold nanotubules as a novel label-free biosensing approach*. Chemical Communications, 2003(20): p. 2560-2561.
32. Lee, S.B., and Martin, C.R., *Electromodulated Molecular Transport in Gold-Nanotube Membranes*. Journal of the American Chemical Society, 2002. **124**: p. 11850-11851.

33. Kobayashi, Y. and Martin, C.R., *Highly sensitive methods for electroanalytical chemistry based on nanotubule membranes*. Analytical Chemistry, 1999. **71**(17): p. 3665-3672.
34. Chun, K.Y., and Stroeve, P., *Protein Transport in Nanoporous Membranes Modified with Self-Assembled Monolayers of Functionalized Thiols*. Langmuir, 2002. **18**: p. 4653-4658.
35. Hou, Z., Abbott, N.L., and Stroeve, P., *Self-Assembled Monolayers on Electroless Gold Impart pH-Responsive Transport of Ions in Porous Membranes*. Langmuir, 2000. **16**: p. 2401-2404.
36. Kohli, P., Wirtz, M., and Martin, C.R., *Nanotube membrane based biosensors*. Electroanalysis, 2004. **16**(1-2): p. 9-18.
37. Huang, S.S., Sheng, C., Yin, Z.F., Shen, J., Li, R.N., and Peng, B., *Immunoreaction-based separation of antibodies using gold nanotubules membrane*. Journal of Membrane Science, 2007. **305**(1-2): p. 257-262.
38. Hatori, H., Takagi, H., and Yamada, Y., *Gas separation properties of molecular sieving carbon membranes with nanopore channels*. Carbon, 2004. **42**(5-6): p. 1169-1173.
39. Ritchie, S.M.C., Kissick, K.E., Bachas, L.G., Sikdar, S.K., Parikh, C., and Bhattacharyya, D., *Polycysteine and other polyamino acid functionalized microfiltration membranes for heavy metal capture*. Environmental Science & Technology, 2001. **35**(15): p. 3252-3258.
40. Yamashita, T., Kodama, S., Ohto, M., Nakayama, E., Hasegawa, S., Takayanagi, N., Kemmei, T., Yamaguchi, A., Teramae, N., and Saito, Y., *Permeation flux of organic molecules through silica-surfactant nanochannels in a porous alumina membrane*. Analytical Sciences, 2006. **22**(12): p. 1495-1500.
41. Jeon, G., Yang, S.Y., Byun, J., and Kim, J.K., *Electrically Actuated Smart Nanoporous Membrane for Pulsatile Drug Release*. Nanoletters, 2011.
42. Baker, L.A., Jin, P., and Martin, C.R., *Biomaterials and biotechnologies based on nanotube membranes*. Critical Reviews in Solid State and Materials Sciences, 2005. **30**(4): p. 183-205.
43. Yu, S.F., Lee, S.B., Kang, M., and Martin, C.R., *Size-based protein separations in poly(ethylene glycol)-derivatized gold nanotubule membranes*. Nano Letters, 2001. **1**(9): p. 495-498.

44. de Lint, W.B.S., Biesheuvel, P.M., and Verweij, H., *Application of the charge regulation model to transport of ions through hydrophilic membranes: One-dimensional transport model for narrow pores (nanofiltration)*. Journal of Colloid and Interface Science, 2002. **251**(1): p. 131-142.
45. Miller, S.A., Young, V.Y., and Martin, C.R., *Electroosmotic flow in template-prepared carbon nanotube membranes*. Journal of the American Chemical Society, 2001. **123**(49): p. 12335-12342.
46. Yuan, H., Cheow, P.S., Ong, J., and Toh, C.S., *Characterization of the electrophoretic mobility of gold nanoparticles with different sizes using the nanoporous alumina membrane system*. Sensors and Actuators B-Chemical, 2008. **134**(1): p. 127-132.
47. Wang, S.N.A., Hua, X., and Lee, L.J., *Electrokinetics induced asymmetric transport in polymeric nanonozzles*. Lab on a Chip, 2008. **8**(4): p. 573-581.
48. Drioli, E. and Giorno, L., *Membrane Operations: Innovative Separations and Transformations*. 2009: Wiley-VCH.
49. Baker, R., *Membrane Technology and Applications*. 2004: Wiley.
50. Rao, S.M. and Zydny, A.L., *High resolution protein separations using affinity ultrafiltration with small charged ligands*. Journal of Membrane Science, 2006. **280**(1-2): p. 781-789.
51. Fissell, W.H., Fleischman, A.J., Humes, H.D., and Roy, S., *Development of continuous implantable renal replacement: past and future*. Translational Research, 2007. **150**(6): p. 327-336.
52. Thombre, A.G., Cardinal, J.R., DeNoto, A.R., and Gibbes, D.C., *Asymmetric membrane capsules for osmotic drug delivery - II. In vitro and in vivo drug release performance*. Journal of Controlled Release, 1999. **57**(1): p. 65-73.
53. Sun, W., Puzas, J.E., Sheu, T.J., Liu, X., and Fauchet, P.M., *Nano- to microscale porous silicon as a cell interface for bone-tissue engineering*. Advanced Materials, 2007. **19**(7): p. 921-+.
54. Fissell, W.H., Humes, H.D., Fleischman, A.J., and Roy, S., *Dialysis and nanotechnology: Now, 10 years, or never?* Blood Purification, 2007. **25**(1): p. 12-17.
55. Motomura, T., Maeda, T., Kawahito, S., Matsui, T., Ichikawa, S., Ishitoya, H., Kawamura, M., Nishimura, I., Shinohara, T., Oestmann, D., Glueck, J., Kawaguchi, Y., Sato, K., and Nose, Y., *Extracorporeal membrane*

- oxygenerator compatible with centrifugal blood pumps.* Artificial Organs, 2002. **26**(11): p. 952-958.
56. Lewinska, D., Piatkiewicz, W., and Rosinski, S., *Pectin coated hollow fiber polypropylene membranes.* International Journal of Artificial Organs, 1997. **20**(11): p. 650-655.
57. Borra, M., Galavotti, D., Bellini, C., Fumi, L., Morsiani, E., and Bellini, G., *Advanced technology for extracorporeal liver support system devices.* International Journal of Artificial Organs, 2002. **25**(10): p. 939-949.
58. Swan, E.E.L., Popat, K.C., and Desai, T.A., *Peptide-immobilized nanoporous alumina membranes for enhanced osteoblast adhesion.* Biomaterials, 2005. **26**(14): p. 1969-1976.
59. Lu, G.Q. and Zhao, X.S., *Nanoporous Materials: Science and Engineering.* Series on Chemical Engineering. Vol. 4. 2004: Imperial College Press.
60. Frisch, H.L. and Mark, J.E., *Nanocomposites prepared by threading polymer chains through zeolites, mesoporous silica, or silica nanotubes.* Chemistry of Materials, 1996. **8**(8): p. 1735-1738.
61. Sasaki, T., Nagaoka, S., Tezuka, T., Suzuki, Y., Iwaki, M., and Kawakami, H., *Preparation of novel organic-inorganic nanoporous membranes.* Polym. Adv. Technol., 2005. **16**: p. 698–701.
62. Fick, A., *Poggendorff's Annel. Physik*, 1855. **94**: p. 59-86.
63. Cussler, E.L., *Diffusion: Mass transfer in fluid systems.* Third Edition ed. 2009: Cambridge University Press.
64. Wijmans, J.G. and Baker, R.W., *The solution-diffusion model - a review.* Journal of Membrane Science, 1995. **107**(1-2): p. 1-21.
65. Goodman, S.R., *Medical Cell Biology.* 3rd ed. 2008: Academic Press.
66. Johnson, L.R., *Essential medical physiology.* Third Edition ed. 2003: Elsevier.
67. Ulbricht, M., *Advanced functional polymer membranes.* Polymer, 2006. **47**: p. 2217–2262.
68. Tsuru, T., *Nano/subnano-tuning of porous ceramic membranes for molecular separation.* Journal of Sol-Gel Science and Technology, 2008. **46**(3): p. 349-361.
69. Whatman. *Nuclepore membranes: Typical data.* 2007.

70. Orelovich, O.L., and Apel, P.Y., *Methods for Preparing Samples of Track Membranes for Scanning Electron Microscopy*. Instruments and Experimental Techniques, 2001. **44**(1): p. 111-114.
71. Apel, P.Y., Blonskaya, I.V., Dmitriev, S.N., Orelovitch, O.L., and Sartowska, B., *Structure of polycarbonate track-etch membranes: Origin of the “paradoxical” pore shape*. Journal of Membrane Science, 2006. **282**: p. 393–400.
72. Gilliam, R.J., Thorpe, S.J., and Kirk, D.W., *A nucleation and growth study of gold nanowires and nanotubes in polymeric membranes*. Journal of Applied Electrochemistry, 2007. **37**(2): p. 233-239.
73. Shao, P., Ji, G., and Chen, P., *Gold nanotube membranes: Preparation, characterization and application for enantioseparation*. Journal of Membrane Science, 2005. **255**: p. 1–11.
74. Losic, D. and Lillo, M., *Porous Alumina with Shaped Pore Geometries and Complex Pore Architectures Fabricated by Cyclic Anodization*. Small, 2009. **5**(12): p. 1392-1397.
75. Kirchner, A., MacKenzie, K.J.D., Brown, I.W.M., Kemmitt, T., and Bowden, M.E., *Structural characterisation of heat-treated anodic alumina membranes prepared using a simplified fabrication process*. Journal of Membrane Science, 2007. **287**(2): p. 264-270.
76. Velleman, L., Triani, G., Evans, P.J., Shapter, J.G., and Losic, D., *Structural and chemical modification of porous alumina membranes*. Microporous and Mesoporous Materials, 2009. **126**(1-2): p. 87-94.
77. Kohli, P., Wharton, J.E., Braide, O., and Martin, C.R., *Template synthesis of gold nanotubes in an anodic alumina membrane*. Journal of Nanoscience and Nanotechnology, 2004. **4**(6): p. 605-610.
78. Bogart, T.E., Dey, S., Lew, K.K., Mohney, S.E., and Redwing, J.M., *Diameter-controlled synthesis of silicon nanowires using nanoporous alumina membranes*. Advanced Materials, 2005. **17**(1): p. 114-+.
79. Rahman, S. and Yang, H., *Nanopillar arrays of glassy carbon by anodic aluminum oxide nanoporous templates*. Nano Letters, 2003. **3**(4): p. 439-442.
80. Ding, G.Q., Zheng, M.J., Xu, W.L., and Shen, W.Z., *Fabrication of controllable free-standing ultrathin porous alumina membranes*. Nanotechnology, 2005. **16**(8): p. 1285-1289.

81. Diggle, J.W., Downie, T.C., and Goulding, C.W., *Anodic oxide films on Aluminium*. Chemical Reviews, 1969. **69**: p. 365.
82. Thompson, G.E., *Porous anodic alumina: Fabrication, characterization and applications*. Thin Solid Films, 1997. **297**(1-2): p. 192-201.
83. Masuda, H. and Fukuda, K., *Ordered metal nanohole arrays made by a 2-step replication of honeycomb structures of anodic alumina*. Science, 1995. **268**(5216): p. 1466-1468.
84. Huczko, A., *Template-based synthesis of nanomaterials*. Applied Physics a-Materials Science & Processing, 2000. **70**(4): p. 365-376.
85. Love, J.C., Estroff, L.A., Kriebel, J.K., Nuzzo, R.G., and Whitesides, G.M., *Self-assembled monolayers of thiolates on metals as a form of nanotechnology*. Chemical Reviews, 2005. **105**(4): p. 1103-1169.
86. Blake, P., Ahn, W., and Roper, D.K., *Enhanced Uniformity in Arrays of Electroless Plated Spherical Gold Nanoparticles Using Tin Presensitization*. Langmuir, 2010. **26**(3): p. 1533-1538.
87. Kobayashi, Y., Tadaki, Y., Nagao, D., and Konno, M., *Deposition of gold nanoparticles on silica spheres by electroless metal plating technique*. Journal of Colloid and Interface Science, 2005. **283**(2): p. 601-604.
88. Sanchez-Castillo, M.A., Couto, C., Kim, W.B., and Dumesic, J.A., *Gold-nanotube membranes for the oxidation of CO at gas-water interfaces*. Angewandte Chemie-International Edition, 2004. **43**(9): p. 1140-1142.
89. De Leo, M., Kuhn, A., and Ugo, P., *3D-ensembles of gold nanowires: Preparation, characterization and electroanalytical peculiarities*. Electroanalysis, 2007. **19**(2-3): p. 227-236.
90. Pereira, F.C., Moretto, L.M., De Leo, M., Zanoni, M.V.B., and Ugo, P., *Gold nanoelectrode ensembles for direct trace electroanalysis of iodide*. Analytica Chimica Acta, 2006. **575**(1): p. 16-24.
91. Demoustier-Champagne, S., and Delvaux, M., *Preparation of polymeric and metallic nanostructures using a template-based deposition method*. Materials Science and Engineering C, 2001. **15**: p. 269–271.
92. Hulteen, J.C., Jirage, K.B., and Martin, C.R., *Introducing Chemical Transport Selectivity into Gold Nanotubule Membranes*. Journal of the American Chemical Society, 1998. **120**: p. 6603-6604.

93. Majumder, M., Chopra, N., and Hinds, B.J., *Effect of tip functionalization on transport through vertically oriented carbon nanotube membranes*. Journal of the American Chemical Society, 2005. **127**(25): p. 9062-9070.
94. Ulbricht, M., Matuszewski, H., Oechel, A., and Hicke, H.G., *Photo-induced graft polymerization surface modifications for the preparation of hydrophilic and low-protein-adsorbing ultrafiltration membranes*. Journal of Membrane Science, 1996. **115**(1): p. 31-47.
95. Popat, K.C., Mor, G., Grimes, C.A., and Desai, T.A., *Surface modification of nanoporous alumina surfaces with poly(ethylene glycol)*. Langmuir, 2004. **20**(19): p. 8035-8041.
96. Sagle, A.C., Van Wagner, E.M., Ju, H., McCloskey, B.D., Freeman, B.D., and Sharma, M.M., *PEG-coated reverse osmosis membranes: Desalination properties and fouling resistance*. Journal of Membrane Science, 2009. **340**(1-2): p. 92-108.
97. Bain, C.D., Biebuyck, H.A., and Whitesides, G.M., *Comparison of Self - Assembled Monolayers on Gold: Coadsorption of Thiols and Disulfides*. Langmuir, 1989. **5**: p. 723-727.
98. Bain, C.D., Troughton, E.B., Tao, Y-T., Whitesides, G.M., and Nuzzo, R.G., *Formation of Monolayer Films by the Spontaneous Assembly of Organic Thiols from Solution onto Gold*. Journal of the American Chemical Society, 1989. **111**: p. 321-335.
99. Chechik, V. and Stirling, C., *Gold-thiol self-assembled monolayers*, in *The chemistry of organic derivatives of gold and silver*, S. Patai and Z. Rappoport, Editors. 1999, John Wiley & Sons Ltd.
100. Martin, C.R., Nishizawa, M., Jirage, K., and Kang, M., *Investigations of the Transport Properties of Gold Nanotubule Membranes*. Journal of Physical Chemistry B, 2001. **105**: p. 1925-1934.
101. Chun, K.Y., and Stroeve, P., *External Control of Ion Transport in Nanoporous Membranes with Surfaces Modified with Self-Assembled Monolayers*. Langmuir, 2001. **17**: p. 5271-5275.
102. Browne, W.R. and Feringa, B.L., *Light Switching of Molecules on Surfaces*. Annual Review of Physical Chemistry, 2009. **60**: p. 407-428.

103. Mu, L., Liu, Y., Cai, S.Y., and Kong, J.L., *A smart surface in a microfluidic chip for controlled protein separation*. Chemistry-a European Journal, 2007. **13**(18): p. 5113-5120.
104. Schmuhl, R., van den Berg, A., Blank, D.H.A., and ten Elshof, J.E., *Surfactant-modulated switching of molecular transport in nanometer-sized pores of membrane gates*. Angewandte Chemie-International Edition, 2006. **45**(20): p. 3341-3345.
105. Liu, Y.L., Zhao, M.Q., Bergbreiter, D.E., and Crooks, R.M., *pH-switchable, ultrathin permselective membranes prepared from multilayer polymer composites*. Journal of the American Chemical Society, 1997. **119**(37): p. 8720-8721.
106. Ku, J.R., Lai, S.M., Ilieri, N., Ramirez, P., Mafe, S., and Stroeve, P., *pH and ionic strength effects on amino acid transport through Au-nanotubule membranes charged with self-assembled monolayers*. Journal of Physical Chemistry C, 2007. **111**(7): p. 2965-2973.
107. Ulbricht, M., Ozdemir, S., and Geissmann, C., *Functionalized track-etched membranes as versatile tool to investigate stimuli-responsive polymers for "smart" nano- and microsystems*. Desalination, 2006. **199**(1-3): p. 150-152.
108. Tokarev, I., Gopishetty, V., Zhou, J., Pita, M., Motornov, M., Katz, E., and Minko, S., *Stimuli-Responsive Hydrogel Membranes Coupled with Biocatalytic Processes*. Acs Applied Materials & Interfaces, 2009. **1**(3): p. 532-536.
109. Yoshida, M., Nagaoka, N., Asano, M., Omichi, H., Kubota, H., Ogura, K., Vetter, J., Spohr, R., and Katakai, R., *Reversible on-off switch function of ion-track pores for thermo-responsive films based on copolymers consisting of diethyleneglycol-bis-allylcarbonate and acryloyl-L-proline methyl ester*. Nuclear Instruments & Methods in Physics Research Section B-Beam Interactions with Materials and Atoms, 1997. **122**(1): p. 39-44.
110. Wang, W.C., Tian, X.D., Feng, Y.P., Cao, B., Yang, W.T., and Zhang, L.Q., *Thermally On-Off Switching Membranes Prepared by Pore-Filling Poly(N-isopropylacrylamide) Hydrogels*. Industrial & Engineering Chemistry Research, 2010. **49**(4): p. 1684-1690.
111. Abidian, M.R., Kim, D.H., and Martin, D.C., *Conducting-polymer nanotubes for controlled drug release*. Advanced Materials, 2006. **18**(4): p. 405-+.

112. Fletcher, B.L., Retterer, S.T., McKnight, T.E., Melechko, A.V., Fowlkes, J.D., Simpson, M.L., and Doktycz, M.J., *Actuatable membranes based on polypyrrole-coated vertically aligned carbon nanofibers*. Acs Nano, 2008. **2**(2): p. 247-254.

CHAPTER 2

EXPERIMENTAL DETAILS

2.1. MEMBRANE FABRICATION

2.1.1. *Fabrication of porous alumina (PA) membranes*

Aluminium foil (99.997 %, Alfa Aesar, USA) was cleaned in acetone with the aid of sonication. Two-step anodisation was performed (Figure 2-1) using an electrochemical cell equipped with a cooling stage set to a temperature of -1°C . The first anodisation step was performed at 60 - 80 V for 5-10 min in 0.3 M oxalic acid. Afterwards, the formed porous oxide film was chemically removed using a mixture of 6 wt% of H_3PO_4 and 1.8% chromic acid for a minimum of 3 h at 75°C . A second anodisation was performed at 80 V for 15 min in 0.3 M oxalic acid (-1°C) to achieve PA membranes with thicknesses of 20 – 30 μm . The aluminium was then removed by immersion in a CuCl_2/HCl solution leaving the PA membrane behind. The barrier oxide layer at the bottom face of the membrane was removed by immersion in 10 wt% H_3PO_4 for 3 h. This process opens the pores to create open channels in the membrane. During the barrier oxide removal, the top face of the PA membrane was protected by masking with nail polish. After pore opening the nail polish was removed by rinsing with copious amounts of acetone.

2.1.2. *Fabrication of gold nanotube membranes*

Electroless deposition onto polycarbonate membranes The procedure for synthesising gold nanotube membranes by electroless gold deposition within porous templates has been previously described by Martin et al. [1]. Firstly, the membranes were immersed in methanol for 30 min to ensure complete wetting. In the first step, referred to as sensitisation, the membrane was immersed in a solution of 0.026 M SnCl_2 and 0.07 M trifluoroacetic acid (Sigma-Aldrich) in a solvent of 50:50 methanol:water for 45 min followed by rinsing in methanol for 5 min. This was followed by the second step, referred to as activation, where the membrane was immersed in a solution of 0.029 M ammoniacal AgNO_3 for 7.5 min. This solution was prepared by the dropwise addition of ammonium hydroxide to an aqueous solution of AgNO_3 (Proscitech, Australia) which turned turbid brown and was stopped once the solution turned clear. The membrane was then rinsed in methanol

for 5 min and immersed in water before placing the membranes in the gold deposition bath. In the third step, referred to as displacement

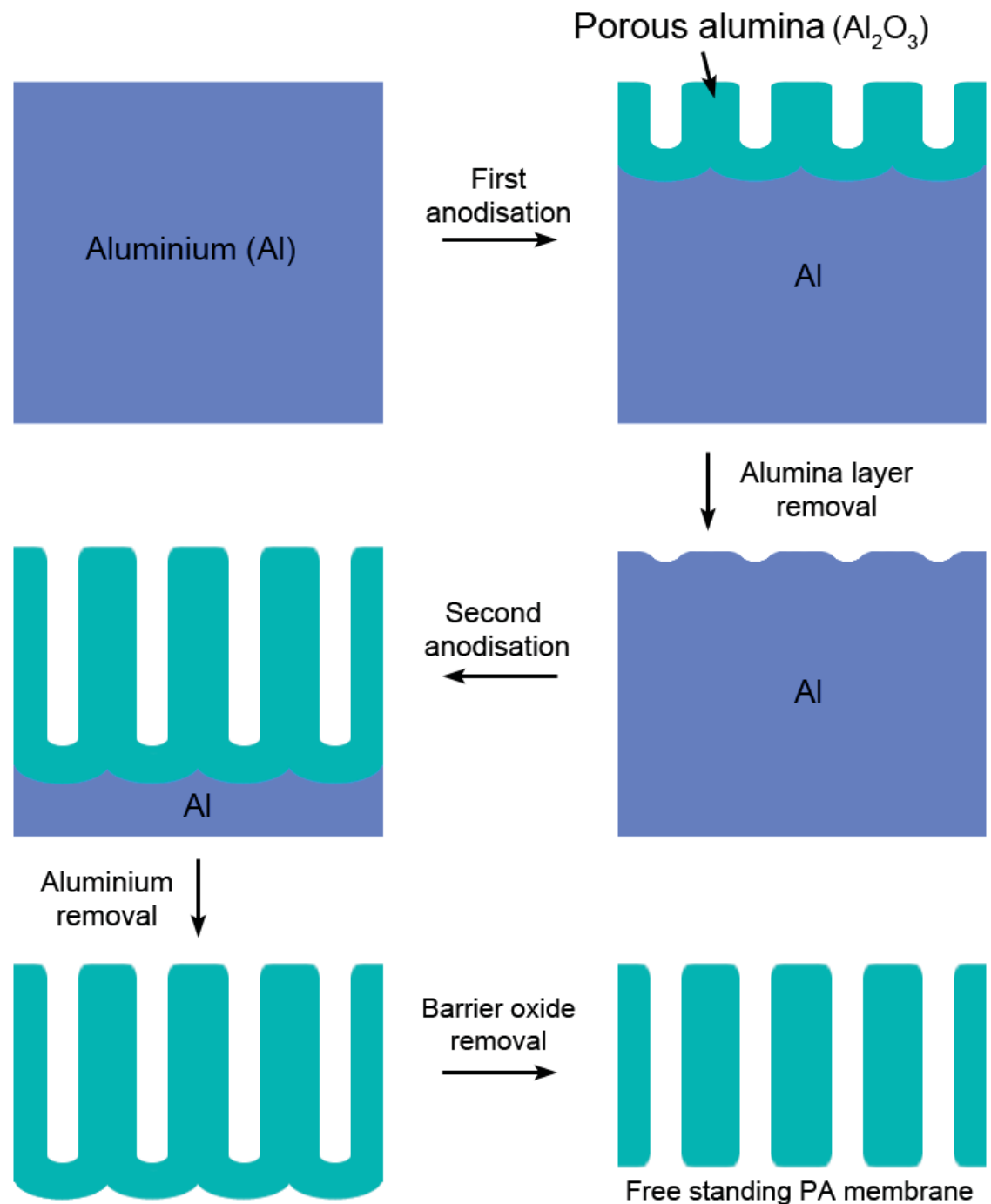


Figure 2-1 Cross sectional schematic of porous alumina fabrication.

deposition, the Ag coated membrane was immersed in the gold deposition solution consisting of 0.079 M $\text{Na}_3\text{Au}(\text{SO}_3)_2$ (Oromerse, Technic Inc. USA), 0.127 M Na_2SO_3 , 0.625 M formaldehyde and 0.025 M NaHCO_3 . The temperature of this bath

was ~ 1 - 4 °C with a pH of 8. The pH was adjusted to 8 through the drop wise addition of 1.8 M H₂SO₄. Gold deposition was allowed to proceed until the desired pore size was obtained. After gold deposition, the membrane was thoroughly rinsed in water and immersed in 25 % HNO₃ for at least 12 h to remove any residual Sn or Ag followed by rinsing in water and air-drying. The samples were flattened between glass slides and heat treated at 160 °C for 30 min then left to cool to room temperature.

2.1.2.1. Electroless deposition onto porous alumina membranes

The electroless deposition procedure for porous alumina is similar to that of polycarbonate with a few alterations. Firstly the porous alumina must be hydroxylated in order to allow for the chelation of tin onto the surface. This is achieved through boiling PA in hydrogen peroxide for 30 min. The membrane is then immersed in hot water for 15 min before placing in the tin sensitisation solution. The tin, silver and gold deposition steps proceed as usual. After gold deposition is completed the membranes are not exposed to nitric acid treatment as this will dissolve the membrane, instead the membranes are only rinsed in water and air-dried.

2.1.3. Fabrication of silica modified porous alumina membranes via atomic layer deposition

Commercial porous alumina membranes were used (Whatman Anodisc, UK) with pore diameters quoted as 20, 100 and 200 nm. The atomic layer deposition (ALD) precursors, tris(tert-butoxy)silanol (t-BuO)₂SiOH, 99.999% purity) and trimethyl aluminium (TMA, (99.9% purity)) were supplied by Sigma–Aldrich. Prior to ALD, membranes were repeatedly washed in ethanol followed by Milli Q water and dried with a nitrogen jet. ALD was carried out in a viscous flow-type reactor (ASM Microchemistry, F - 120) by collaborators from ANSTO, Sydney. To deposit SiO₂ by ALD the PA membranes were exposed to tri(tert-butoxy)silanol, and TMA as the precursor couple [2]. Clean PA membranes with different pore sizes (20, 100 and 200 nm), with the top side facing the flow of precursors, were placed in the chamber. The precursors were carried to the membrane by a flow of nitrogen gas, which was also used to purge the reactor between precursor pulses. The temperature of

deposition was 225 °C. The sequential pulse and purge regime was 1s/1s/5s/5s for the particular reaction sequence TMA/purge/(t-BuO)₂- SiOH/purge. SiO₂ thin-films were grown at 3, 5, 7, 10, 15 and 20 cycles in order to obtain conformal coatings with different thicknesses on the PA pores and hence reduce pore diameters. Silicon wafers were also coated with SiO₂ for reference purposes and the thicknesses of the deposited silica films were determined by spectroscopic ellipsometry (SOPRA GES5E). A growth rate of 2.5 – 3 nm/cycle was determined for the ALD process.

2.2. SURFACE FUNCTIONALISATION OF MEMBRANES

2.2.1. *Thiol functionalisation of gold coated membranes*

The thiol molecules; (1-decanethiol, 1H,1H,2H,2H-perfluorodecanethiol and cysteamine) were purchased from Sigma-Aldrich (Australia) and were used to create SAMs on the surfaces of the gold nanotube membranes. Prior to self assembly, the membrane was thoroughly rinsed in ethanol. The membranes were functionalised by immersion in a 3 mM solution of the thiol in ethanol for 24 h under nitrogen atmosphere, followed by rinsing in ethanol and water. The functionalised membranes were then stored in ethanol.

2.2.2. *Functionalisation of silica modified alumina membranes*

The surfaces of the SiO₂-PA membranes were hydroxylated under water plasma at a pressure of 0.2 atm for 1 min. The water plasma process forms OH groups over both SiO₂ and alumina surfaces [3-4]. The samples were then functionalised with the hydrophobic silane, perfluorodecyldimethylchlorosilane (PFDS, Gelest Inc.) by immersion in a 0.1 v % solution of the silane in dry toluene for 2 h under nitrogen atmosphere [4]. The silane reacts with the OH groups on the Al and Si surfaces to form a covalently bonded self assembled monolayer. The membrane was then thoroughly rinsed in dry toluene followed by dry dichloromethane and dried in air.

2.3. CHARACTERISATION OF MEMBRANES

2.3.1. *Scanning and transmission electron microscopy*

2.3.1.1. *SEM and TEM of gold coated polycarbonate membranes*

Scanning electron microscopy (SEM) and energy dispersive x-ray microscopy (EDAX) (Philips XL30) was used to characterise the deposition of gold onto the membranes. The membrane samples were cut into small pieces and mounted on a holder with double sided conductive tape. If required, the top and bottom gold surfaces of the membrane were removed by simply wiping the membrane with a cotton tip immediately after deposition, whilst the membrane was still wet. The gold nanotubes within the pores were liberated from the template support by immersion into dichloromethane resulting in a suspension of gold nanotubes. The suspension was deposited onto porous alumina or porous silicon substrates and rinsed with excess dichloromethane to ensure entire dissolution of the polycarbonate. For imaging uncoated polycarbonate membranes the samples were coated with ~ 5 nm of platinum (Quorumtech K757X sputter coater). Pore size distributions were measured using Adobe Photoshop CS5.

For transmission electron microscopy (TEM) (Philips CM100) analysis, cross sections of the gold coated membranes were obtained by microtoming resin encapsulated gold membranes. These cross sections were affixed onto copper TEM grids. The liberated gold nanotubes were also viewed via TEM by dropping the suspension of dichloromethane dissolved nanotubes onto TEM grids and allowing to air dry.

2.3.1.2. *SEM and TEM of gold coated porous alumina membranes*

Philips XL30 and the Helios Dualbeam Nanolab 600 scanning electron microscopes were used to view the porous alumina samples. Cross sections of the gold coated membranes were obtained by fracturing the membrane. In order to view the gold nanotubes formed within the pores, the PA template was removed by dissolution in 10 wt% H₃PO₄. Uncoated PA membranes were coated with 5 nm platinum

(Quorumtech K757X sputter coater). Pore size distributions were measured using Adobe Photoshop CS5.

2.3.1.3. SEM of silica modified alumina membranes

Surface characterisation of PA membranes before and after ALD silica deposition was performed using a SEM (Philips XL 30). The membrane samples were coated with a few nanometres of platinum. Images with a range of scan sizes and at normal incidence and at an angle of 40° were acquired to characterise the pore structures of silica coated PA membranes. Pore size distributions were determined from SEM images using image processing software (Image J, NIH, USA).

2.3.2. Dynamic secondary ion mass spectrometry (SIMS) and ellipsometry characterisation of silica coated PA membranes

Elemental depth profiles of selected ALD coated PA samples were obtained by dynamic SIMS using a Cameca ims 5f spectrometer by collaborators from ANSTO (Sydney). A Cs⁺ primary ion beam was rastered over an area of 50 μm x 50 μm was used for depth profiling. Secondary caesium cluster ions (MCs⁺) from a ~ 15 μm diameter central region of the sputtered crater were detected. Ion beam currents of 2 and 10 nA were used to sputter depth profile the SiO₂ surface film. Thickness measurements of ALD deposited silica films on silicon wafers used as controls were performed using a high resolution spectroscopic ellipsometer SOPRA GES5E (France). The measurements were carried out at a specific wavelength of ~ 600 nm as the angles of incidence and reflected light detection were varied between 40° and 85°. A series of samples fabricated using different deposition times were characterised to establish the deposition rate.

2.3.3. Electrochemical characterisation of gold nanotube membranes

Electrochemical characterisation of bare and modified gold nanotube membranes was performed using the electrochemical system CHI 600 (CH Instrument, USA). Current-voltage curves were recorded versus an Ag/AgCl saturated KCl reference

electrode and a Pt mesh auxiliary electrode. Electrochemical measurements were performed in U-tube permeation cell where the active area of electrode is defined using an O-ring pressed against the gold membrane. Electrolyte solutions were purged with argon for at least 30 minutes prior to measurements and blanketed in argon throughout the experiments. To assess the quality of thiol modified gold membranes two cyclic voltammetry (CV) measurements were performed using a redox probe (1 mM potassium ferricyanide), and electrochemical reduction of gold oxide (0.1 M sulphuric acid) [5-6]. Heterogeneous electron-transfer measurements for the assessment of the passivating ability of the films were conducted in 1 mM potassium ferricyanide in 0.2 M KCl. Applied potential windows of -0.5 to +0.8 V with scan rates between 25 and 200 mVs⁻¹. Electrochemical stripping of gold oxide was performed in 0.1 M sulphuric acid at potentials of -0.5 to 1.5 V at scan rates of 100 mVs⁻¹. The integrated charge, $Q(\mu\text{C cm}^{-2})$, under the oxide removal peak of the SAM-modified electrode was used as a measure of the total fractional pinhole area, $1 - \theta$ (where θ is the SAM coverage). Stripping was followed by an additional scan in the same voltage range to verify the total removal of the oxide in the first scan with the second reduction scan used as basis for calculations. Additionally, repeated cycling for up to 25 cycles was used as a guide to the robustness of the SAMs on each substrate.

2.3.4. *Contact angle measurements*

Effects of surface modifications were investigated using contact angle measurements. Contact angle experiments were performed with a custom built measurement system. Samples were affixed to a glass slide and a 1 μL drop of water was deposited onto the surface of the membrane and the image was captured on a fixed camera. ImageJ software was used to determine the contact angle of the droplet on the surface. The mean value of the contact angles was calculated from at least 3 individual measurements taken at different locations on the examined substrates.

2.3.5. Raman spectroscopy of 3-mercaptopbenzoic acid on gold coated PA membranes

SERS spectra were recorded with a LabRam II Raman spectrometer (Horiba Jobin-Yvon) coupled to an Olympus confocal microscope and equipped with a HeNe laser operating at 632.8 nm as the excitation source (laser power 100 µW at sample, 100× Olympus objective and laser spot diameter 1 µm). The acquisition time for each spectrum was 60 s and the spectral resolution 4 cm⁻¹. A 2 µm step size was used for the line scans.

2.4. INVESTIGATION OF THE TRANSPORT PROPERTIES OF MEMBRANES

2.4.1. Transport experiments

Transport experiments were performed using a home-made U-tube permeation cell in which the membrane separates two half-cells; the feed cell and the permeate cell (Figure 2-2). A hole was punched into thin PDMS sheets to act as o-rings between the membrane and the cell with one sheet placed on either side of the membrane. The diameter of the hole in the PDMS on the feed side of the membrane presents the effective area of the membrane exposed to the feed solution. Various dyes were used to probe the transport properties of the membranes. The structures of the dyes used in these studies are shown in (Figure 2-3). Separate permeation experiments were performed in which a 1mM aqueous solution of the dye was added to the feed cell while pure water was added to the permeate cell. The diffusion of the dye from the feed cell to the permeate cell was continuously monitored with a UV-Vis fibre optic spectrophotometer (Ocean Optics, USA, Figure 2-2b) at the maximum peak absorbance. The peak absorbance was logged (Spectrasuite, Ocean Optics) every 10 s. The flux of the dyes through each of the membranes was calculated by correlating the maximum absorbance with the concentration of the dye. Concentration calibration plots were obtained by measuring the peak absorbance for a set of dye solutions with known concentration.

2.4.2. Measurement of dye oil:water partition coefficients

Hydrophobic and hydrophilic probe dyes were chosen for transport experiments based on their oil:water partition coefficients. Laboratory shake flask experiments were conducted as according to OECD guideline 107 [7] using n-octanol (Sigma-Aldrich) and Milli-Q water. The octanol and water were saturated with water and octanol respectively prior to the experiments and herein reference to octanol and water refers to their saturated solutions. All dyes were dissolved in water to obtain a concentration of 1 mM. Octanol and water were added to centrifuge tubes to obtain an octanol:water ratio of 1:1, 1:2 and 2:1 with a total volume of 8 mL. Each ratio was carried out in triplicate. The dyes were added to the centrifuge tubes and the phases were mixed by vortex for 10 min and then centrifuged at 1000 rpm for 10 min. The water phase was extracted and the concentration in the water phase was determined via UV-Vis spectroscopy (Ocean Optics system, USA). The dye concentrations were determined only from the water phase and the concentration of the dyes in the octanol phase was calculated by subtraction of the concentration in the water phase.

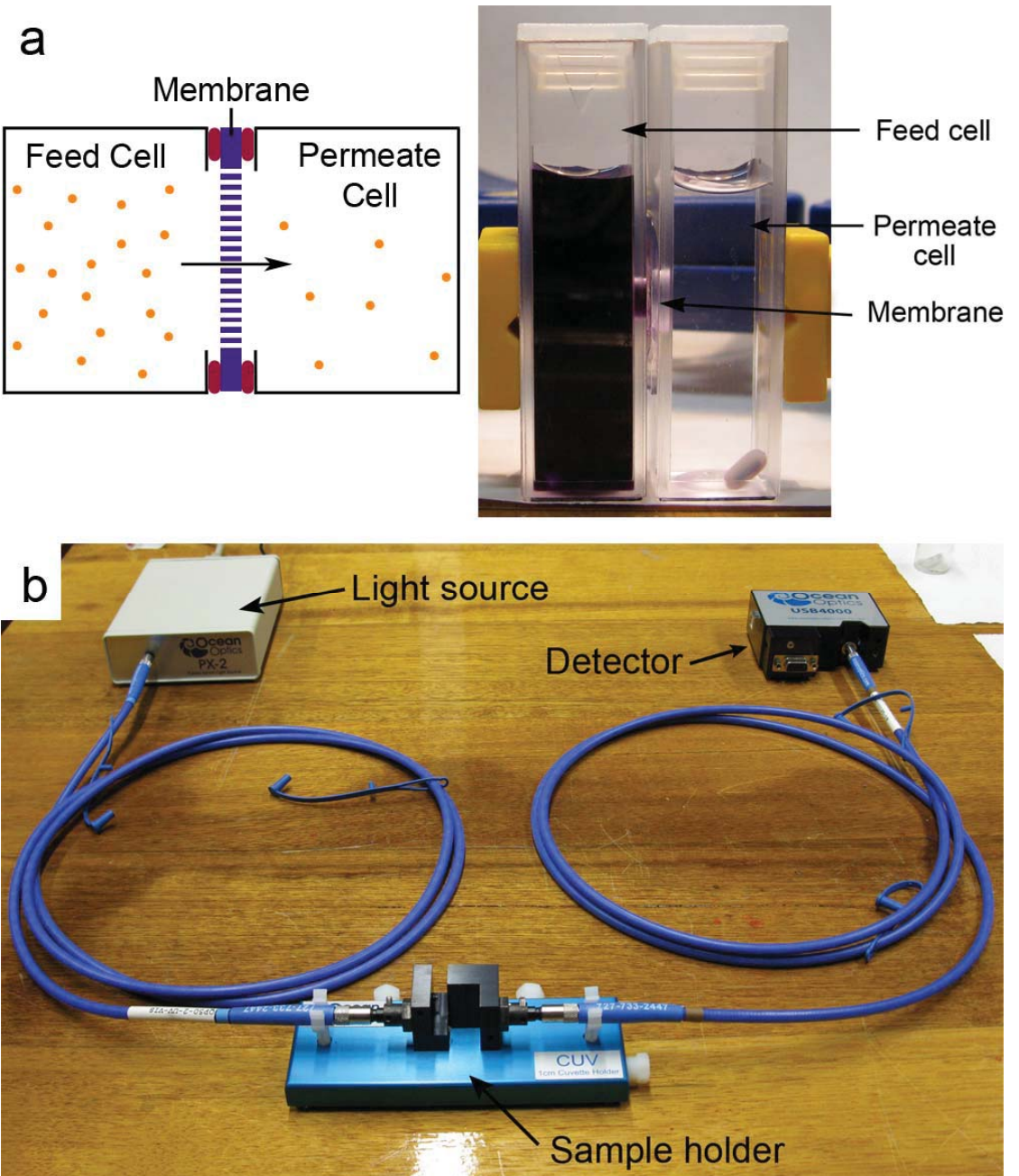
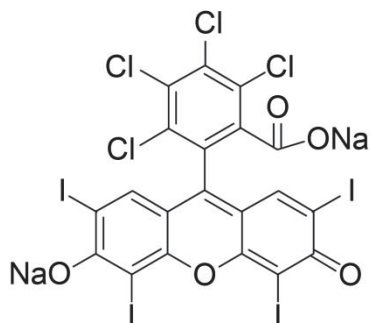
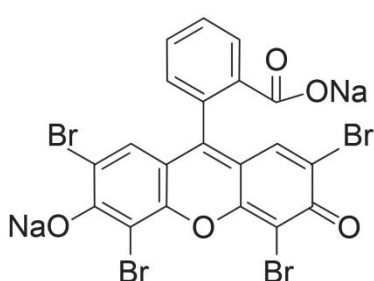


Figure 2-2 (a) Schematic and photo of the permeation cell set up used in these studies. (b) Photo of the Ocean Optics UV-Vis system.

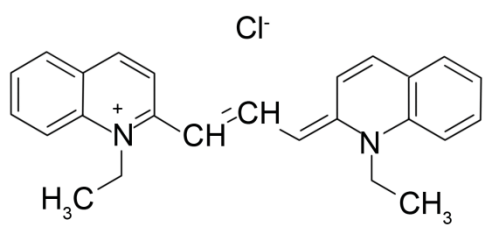
(a) Rose bengal



(b) Eosin yellow



(c) Pinacyanol chloride



(d) Tris(2,2'-bipyridyl)dichlororuthenium(II) hexahydrate

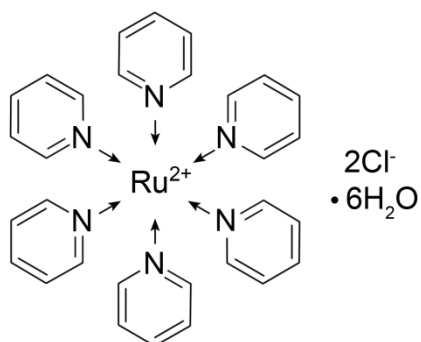


Figure 2-3 Structures of probe dye molecules used in the transport experiments.

2.5. SYNTHESIS OF FLUORINATED AZOBENZENE FOR THE DEVELOPMENT OF

SWITCHABLE MEMBRANES

2.5.1. *Synthesis of 4-(4-trifluoromethoxyphenylazo)phenol (1)*

4-(Trifluoromethoxy)aniline (75 mmol) was added dropwise under heating ($\sim 60^\circ\text{C}$) to a mixture of 21 ml concentrated sulphuric acid and 21 ml water. This reaction yields a white foam. After cooling the solution was diazotised by the dropwise addition of a solution of 7 g sodium nitrite in 40 ml water at $0 \sim 5^\circ\text{C}$ to the acid mixture. The solution was stirred for 1 h. The diazotisation solution was slowly added to a solution of 7.5 g phenol, 3 g sodium hydroxide and 47 g sodium carbonate in 270 ml water at $0 \sim 5^\circ\text{C}$. The yellow coloured precipitate was filtered off, dried under vacuum and recrystallised from n-hexane (Figure 2-4).

2.5.2. *Synthesis of 7-[*(trifluoromethoxyphenylazo)phenoxy*]pentanoic acid (2)*

6-bromohexanoic acid (23.1 mmol) was added to a mixture of 4-(4-trifluoromethoxy phenylazo)phenol (19.0 mmol) and potassium hydroxide (42.4 mmol) in 150 ml ethanol and the mixture was refluxed at 70 °C for 20 h. The solution was cooled to room temperature then the inorganic salts were removed by filtration. The filtrate was acidified with 40 ml acetic acid, and then refluxed for 30 min. The solvent was removed in vacuo and 200 ml chloroform was added. The organic layer was washed three times with water and dried over sodium sulfate. Recrystallisation from acetonitrile afforded orange crystals (Figure 2-4).

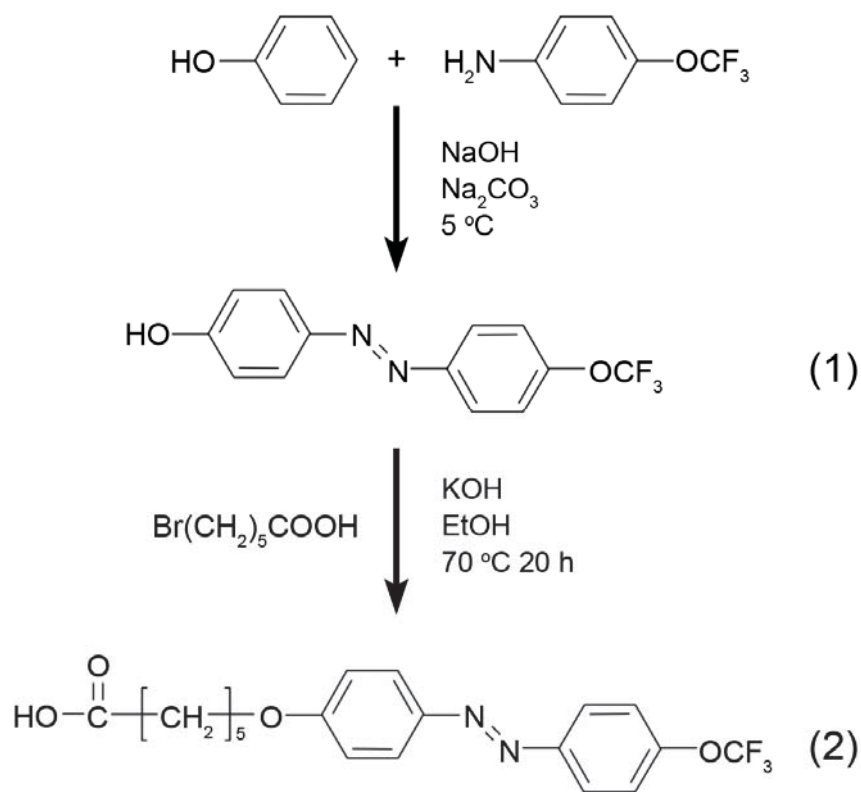


Figure 2-4 Scheme of the synthesis of 4-(4-trifluoromethoxyphenylazo)phenol (1) (intermediary) and 7-[*(trifluoromethoxyphenylazo)phenoxy*]pentanoic acid (2).

2.6. REFERENCES

1. Menon, V.P., and Martin, C.R., *Fabrication and Evaluation of Nanoelectrode Ensembles*. Analytical Chemistry, 1995. **67**: p. 1920- 1928.
2. Hausmann, D., Becker, J., Wang, S.L., and Gordon, R.G., *Rapid vapor deposition of highly conformal silica nanolaminates*. Science, 2002. **298**(5592): p. 402-406.
3. Ravoo, B.J., Reinhoudt, D.N., and Onclin, S., *Engineering Silicon Oxide Surfaces Using Self-Assembled Monolayers*. Angewandte Chemie-International Edition, 2005. **44**: p. 6282 – 6304.
4. Jani, A.M.M., Anglin, E.J., McInnes, S.J.P., Losic, D., Shapter, J.G., and Voelcker, N.H., *Nanoporous anodic aluminium oxide membranes with layered surface chemistry*. Chemical Communications, 2009(21): p. 3062-3064.
5. Losic, D., Shapter, J.G., and Gooding, J., *Atomically Flat Gold for Biomolecule Immobilisation and Imaging*. Australian Journal of Chemistry, 2001. **54**: p. 643-648.
6. Losic, D., Shapter, J.G., and Gooding, J.J., *Influence of surface topography on alkanethiol SAMs assembled from solution and by microcontact printing*. Langmuir, 2001. **17**(11): p. 3307-3316.
7. *Guideline for the testing of chemicals - partition coefficient (n-octanol/water): shake flask method*. 1995, Paris: OECD Organisation for Economic Cooperation and Development

CHAPTER 3

RAMAN SPECTROSCOPY OF THIOLS ADSORBED INSIDE THE PORES OF GOLD- ALUMINA MEMBRANES

The surface enhanced Raman scattering (SERS) effect was employed to confirm and characterise the formation of SAMs of 3-mercaptobenzoic acid (mMBA) on the surfaces of the gold coated alumina membranes. The investigation of the coverage and reproducibility of SAMs within porous matrices is of utmost importance in the design of filtration membranes and sensing platforms.

3.1. INTRODUCTION

Much of the work outlined in this thesis involves the implementation of various gold coated membranes for the investigation of surface chemistry driven transport phenomena. Due to their highly ordered structure and ease of surface functionalisation, gold coated porous alumina (Au-PA) membranes provide an ideal model for studying the impact of surface chemistry on molecular transport through membranes. Research into employing surface chemistry to improve transport selectivity and sensing is relatively recent but is essential for the development of membrane materials. Through further characterisation of SAMs within membranes more efficient separation processes can be devised. Consequently it is imperative to confirm the nature of SAMs within pores in order to elucidate their full impact on the transport phenomena through membranes. Whilst enormous effort has been made to investigate and characterise SAMs, the characterisation of SAMs within restricted spaces such as pores is currently poorly understood and difficult to probe [1].

There are numerous analytical techniques capable of investigating the structure and formation of SAMs of thiols on gold including XPS, FTIR, Raman and electrochemistry. Many of these methods are used to study SAMs on planar gold surfaces providing both qualitative and quantitative information about SAMs [2-3]. In particular, Surface Enhanced Raman Spectroscopy (SERS) is a powerful analytical tool due to the immense enhancement of the Raman scattering of a molecule [3]. The SERS effect allows very low concentrations or even single molecules to be detected when they are adsorbed onto roughened metal surfaces such as gold, silver and copper [7, 8]. Extensive research has been focussed on the fabrication of new metal structures for use as SERS substrates for sensing applications. Recently, metal nanorods, tubes and nanoporous metals have been exploited as SERS substrates [8-10].

The mechanism of electroless gold deposition is the nucleation and growth of gold nanoparticles [4]. Since the SERS effect is known to occur for nanoparticles [5] then electrolessly coated PA membranes can potentially provide a roughened gold surface suitable for use as a SERS substrate [5, 6]. These gold nanotube membranes have the potential to develop into SERS active substrates for ultrasensitive sensing

technologies. These technologies require reproducible, reusable, stable and tuneable SERS substrates. Gold coated porous alumina membranes present an extremely reproducible material due to highly ordered and controlled alumina fabrication and uniform gold deposition.

The aim of this chapter is to explore the application of the SERS effect to confirm and characterise the deposition of 3-mercaptopbenzoic acid (mMBA) on the interfaces of a gold coated PA membrane and within the confines of the pores (Figure 3-1). In addition, Raman spectroscopy is capable of spatially resolved techniques such as mapping and depth profiling which is used to identify and characterise the distribution of mMBA assembly along the length of the pores. To our knowledge, this is the first attempt to characterise SAMs within pores and probe their spatial distribution using scanning cross-sectional Raman spectroscopy.

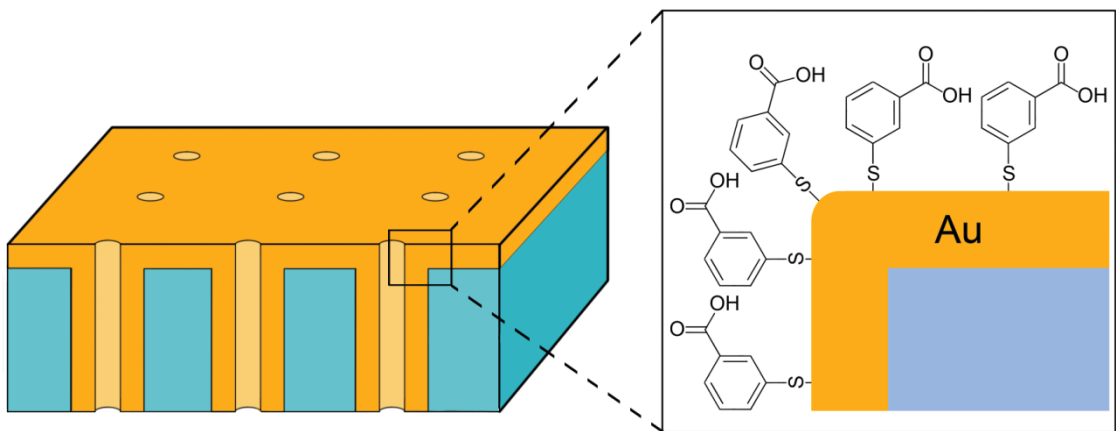


Figure 3-1 Schematic of electrolessly gold coated porous alumina membranes and functionalisation of the gold surfaces with 3-mercaptopbenzoic acid.

3.2. EXPERIMENTAL DETAILS

3.2.1. *Fabrication of porous alumina membranes*

Porous alumina was fabricated as outlined in section 2.1.1. The second anodisation was performed under 80 V for 15 min in 0.3 M oxalic acid (-1 °C) to achieve PA with thicknesses of 20 – 30 µm. The barrier oxide layer at the bottom face of the membrane was removed by immersion in 10 wt% H₃PO₄ for 3 h.

3.2.2. Electroless gold deposition

Electroless gold deposition onto porous alumina membranes was carried out as stated in section 2.1.2.1 with the following adjustments. Prior to tin sensitisation the bottom face of the membrane was coated with nail polish and dried in air in order to block gold deposition on this face. The tin and silver deposition steps proceeded as usual. A gold deposition time of 19 h was used in this study after which the nail polish film was removed with copious rinsing in acetone then allowed to air-dry.

3.2.3. Thiol functionalisation of gold nanotube membranes

The Au-PA membranes were functionalised with 3-mercaptopbenzoic acid (mMBA, Sigma-Aldrich) by immersion in a 3 mM solution in ethanol for 24 h, followed by rinsing in ethanol and water then air dried.

3.2.4. Raman spectroscopy of MBA on Au-PA membranes

SERS spectra were obtained as outlined in section 2.3.5. A cross section of the membrane was obtained by snapping the sample in half and then clamped in a custom built holder in order to orient the cross section to face the Raman objective.

3.3. RESULTS AND DISCUSSION

3.3.1. Structural characterisation of gold – alumina (Au-PA) membranes

SEM was used to examine the surface morphology of the Au-PA membranes (Figure 3-2a). The electroless deposition of gold provided a significant reduction in the pore diameter of the Au-PA membrane in comparison with the uncoated PA membranes. Pore size measurements of PA templates and Au-PA membranes were calculated through the analysis of SEM images. The original PA template pore size is 170.0 ± 21.1 nm. After electroless deposition the pore diameter of the Au-PA membranes have been reduced to 57.0 ± 12.5 nm (Figure 3-2d). In this work, gold deposition parameters were carefully chosen to provide optimum films. It is well documented that the gold deposition kinetics can be varied by changing the concentration of gold,

pH, and temperature of the gold deposition bath [6-7]. In our case we have reduced the pH of the gold deposition bath to 8 to decrease the rate of deposition of gold in order to achieve a more homogenous gold layer in addition to preventing the dissolution of alumina which occurs at high pH. Figure 3-2b displays an SEM image of an Au-PA membrane where the surface gold layer has been removed by scratching off the top layer of gold with a scalpel. The image clearly shows the tips of the gold nanotubes and presents a clearer indication of the magnitude of the reduction in the pore diameters due to the increase in the thickness of the gold. The outer diameter of the gold nanotubes corresponds to the pore diameter of the original PA template. Figure 3-2c presents an SEM image of the cross section of the Au-PA membrane after fracturing the membrane. The thickness of the membrane is found to be $\sim 21 \mu\text{m}$.

To confirm that gold deposition occurred inside the pores of the membrane, the supporting alumina template was dissolved revealing the gold nanotube structures (Figure 3-3a). A standing array of gold nanotubes is formed supported by the existing gold layer which was present on the top face of the membrane. Figure 3-3c presents the EDAX analysis of the nanotubes array confirming their composition of gold. The tubular shape of the gold is obvious, therefore confirming successful gold attachment to the pore walls. The length of the gold nanotubes obtained matches the thickness of the PA template thus signifying that the gold deposition has extended through the entire thickness of the membrane. Given that one side of the membrane was completely blocked with nail polish during the gold deposition stages, this suggests that electroless gold deposition is a reliable technique for coating thick porous materials. The section of the gold nanotube immediately adjacent to the top face of the membrane exhibits dense gold packing (Figure 3-3a). However, some pinholes in the gold nanotubes can be observed which becomes more prevalent in the nanotube regions of $> 5 \mu\text{m}$ depth into the membrane (Figure 3-3b). Therefore although gold deposition can occur throughout the length of the pore, it appears that the quality of the gold deposition diminishes slightly at depths greater than $5 \mu\text{m}$.

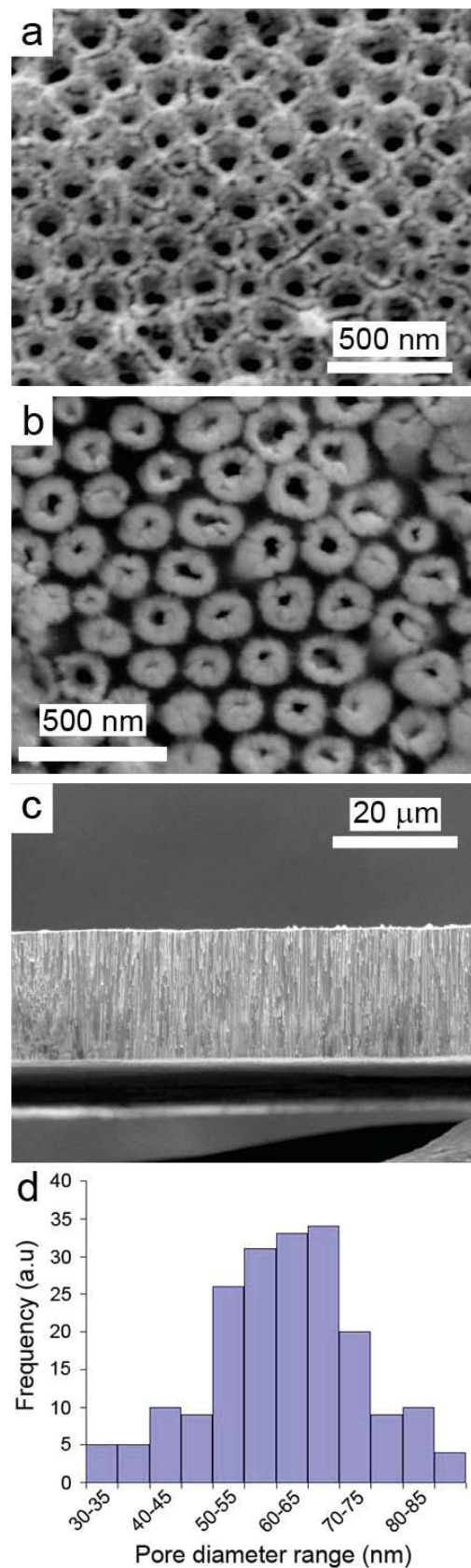


Figure 3-2. SEM images of a) the surface of an Au-PA membrane and b) an area of the membrane where the gold surface layer was cleaved exposing the tips of the gold nanotubes formed within the pores. c) cross section of the Au-PA membrane. d) pore size distribution of Au-PA membranes.

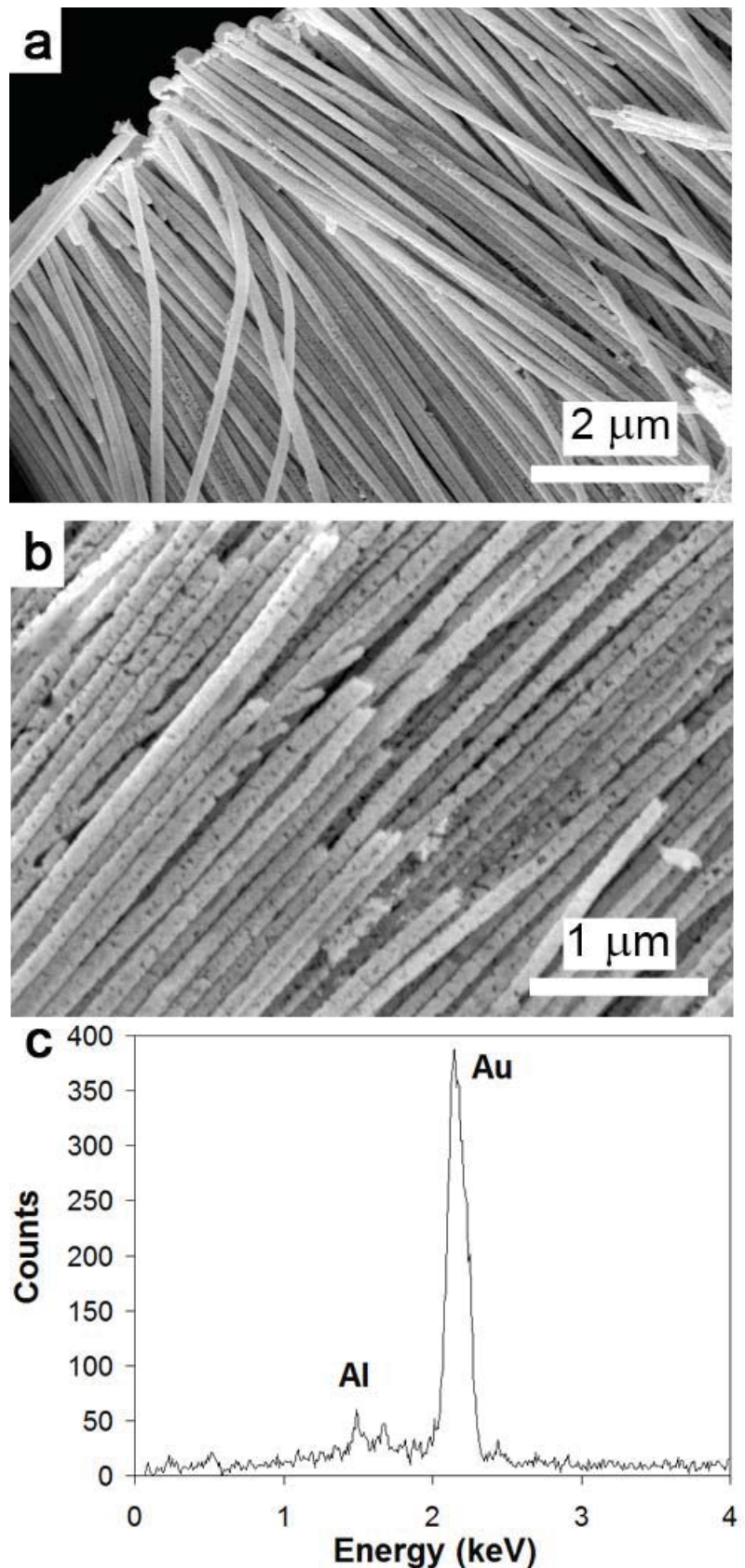


Figure 3-3 SEM images of a section of liberated gold nanotubes after dissolution of the porous alumina from the top of the membrane (a) and from the centre of the membrane (b). EDAX analysis of the nanotube array confirming their composition of gold (c).

3.3.2. Characterisation of SAMs within the pores of Au-PA membranes by Raman spectroscopy

Figure 3-4 shows the normal Raman spectrum of pure mMBA and the SERS spectrum of mMBA assembled on the surface of an Au-PA membrane. The SERS spectrum of mMBA on gold (Figure 3-4b) is dominated by bands at 1570 cm^{-1} , 1130 cm^{-1} , 1080 cm^{-1} , 1000 cm^{-1} and 840 cm^{-1} which involve CC stretching, HCC and CCC bending vibrations of the benzene ring [8]. The assignments are performed by a comparison with the Raman spectra of disubstituted benzenes [8-9] and 4-mercaptobenzoic acid [9-12]. The SERS enhancement is not observed for all vibrational modes of mMBA and the Raman peaks in the SERS spectrum are systematically red shifted by $3 - 10\text{ cm}^{-1}$ in comparison to bulk mMBA (Figure 3-4). The vibrational shifts are due in part to the charge transfer occurring between the gold surface and mMBA [10]. The dissociation of the SH group of mMBA at the gold surface results in formation of a coordinative bond between the gold and the sulphur moiety, allowing charge transfer between the gold and mMBA.

In bulk mMBA, stretching $\nu(\text{SH})$ bands at about 2600 cm^{-1} and bending $\beta(\text{SH})$ bands at 915 cm^{-1} are observed in Figures 3-4a and 3-4c. The SH group of mMBA dissociates on a gold surface and hence there are no prominent bands corresponding to the SH group vibrations in the SERS spectra (Figure 3-4b and d). The CH stretching vibrations are observed at $\sim 3100\text{ cm}^{-1}$ in bulk mMBA and are not observed in the SERS spectrum (Figure 3-4d). According to the so-called SERS selection rules [11-12] the absence of CH stretching bands in the SERS spectra would indicate that the benzene ring of mMBA is lying flat on the gold surface. It should be pointed out that this selection rule may apply if the C-H bonds are close and perpendicular to the surface [12]. For example in 4-mercaptobenzoic acid (pMBA) the C-H bonds are almost parallel to the surface when the molecule is perpendicular to the surface. We noted that interpretations of SERS spectra in literature are often contradictory about molecule orientations. The C-H stretching bands are in general not detected on the SERS spectra of pMBA but different authors reached different conclusions; the molecules could be parallel [10], perpendicular [13] or tilted [14-15] with respect to the surface plane. However, other techniques are certainly more adapted for deducing quite precisely molecular orientations at a metallic surface. Orientations of the three

isomers of mercaptobenzoic acid (pMBA, mMBA and 2-mercaptobenzoic acid oMBA) on gold have been determined precisely by means of carbon K-edge NEXAFS spectroscopy [16]. Only oMBA is quite flat on the surface with a tilt angle of about 50° with respect to the normal of the surface whereas the tilt angle for pMBA and mMBA is in the range 25 - 30°. Infrared reflection spectroscopic techniques are also well adapted to determine, at least qualitatively, the orientation of the molecules at the surface of a metal. For pMBA, there is a general agreement that the molecules are almost perpendicular to the surface [14, 15]. In conclusion we cannot claim that mMBA molecules are lying flat on the gold surface because C-H stretching bands are not observed. Most likely mMBA molecules adopt a tilted orientation which is the common orientation of thiols on a planar gold surface [2].

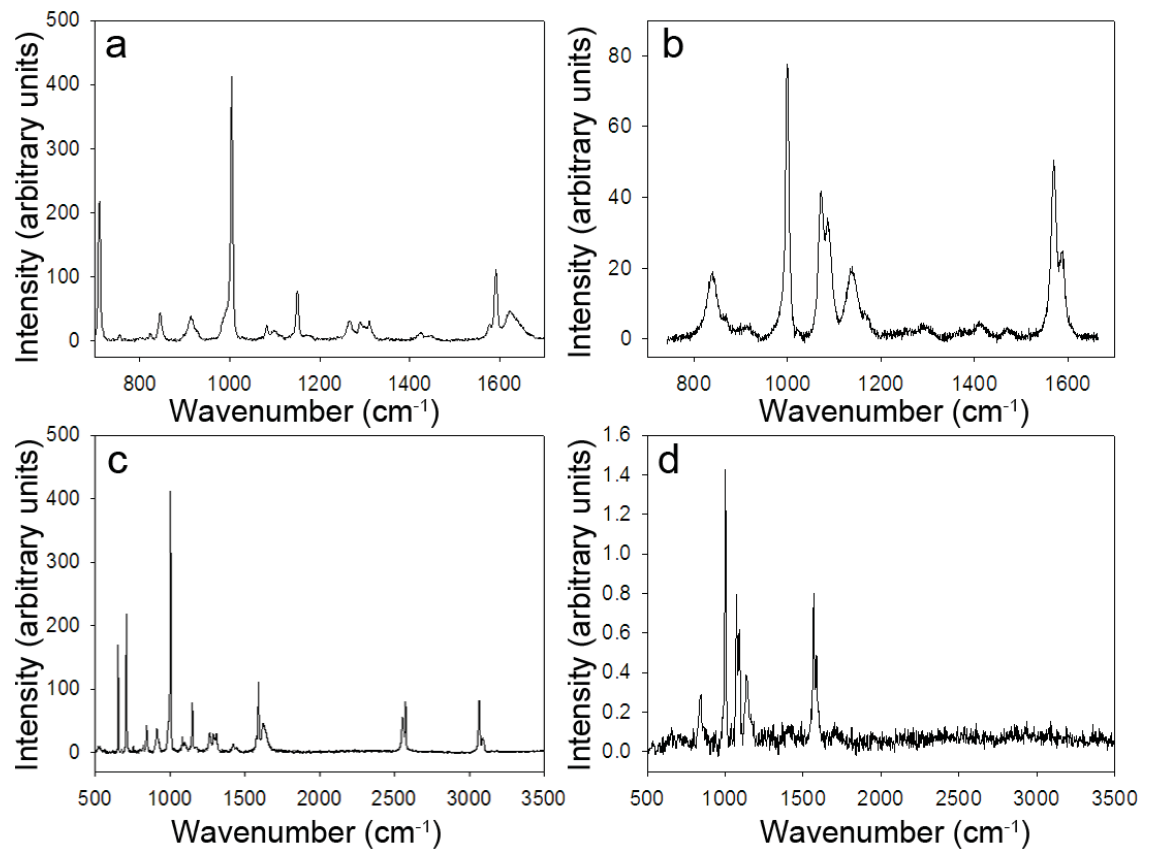


Figure 3-4 Normal Raman spectrum of pure mMBA (a) and SERS spectrum of an mMBA monolayer on gold (b). Normal Raman spectrum of solid mMBA (c) and SERS spectrum of mMBA on an Au-PA membrane (d) over an extended wavenumber range.

A comparison of the SERS spectra of mMBA on the top surface of the membrane and within the pores of the membrane is displayed in Figure 3-5 a & b respectively.

The main trend observed for multiple mMBA modified Au-PA membranes was that the intensity of the vibrations are greater in the case where the mMBA is assembled within the pores. The top surface of the membrane is almost completely covered in gold (Figure 3-2a), allowing the thiols to assemble everywhere on the surface, while the cross section of the membrane will only have the inner surface of the gold nanotubes available for thiol assembly. Given that the inner diameter of the gold nanotubes was found to be 57 nm with an interpore distance of 170 nm then the surface area of gold on the cross section will be the similar if not less than the surface area of gold on the top of the membrane. Therefore there will be less thiol molecules assembled on the cross section than the top surface of the membrane indicating that the increase in the SERS signal is most likely attributed to a greater SERS enhancement due to the curvature of the inner surface of the gold nanotubes.

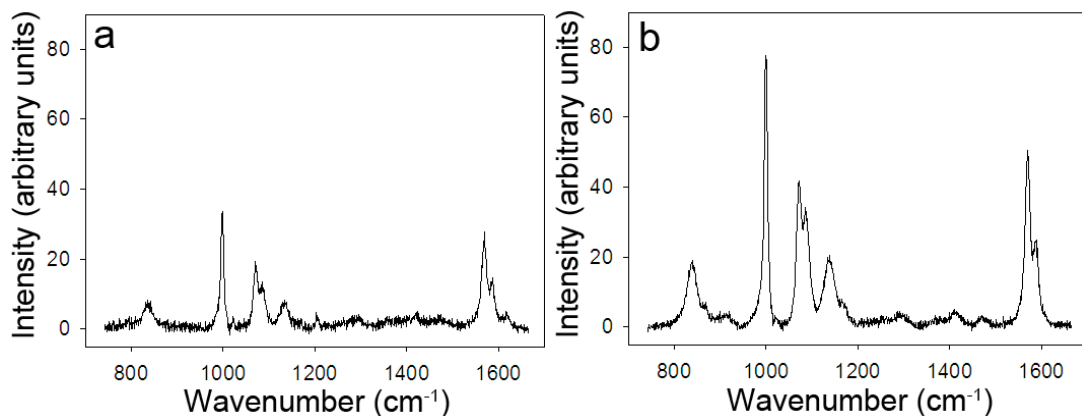


Figure 3-5 Raman spectra of mMBA when it is attached to the top surface (a) and within the pores (b) of the gold coated membrane.

Raman spectroscopy offers the ability to map surfaces for chemical species. Line scans were implemented in this study to determine the presence of thiol molecules across the thickness of the functionalised Au-PA membranes. Figure 3-6a presents the SERS spectra for mMBA at 4 μm increments along the cross section of a fractured mMBA-Au-PA membrane. The laser was scanned outside of the top face and ended below the bottom face of the membrane. Therefore the position of the scan is associated with the position of the laser at that particular acquisition, not the depth into the membrane. Firstly it is confirmed that thiols are present throughout the thickness of the membrane as a thiol signal is observed across the line scan. This result supports the applicability of using thiol modification to alter the chemical environment within porous materials. A common trend is observed with the cross

section line scans across mMBA-Au-PA membranes. Generally the intensity of the peaks increases at the middle of the membrane or towards the bottom face of the membrane (Figure 3-6a). There are several possibilities to explain these unexpected results including morphology and thickness of the gold nanotubes, structural changes in the internal gold surface and quality of the mMBA layer. The formation of bottle necked pores during gold deposition is highly likely as the deposition of gold will preferentially deposit on the face of the membrane. Bottle necked pores result in a smaller inner diameter of the nanotube at the top face of the membrane and slightly larger inner tube diameters within the membrane (Figure 3-7). As the bottom face of the membrane was sealed with nail polish during the gold deposition stages, then the bottle necked pore would only occur at the top face of the membrane. Furthermore, inhomogeneous gold deposition would likely result in a gradual decrease of the thickness of the nanotube wall along the length of the pore due to difficulties in the gold deposition solution penetrating into the depths of the pores. Therefore this gradual increase of the pore diameter from the top to the bottom of the membrane will result in the gradual increase of the peak intensity which is seen over the first 12 μm of the scan (Figure 3-6b). The peak at 1000cm^{-1} was chosen for this plot as it is the best representation of the 3-mba coverage, it is characteristic to 3-mba and is the most intense peak. As the thiols can only assemble on the inner surface of the gold nanotubes there is therefore less area for the thiols to assemble within the section of gold nanotubes closer to the top face of the membrane resulting in lower peak intensities. As the line scan continues towards the bottom of the membrane, the inner diameter of the gold nanotubes become larger and can therefore accommodate more thiol molecules. The pinhole defects in the gold nanotubes can be observed at depths $> 5 \mu\text{m}$ (Figure 3-3b) can also attribute to the increase in the peak intensities. A larger signal can arise due to the increased surface area and roughness caused by the pinholes. The peak intensity stabilises at a laser position greater than 12 μm (Figure 3-6b), signifying the regularity of the gold nanotube structure over this region.

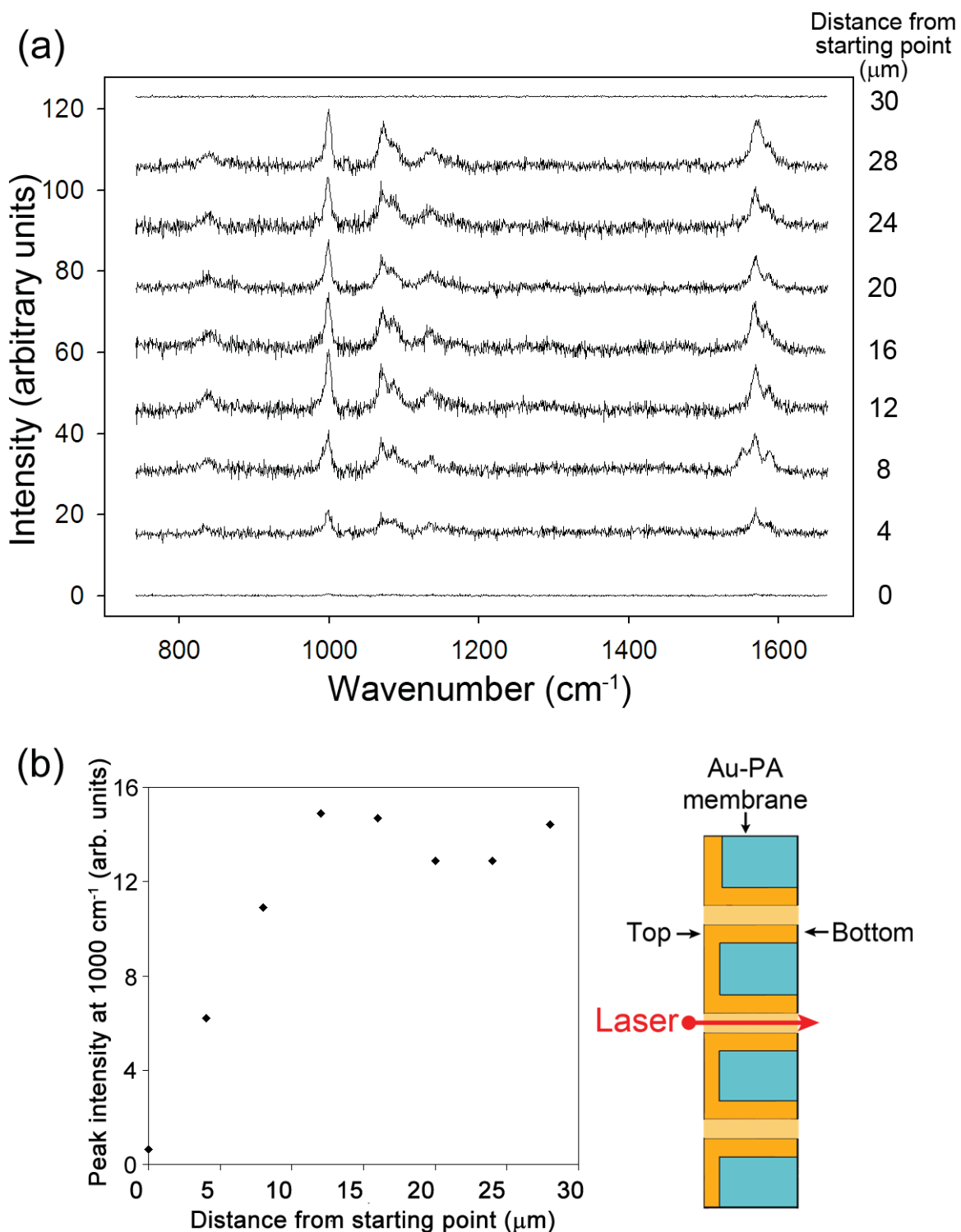


Figure 3-6 a) Raman spectra of the cross section of an mMBA functionalised Au-PA membrane. b) Plot of the peak height obtained at 1000 cm^{-1} for $4 \mu\text{m}$ increments across a cross section of an Au-PA membrane. Scans were taken in $4 \mu\text{m}$ increments starting above the top surface of the membrane. Position $0 \mu\text{m}$ is the position of the laser at the starting point of the line scan. The line scan finishes below the bottom surface of the membrane.

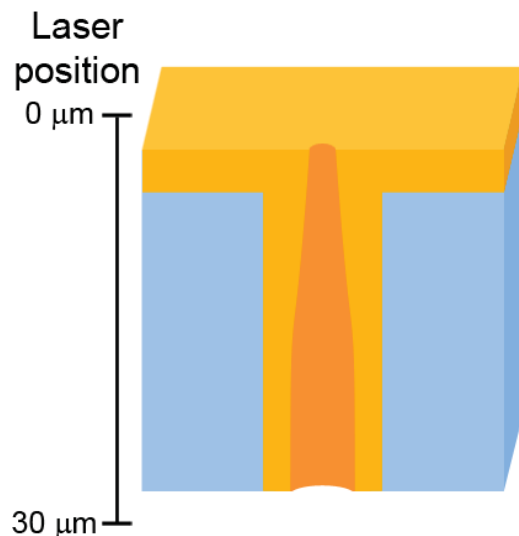


Figure 3-7 Schematic of a cross section of Au-PA exhibiting a bottle neck shaped pore.

3.4. CONCLUSION

Electroless deposition was utilised to coat porous alumina membranes with gold. The gold surfaces were functionalised with 3-mercaptobenzoic acid and the layer was subsequently characterised with Raman spectroscopy. This study confirmed the deposition of the thiol SAM throughout the length of the pore. Due to the curvature of the gold within the pores, there was an increased SERS effect when viewing the cross section of mMBA-Au-PA membranes. Higher peak intensities in the Raman spectra were observed for mMBA assembled in the middle of the membrane and towards the bottom of the membrane. We postulated that this effect was due to the formation of bottle necked pores which resulted in a smaller pore diameter at the top of the membrane and hence less surface area available for thiol assembly. Furthermore, inhomogeneous gold deposition at $> 5 \mu\text{m}$ depth into the membrane caused structural pinhole defects in the gold nanotubes to occur thus increasing the roughness and surface area of the gold in these sections which can contribute to the increased SERS signal. These gold nanotube membranes have the potential to develop into SERS active substrates for ultrasensitive sensing technologies. These technologies require reproducible, reusable, stable and tuneable SERS substrates. Gold coated porous alumina membranes present an extremely reproducible material due to highly ordered and controlled alumina fabrication and uniform gold deposition.

3.5. REFERENCES

1. Jirage, K.B., Hulteen, J.C., and Martin, C.R., *Effect of thiol chemisorption on the transport properties of gold nanotubule membranes.* Analytical Chemistry, 1999. **71**(21): p. 4913-4918.
2. Finklea, H.O., *Self-assembled monolayers on electrodes*, in *Encyclopedia of Analytical Chemistry*, R.A. Meyers, Editor. 2006, John Wiley & Sons Ltd: Chichester.
3. Fleischm.M, Hendra, P.J., and McQuilla.Aj, *Raman-spectra of pyridine adsorbed at a silver electrode.* Chemical Physics Letters, 1974. **26**(2): p. 163-166.
4. Gilliam, R.J., Thorpe, S.J., and Kirk, D.W., *A nucleation and growth study of gold nanowires and nanotubes in polymeric membranes.* Journal of Applied Electrochemistry, 2007. **37**(2): p. 233-239.
5. Mu, C., Zhang, J.P., and Xu, D.S., *Au nanoparticle arrays with tunable particle gaps by template-assisted electroless deposition for high performance surface-enhanced Raman scattering.* Nanotechnology, 2010. **21**(1).
6. Jirage, K.B., Hulteen, J.C., Martin, C.R., *Nanotubule-Based Molecular-Filtration Membranes.* Science, 1997. **278**: p. 655-658.
7. De Leo, M., Pereira, F.C., Moretto, L.M., Scopece, P., Polizzi, S., and Ugo, P., *Towards a better understanding of gold electroless deposition in track-etched templates.* Chemistry of Materials, 2007. **19**(24): p. 5955-5964.
8. Mayo, D.W., Miller, F.A., and Hannah, R.W., *Course Notes on the Interpretation of Infrared and Raman Spectra*, ed. J.W.a.S. Ltd. 2003.
9. Varsanyi, G., *Assignments for Vibrational Spectra of Seven Hundred Benzene Derivatives.* 1974: Wiley: New York.
10. Fleger, Y., Mastai, Y., Rosenbluh, M., and Dressler, D.H., *Surface enhanced Raman spectroscopy of aromatic compounds on silver nanoclusters.* Surface Science, 2009. **603**(5): p. 788-793.
11. Suh, J.S. and Moskovits, M., *Surface-enhanced Raman-spectroscopy of amino-acids and nucleotide bases adsorbed on silver.* Journal of the American Chemical Society, 1986. **108**(16): p. 4711-4718.

12. Moskovits, M. and Suh, J.S., *Surface geometry change in 2-naphthoic acid adsorbed on silver*. Journal of Physical Chemistry, 1988. **92**(22): p. 6327-6329.
13. Yuan, Y.X., Ling, L., Wang, X.Y., Wang, M., Gu, R.A., and Yao, J.L., *Surface enhanced Raman spectroscopic readout on heavy metal ions based on surface self assembly*. Journal of Raman Spectroscopy, 2007. **38**(10): p. 1280-1287.
14. Michota, A. and Bukowska, J., *Surface-enhanced Raman scattering (SERS) of 4-mercaptopbenzoic acid on silver and gold substrates*. Journal of Raman Spectroscopy, 2003. **34**(1): p. 21-25.
15. Ma, W.Q., Fang, Y., Hao, G.L., and Wang, W.G., *Adsorption Behaviors of 4-Mercaptobenzoic Acid on Silver and Gold Films*. Chinese Journal of Chemical Physics, 2010. **23**(6): p. 659-663.
16. Barriet, D., Yam, C.M., Shmakova, O.E., Jamison, A.C., and Lee, T.R., *4-mercaptophenylboronic acid SAMs on gold: Comparison with SAMs derived from thiophenol, 4-mercaptophenol, and 4-mercaptopbenzoic acid*. Langmuir, 2007. **23**(17): p. 8866-8875.

CHAPTER 4

COMPARISON OF ALKANETHIOL AND FLUORINATED THIOLS ON THE TRANSPORT PROPERTIES OF GOLD COATED POLYCARBONATE MEMBRANES

The effect of the surface chemistry on the transport properties of gold nanotube membranes has been explored through functionalisation with self assembled monolayers. The transport properties and the selectivity of fluoro-derivatised membranes (1H,1H,2H,2H-perfluorodecanethiol) towards hydrophobic and hydrophilic molecules was compared with a membrane modified with an analogous alkanethiol; 1-decanethiol.

4.1. INTRODUCTION

Electroless deposition is used to form gold nanotube membranes via a process which finely coats any surface to which it is applied with gold. When applied to porous membranes gold nanotubes are formed within the pores of the membrane (chapter 1, Figure 6) [1-6]. Gold nanotube membranes can be made chemically sensitive through functionalisation with thiols, which form self assembled monolayers (SAMs) on the surfaces and within the pores of the membrane [7]. It has been demonstrated that the enhancement of transport selectivity can be achieved by exploiting chemical features of the membrane or molecules being transported and tuning the interactions between the two [7].

Studies involving gold nanotube membranes have shown that thiol modification is an elegant approach to form membranes with molecular selectivity based on different/hydrophobic/hydrophilic properties [7]. However, concerns in recent years were raised in the implementation of thiol chemistry on commercial devices due to their poor durability under ambient and extreme conditions [8]. Dynamic studies of alkanethiol on gold surfaces have revealed several serious disadvantages of SAMs [9]. In particular there is concern for their thermal instability, UV photo-oxidation and the changing of SAM structures over time [10-12]. The evidence of maturation of SAMs has shown that over a period of several months there are dramatic changes in their structure and integrity [13]. SAMs made from fluorinated thiols have great promise to resolve some of these issues because of their potential to produce an extremely low surface energy and highly hydrophobic surface [14-15]. Several studies have shown fluorinated SAMs on gold to be robust and relatively defect free [16-18]. Fluorinated surfaces derive their characteristics from the unique molecular properties associated with C-F bond that imparts a specific, unique chemistry and physics at interfaces. Their low surface tension and low electrostatic loading can play an essential role in antifouling applications and are promising in membrane applications [15, 19].

In this work we propose to impart chemical selectivity to gold nanotube membranes by incorporating the highly hydrophobic and durable thiol, perfluorodecanethiol (PFDT). To determine the effectiveness and stability of gold nanotube membranes

modified with fluorinated SAMs comparative studies using a hydrophobic alkanethiol of comparable chain length, decanethiol (DT), have been explored. The selectivity of these membranes towards hydrophobic and hydrophilic organic molecules is presented.

4.2. EXPERIMENTAL DETAILS

4.2.1. *Electroless gold deposition onto polycarbonate membranes*

Gold coated polycarbonate (Au-PC) membranes were fabricated through the gold deposition procedure outlined in section 0 with the following modifications. A gold deposition time of 20 h for all samples was used in this study. After gold deposition, the membrane was thoroughly rinsed in water and immersed in 25 % HNO₃ for at least 12 h to remove any residual Sn or Ag followed by rinsing in water and air-drying.

4.2.2. *Investigation of gold nanotube membrane transport properties*

Transport experiments were carried out as stated in section 2.4.1. In this particular study ethanolic solutions of the hydrophobic dye, pinacyanol chloride (PCN), and the hydrophilic dye, rose bengal (RB), were used to probe the transport properties of the membranes. Their absorption spectra were monitored at 606.09 nm for PCN and 552.20 nm for RB.

4.3. RESULTS AND DISCUSSION

4.3.1. *Fabrication and characterisation of gold - polycarbonate membranes*

The surface morphology of gold nanotube membranes fabricated by gold deposition of PC membranes with an 80 nm pore diameter is presented in Figure 4-1a. Through coating the porous membrane a significant decrease in the pore diameter is seen in comparison with uncoated membranes (Figure 4-1a inset). The clustered gold surface

seen on the membranes is the typical morphology of gold films prepared by electroless deposition. In this work, gold deposition parameters were carefully chosen to provide preparation of optimum films. A pH of 8 was chosen for the gold deposition bath as it decreases the rate of the deposition reaction as a result of the reduction of gold by formaldehyde. This approach has been shown to allow a more homogeneous layer of gold to form and provides preferential deposition within the pores [4].

To confirm that gold deposition occurred inside the pores as well as on the top of membrane surface TEM image of a microtomed section of a gold plated membrane is shown in Figure 4-1b. The gold particles (black dots) line the entire length of the pore, confirming gold deposition is taking place within the depths of the pore and the gold on the face does not obstruct the pore openings. Furthermore SEM of liberated gold nanotubes after chemical etching or dissolution of the PC membrane confirmed the presence of gold down the length of the pore (Figure 4-1 c & d).

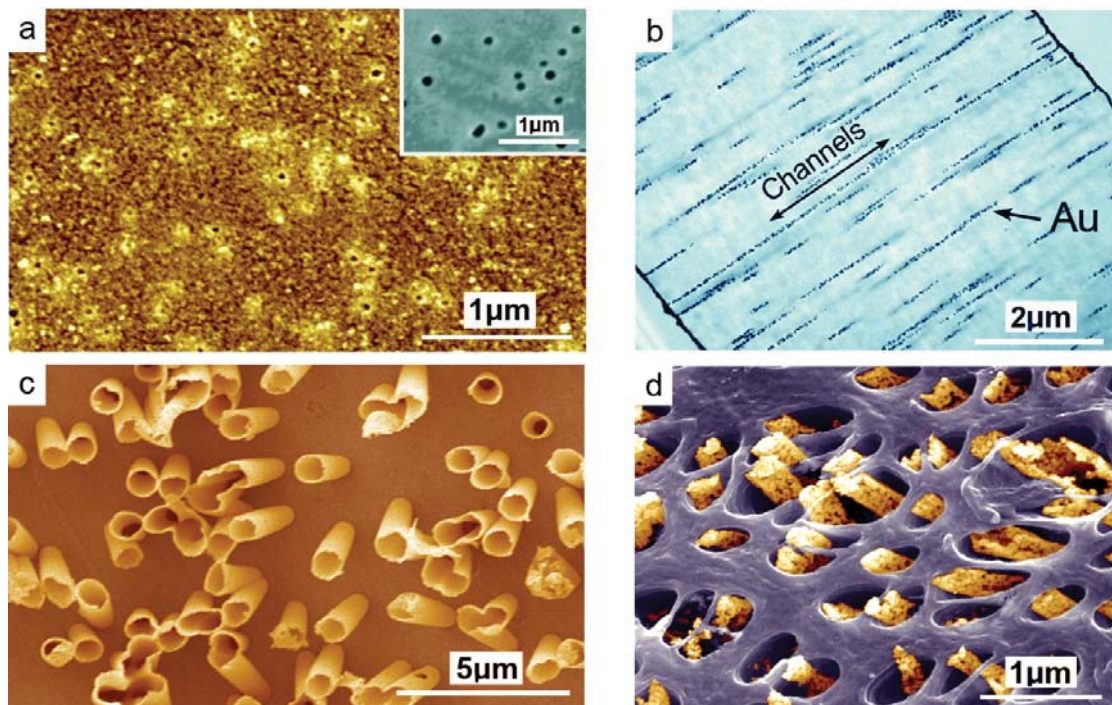


Figure 4-1. a) SEM image showing the surface morphologies of gold nanotube membranes prepared using a polycarbonate membrane as the template with a nominal pore diameter of 80nm. Inset: uncoated polycarbonate membrane. b) TEM cross section of 30nm PC membrane plated with gold for 20h. c) Fully dissolved PC membrane resulting in a standing array of gold nanotubes supported by the

surface gold layer (PC pore diameter: 800 nm). d) Surface etched Au-PC membrane revealing the tips of the gold nanotubes (PC pore diameter: 200 nm).

4.3.2. Electrochemical characterisation of thiol modified gold - polycarbonate membranes

PFDT and DT functionalised Au-PC membranes were probed for passivating properties of their self-assembled monolayers by ferricyanide as a redox probe. Figure 4-2a shows comparative cyclic voltammetry (CV) measurements of bare and modified Au-PC membranes. The shape of the CV peak is used to assess the quality of the monolayer as it provides information regarding the electron-transfer of the redox probe through the monolayer [20]. The peak-shaped CV of DT-Au-PC membranes indicate diffusion-limited electron transfer characteristic of closely spaced defect sites or large bare areas of uncoated gold. PFDT-Au-PC membranes give a peak-less CV with lower current densities which indicates a denser monolayer with lower defects in comparison with DT. To estimate the fraction of these defects, CV results of gold oxide stripping experiments are shown in Figure 4-2b. A significantly larger reduction peak for DT in comparison with PFDT confirms that the DT monolayer is more defective. These observations are not surprising as it is known that fluorocarbon chains assume a helical conformation making them more rigid than analogous hydrocarbon chains [21]. The perfluorocarbon helices are intramolecularly stabilised and will maintain their helical conformation whereas hydrocarbon chains do not have this degree of intermolecular stability [14, 23]. These factors all contribute to the enhanced stability of fluorocarbon SAMs against mechanical friction, thermal stress and extreme acid/base conditions [8].

The electrochemical results presented provide information on the SAMs properties of the top surface of the membranes rather than inside the pores. These results do not provide an indication of the quality inside the pores. The structure of thiols within confined spaces such as pores is poorly understood and very difficult to probe [22]. Given the highly curved surface it is very likely that the SAM is not as well ordered or well-packed as on a planar surface which was found to be the case in several other studies [7, 22]. However, as on the planar surface, it would be reasonable to expect

the perfluorinated chains to form higher quality layers in the pores than alkane chains.

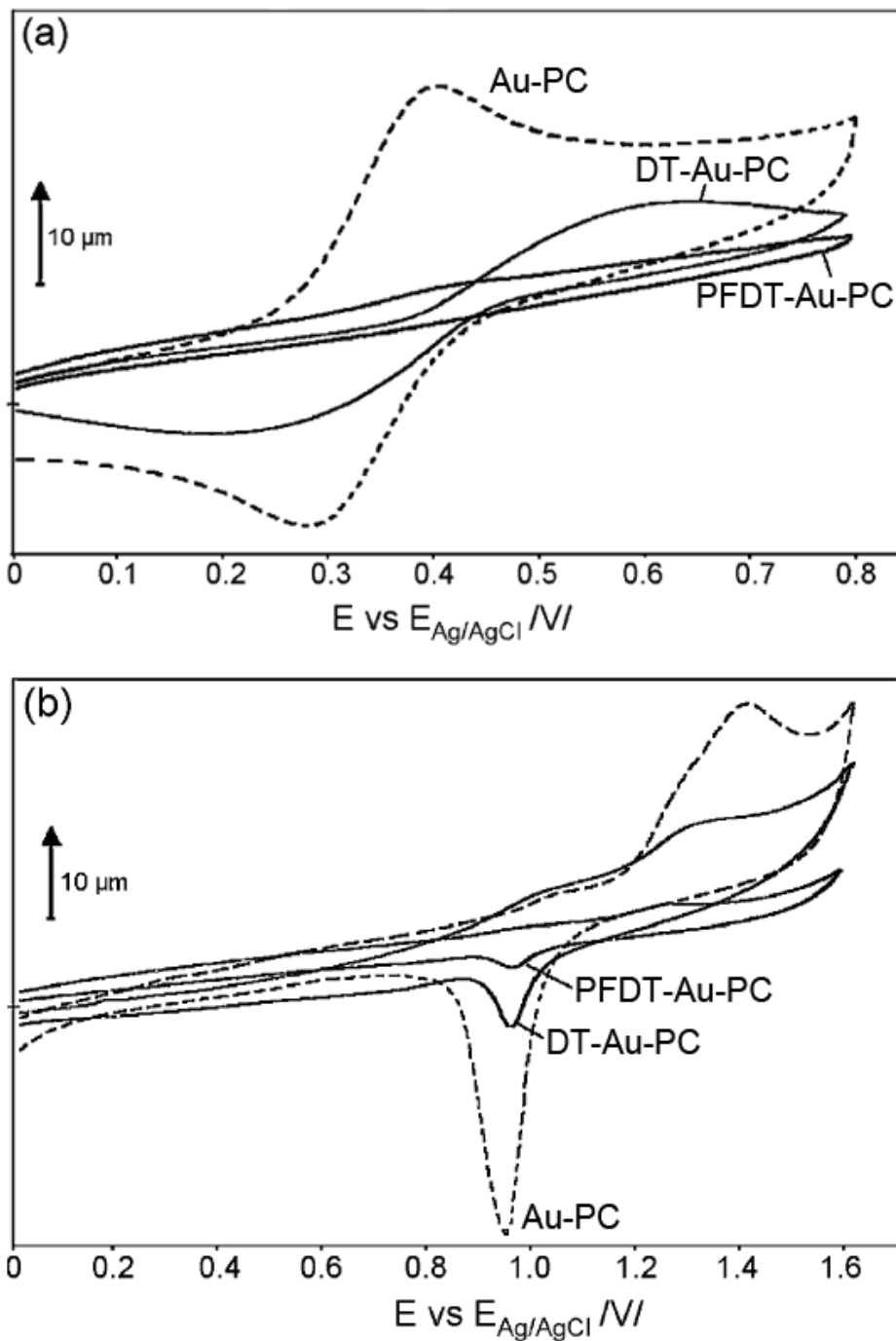


Figure 4-2. Typical CVs obtained for unmodified, and thiol-modified gold nanotube membranes, PFDT-Au-PC and DT-Au-PC in (a) an electron-transfer experiment performed using a redox probe 1 mM ferricyanide in 0.2 M KCl (scan rate 100 mVs^{-1}) and (b) a gold reduction experiment performed in 0.1 M sulphuric acid (scan rate 100 mVs^{-1}).

4.3.3. Transport and selectivity of gold - polycarbonate membranes

The transport and selectivity properties of PFDT and DT modified gold nanotube membranes were explored using two molecular dyes: pinacyanol chloride (PCN) that has dominant hydrophobic properties and rose bengal (RB) with more hydrophilic properties. A summary of the permeation data of these dyes through functionalised and unfunctionalised membranes are shown in Table 4-1. The flux of the dyes through each of the membranes was documented and the ratio of the flux for PCN and the flux for RB (selectivity ratio) was determined. For an unfunctionalised membrane we find that the flux of RB is 7.3 times smaller than PCN. The observed difference in transport is due to the fact that PCN is smaller than RB and so can pass through the membrane more easily.

Table 4-1. Transport and selectivity properties of functionalised and bare gold nanotube membranes (errors obtained from three replicate measurements).

	Flux of permeate molecule (mol cm ⁻² h ⁻¹)		Selectivity PCN:RB
	PCN	RB	
Au-PC	4.02×10^{-8} $\pm 2.64 \times 10^{-9}$	5.53×10^{-9} $\pm 1.45 \times 10^{-9}$	7.27
DT-Au-PC	4.23×10^{-8} $\pm 3.71 \times 10^{-9}$	4.94×10^{-9} $\pm 5.37 \times 10^{-10}$	8.56
PFDT-Au-PC	3.76×10^{-8} $\pm 1.47 \times 10^{-9}$	2.31×10^{-9} $\pm 2.03 \times 10^{-10}$	16.28

Figure 4-3 represents the transport of both probe dyes through the membranes functionalised with the alkane thiol, DT and the fluorinated thiol, PFDT. The data confirms that both functionalised membranes favour transport of the hydrophobic dye over the hydrophilic dye. Thus through functionalising the membrane with a hydrophobic thiol it has become chemically sensitive, favouring the transport of hydrophobic species. However, the PFDT-Au-PC membrane shows improved transport of hydrophobic molecules over hydrophilic molecules compared to the DT-Au-PC membrane. From Table 4-1 it can be seen that the selectivity ratio through the PFDT-Au-PC membrane is 16.27 whereas the DT-Au-PC membrane has a selectivity

ratio of only 8.56. The selectivity ratio of the PFDT-Au-PC membrane has increased by 124% in comparison to the unfunctionalised membrane while the DT-Au-PC membrane has only increased a small amount (18 %). From Table 4-1, the flux of PCN through unfunctionalised and functionalised membranes are very similar, indicating that the transport of the hydrophobic dye is not largely affected by the introduction of a hydrophobic SAM to the membrane. The addition of thiols would be expected to decrease the membrane pore size and consequently decrease the transport. However, it is important to consider the partition effect during the diffusion of molecules through the thiol modified pores of the membrane. The partitioning of organic solutes through various membranes and molecular structures such as SAMs and lipid bilayers and their impact on transport properties have been explored and reported in literature [23-26]. In our case it is likely that PCN can partition into the thiol layers as well as the solvent at the centre of the pore. This is further verified in terms of Fick's law of diffusion;

$$J = P(C_1 - C_2) \quad \text{Eq. (2)}$$

Where J is the flux across the membrane, P is the permeability constant, C_1 is the concentration in the feed cell and C_2 is the concentration in the permeate cell [27]. The permeability constant of the membrane is proportional to the diffusion coefficient and the partition coefficient of the dye into the membrane. For the case of an unfunctionalised and functionalised membrane, the area and concentration difference are the same and PCN provides similar transport rates (Table 4-1) which means the permeability constants must be comparable (Eq. 2). This is perhaps a surprising result as the narrowing of the pores by the adsorbed monolayer would be expected to hinder the diffusion. As mentioned in section 4.3.3 given the highly curved surface within the pores it is very likely that the SAM is not well ordered or well-packed [7, 22]. Therefore the thickness of the thiol layer within the pores will be small and there will be only slight narrowing of the pores due to the adsorbed monolayer. However, in the case where the molecules being transported can dissolve into the monolayer [7, 22], diffusion across the membrane can occur through the thiol layer and through the centre of the pore. The partition of the dye from the pore into the thiol layer will alter the concentration gradient between the feed cell and the solvent inside the pore. An overall increase in the concentration gradient in the pore would be expected which would increase the flow across the membrane compensating for the narrower pore size.

It is also important to consider the adsorption and retention of the dye onto the functional layer or gold surface. PFDT is highly antifouling and therefore the dye is highly unlikely to adsorb and be retained by the functional layer. Consequently the PFDT layer will permit the passage of hydrophobic molecules and the reduction of the flux of the hydrophilic dye is due to the hydrophobic-hydrophilic effects as described. However, DT is not antifouling and therefore the dye may adsorb onto the layer and become retained, thus decreasing the effective pore diameter of the membrane and lowering the transport rate of the dye. Adsorption of the dye onto the DT layer would also result in an increase in the concentration of the dye immediately within the membrane and hence generate less driving force for the dye to transport from the feed cell into the membrane. However the PCN transport rate is found to increase slightly after DT modification and therefore adsorption doesn't appear to be influencing the flux. The hydrophilic dye flux is found to decrease after DT modification which may be attributed to adsorption of the dye onto the DT layer. If adsorption is used to explain the transport properties of the DT membrane then RB can adsorb to the DT layer while PCN does not adsorb. To determine whether the transport effects are due to hydrophilic-hydrophobic interactions or adsorption effects, it would be desirable to perform the experiments using a range of dyes.

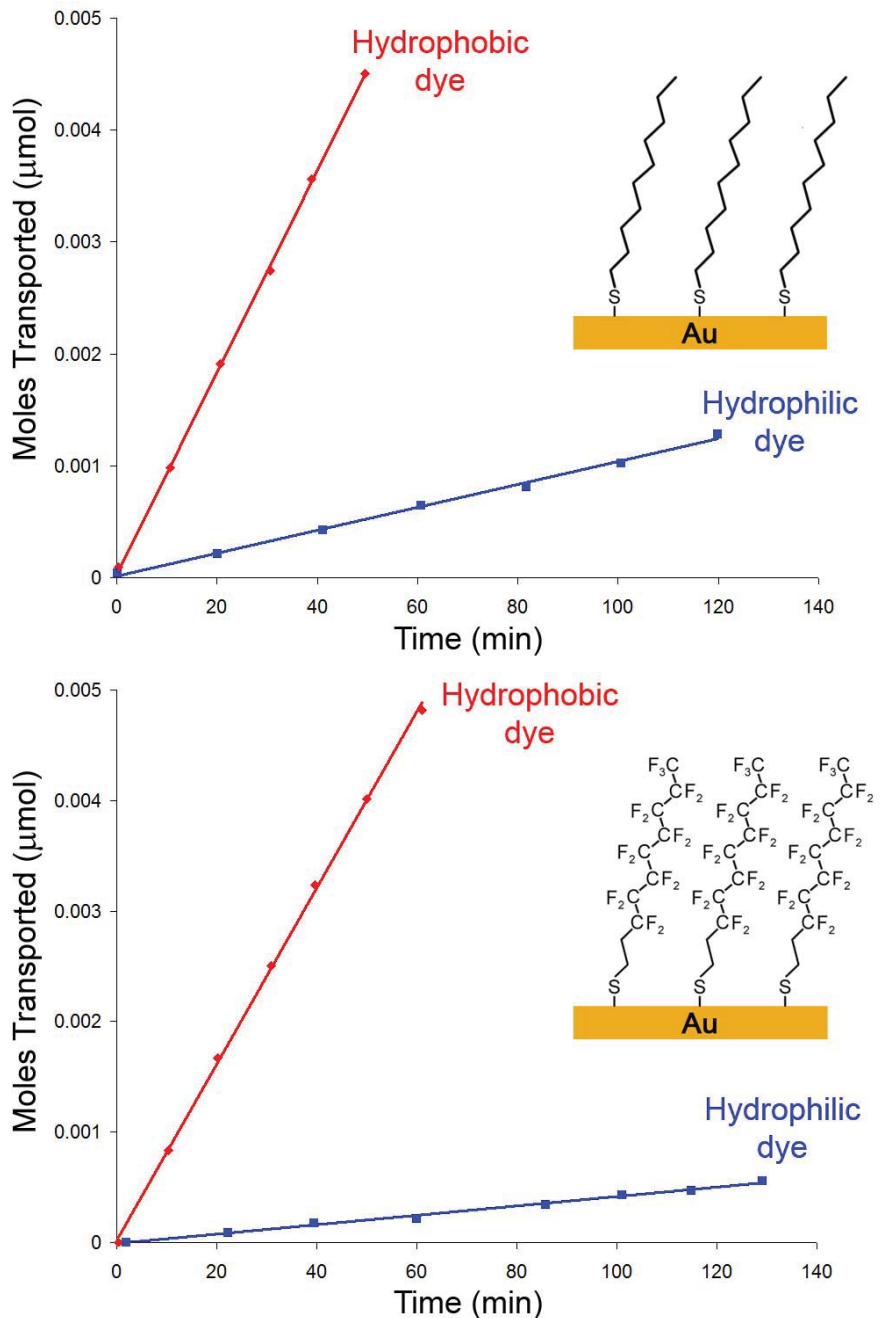


Figure 4-3 Transport of a hydrophobic (PCN) and hydrophilic (RB) dye through a gold nanotube membrane functionalised with the hydrophobic thiols a) decanethiol and b) perfluorodecanethiol.

Figure 4-4 directly compares the hindrance of the PFDT and DT modified membranes towards the transport of the hydrophilic dye, RB. The introduction of either hydrophobic thiol decreases the rate of transport of the hydrophilic species through the pore in comparison with unmodified membranes. This is expected as the membranes exhibit a hydrophobic environment that the hydrophilic dye would have difficulty partitioning into. However, this result clearly shows that the PFDT

derivatised membrane is more effective at rejecting the hydrophilic dye than the DT membrane. Unlike the case for the hydrophobic dye, PCN, it is unlikely that the hydrophilic dye, RB, will partition into the organic monolayer and hence the reduction of the transport rate is attributed to the reduction in the pore diameter from the adsorbed monolayer and the rejection of hydrophilic species from the hydrophobic surface. Electrochemical characterisation of PFDT on the membrane surface showed a more ordered, dense, and less defective monolayer film in comparison with DT. Even though the thiols are not well ordered or well packed within pores [7, 22] it is expected that the PFDT layer within a pore will form a higher quality layer than a DT layer and hence yield a smaller pore. DT monolayers form a thinner layer than PFDT as a consequence of weaker intermolecular forces and a more disordered configuration, leading often to collapsed DT molecules [14]. This explains the lower transport rate observed as the effective pore diameter of a PFDT-membrane would be smaller than a DT-membrane.

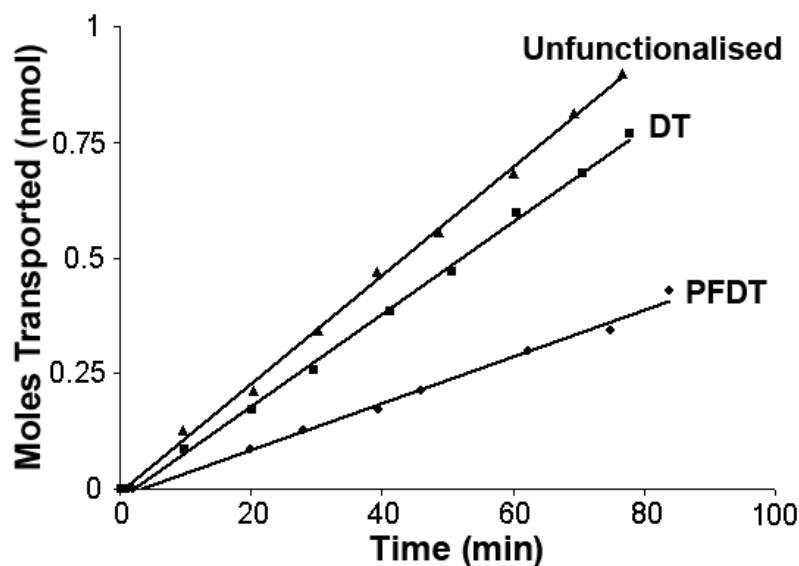


Figure 4-4 Transport of the hydrophilic dye (RB) through an unfunctionalised membrane and membranes functionalised with decanethiol and perfluorodecanethiol.

4.4. CONCLUSIONS

Gold nanotube membranes were successfully synthesised using the electroless deposition technique, forming gold nanotubes within the pores of a porous polycarbonate membrane. The functionalisation of gold nanotube membranes with

SAMs of fluorinated thiols (PFDT) was demonstrated showing that the transport and selectivity properties of gold nanotube membranes can be varied by functionalisation using thiol chemistry. PFDT functionalised membranes showed excellent sensitivity for the transport of hydrophobic molecules over hydrophilic molecules. Their transport, selectivity and stability properties were superior in comparison to membranes functionalised with alkanethiol monolayers such as decanethiol.

4.5. REFERENCES

1. Demoustier-Champagne, S., and Delvaux, M., *Preparation of polymeric and metallic nanostructures using a template-based deposition method*. Materials Science and Engineering C, 2001. **15**: p. 269–271.
2. Nishizawa, M., Menon, V.P., and Martin, C.R., *Metal Nanotubule Membranes with Electrochemically Switchable Ion-Transport Selectivity*. Science, 1995. **268**: p. 700-702.
3. Menon, V.P., and Martin, C.R., *Fabrication and Evaluation of Nanoelectrode Ensembles*. Analytical Chemistry, 1995. **67**: p. 1920- 1928.
4. Gilliam, R.J., Thorpe, S.J., and Kirk, D.W., *A nucleation and growth study of gold nanowires and nanotubes in polymeric membranes*. Journal of Applied Electrochemistry, 2007. **37**(2): p. 233-239.
5. De Leo, M., Kuhn, A., and Ugo, P., *3D-ensembles of gold nanowires: Preparation, characterization and electroanalytical peculiarities*. Electroanalysis, 2007. **19**(2-3): p. 227-236.
6. De Leo, M., Pereira, F.C., Moretto, L.M., Scopece, P., Polizzi, S., and Ugo, P., *Towards a better understanding of gold electroless deposition in track-etched templates*. Chemistry of Materials, 2007. **19**(24): p. 5955-5964.
7. Hulteen, J.C., Jirage, K.B., and Martin, C.R., *Introducing Chemical Transport Selectivity into Gold Nanotubule Membranes*. Journal of the American Chemical Society, 1998. **120**: p. 6603-6604.
8. Fukushima, H., Seki, S., Nishikawa, T., Takiguchi, H., Tamada, K., Abe, K., Colorado, R., Graupe, M., Shmakova, O.E., and Lee, T.R., *Microstructure, wettability, and thermal stability of semifluorinated self-assembled monolayers (SAMs) on gold*. Journal of Physical Chemistry B, 2000. **104**(31): p. 7417-7423.
9. Schlenoff, J.B., Li, M., and Ly, H., *Stability and self-exchange in alkanethiol monolayers*. Journal of the American Chemical Society, 1995. **117**(50): p. 12528-12536.
10. Zamborini, F.P. and Crooks, R.M., *Corrosion passivation of gold by n- alkanethiol self-assembled monolayers: Effect of chain length and end group*. Langmuir, 1998. **14**(12): p. 3279-3286.

11. Schoenfisch, M.H. and Pemberton, J.E., *Air stability of alkanethiol self-assembled monolayers on silver and gold surfaces*. Journal of the American Chemical Society, 1998. **120**(18): p. 4502-4513.
12. Delamarche, E., Michel, B., Kang, H., and Gerber, C., *Thermal-stability of self-assembled monolayers*. Langmuir, 1994. **10**(11): p. 4103-4108.
13. Horn, A.B., Russell, D.A., Shorthouse, L.J., and Simpson, T.R.E., *Ageing of alkanethiol self-assembled monolayers*. Journal of the Chemical Society-Faraday Transactions, 1996. **92**(23): p. 4759-4762.
14. Tamada, K., Ishida, T., Knoll, W., Fukushima, H., Colorado, R., Graupe, M., Shmakova, O.E., and Lee, T.R., *Molecular packing of semifluorinated alkanethiol self-assembled monolayers on gold: Influence of alkyl spacer length*. Langmuir, 2001. **17**(6): p. 1913-1921.
15. Miura, Y.F., Takenaga, M., Koini, T., Graupe, M., Garg, N., Graham, R.L., and Lee, T.R., *Wettabilities of self-assembled monolayers generated from CF₃-terminated alkanethiols on gold*. Langmuir, 1998. **14**(20): p. 5821-5825.
16. Alves, C.A. and Porter, M.D., *Atomic force microscopic characterization of a fluorinated alkanethiolate monolayer at gold and correlations to electrochemical and infrared reflection spectroscopic structural descriptions*. Langmuir, 1993. **9**(12): p. 3507-3512.
17. Chidsey, C.E.D. and Loiacono, D.N., *Chemical functionality in self-assembled monolayers: structural and electrochemical properties*. Langmuir, 1990. **6**(3): p. 682-691.
18. Cosmacini, E. and Veronesi, V., *A study of the tribological behaviour of perfluoro-polyethers*. Wear, 1986. **108**.
19. Grampel, R.D.v.d., *Surfaces of Fluorinated Polymer Systems*. 2002: Technische Universiteit Eindhoven.
20. Finklea, H.O., *Self-assembled monolayers on electrodes*, in *Encyclopedia of Analytical Chemistry*, R.A. Meyers, Editor. 2006, John Wiley & Sons Ltd: Chichester.
21. Liu, G.Y., Fenter, P., Chidsey, C.E.D., Ogletree, D.F., Eisenberger, P., and Salmeron, M., *An unexpected packing of fluorinated n-alkane thiols on Au(111): A combined atomic force microscopy and x-ray diffraction study*. Journal of Chemical Physics, 1994. **101**(5): p. 4301-4306.

22. Jirage, K.B., Hulteen, J.C., and Martin, C.R., *Effect of thiol chemisorption on the transport properties of gold nanotubule membranes*. Analytical Chemistry, 1999. **71**(21): p. 4913-4918.
23. Bemporad, D., Essex, J.W., and Luttmann, C., *Permeation of small molecules through a lipid bilayer: A computer simulation study*. Journal of Physical Chemistry B, 2004. **108**(15): p. 4875-4884.
24. Paula, S., Volkov, A.G., VanHoek, A.N., Haines, T.H., and Deamer, D.W., *Permeation of protons, potassium ions, and small polar molecules through phospholipid bilayers as a function of membrane thickness*. Biophysical Journal, 1996. **70**(1): p. 339-348.
25. Janshoff, A. and Steinem, C., *Transport across artificial membranes - an analytical perspective*. Analytical and Bioanalytical Chemistry, 2006. **385**(3): p. 433-451.
26. Ulbricht, M., *Advanced functional polymer membranes*. Polymer, 2006. **47**: p. 2217–2262.
27. Lodish, H., Darnell, J., Matsudaira, P., Baltimore, D., and Berk, B., *Molecular cell biology*. 1995: W. H. Freeman Company.

CHAPTER 5

THE EFFECTS OF SURFACE FUNCTIONALITY POSITIONING ON THE TRANSPORT PROPERTIES OF MEMBRANES

Several hybrid membrane structures based on polycarbonate membranes were created in which gold was deposited on different areas on the membrane; on one of the membrane interfaces, within the pores of the membrane and completely coating all surfaces of the membrane. Gold-thiol chemistry was exploited in which the thiols only assembled on the gold coated regions of the membrane thus providing controlled positioning of functional regions. The effects of the controlled positioning of functional groups on the transport properties of the membrane were investigated.

5.1. INTRODUCTION

Surface modification can result in highly selective separations due to the chemical interaction between the permeate and the molecules on the surface [1-2] and can also be used to produce anti-fouling surfaces [3]. However, the application of surface modification in commercial membranes is not widely considered other than their use as anti-fouling coatings [4-6]. Research into exploiting surface chemistry to enhance transport selectivity and sensing is relatively new but is exceedingly important especially in the biotechnology industry, which requires separation of complex, and often quite similar, biomolecules and controlled delivery of drugs. Consequently, surface modification is an important factor in membrane design as it has the potential to increase the flux, selectivity and stability of the membrane.

Polycarbonate membranes were used in this study due to their uniform cylindrical pores and narrow pore size distribution [4]. These membranes can be considered model systems for investigating membrane transport phenomena. Therefore in regards to the pore structure, polycarbonate membranes bear a much closer resemblance to an ideal membrane structure. However, polycarbonate membranes do not offer a suitable surface to proceed with further surface chemistry modifications. Therefore, electroless deposition was used to coat the polycarbonate membranes with gold, this procedure provides the ability to tailor surface properties by chemical and biochemical functionalisation [8-14]. A range of molecules can be attached to gold via a thiol linkage [5-6], thereby altering the membrane surfaces with functional groups. The immobilisation of appropriate functional groups on the membrane surface allows for selective transport of permeate molecules [1].

The groundwork for this study is based on the experiments described in chapter 4. This chapter presents the investigation of the effect on the transport properties of membranes functionalised with SAMs. In particular, the effect of the positioning of functional groups on the membrane has previously not been investigated. Such studies are important to give insight into how surface modifications may impact the transport properties of porous membranes in order to develop more efficient separation processes. Therefore in our work we have devised a set of membranes in

which only specific regions of the membrane are functionalised. We have used the electroless gold deposition method and gold sputter coating to provide control over which areas of the membrane are coated in gold and hence the areas of the membrane that can be subsequently functionalised with SAMs of thiols. In this work we produced several differently structured gold nanotube membranes based on polycarbonate membranes. This was achieved by coating different areas of the polycarbonate membrane with gold, one with gold coating the membrane entirely (external surfaces and within the pores); $\text{Au}_{(\text{ext}+\text{pore})}\text{PC}$ membrane, one with gold coated only within the pores; $\text{Au}_{(\text{pore})}\text{PC}$ membrane and a membrane coated in gold only one interface; $\text{Au}_{(\text{ext})}\text{PC}$ membrane (Figure 5-1). Here interface refers to the face of the membrane that will be facing the feed solution during transport studies. The membranes were later functionalised with thiols in which the thiols only assembled on the areas of the membrane where gold has been deposited (Figure 5-1).

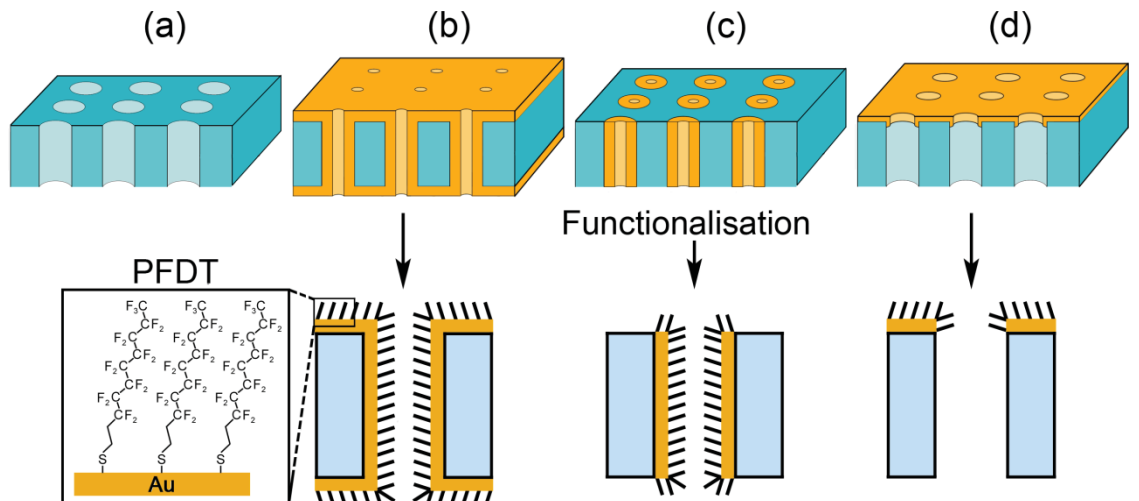


Figure 5-1 Schematics of the hybrid gold-polycarbonate structures investigated in this study; (a) unmodified PC, (b) $\text{Au}_{(\text{ext}+\text{pore})}\text{PC}$, (c) $\text{Au}_{(\text{pore})}\text{PC}$ and (d) $\text{Au}_{(\text{ext})}\text{PC}$ and corresponding cross sectional images of the membranes after functionalisation, displaying the areas PFDT is adsorbed on.

5.2. EXPERIMENTAL DETAILS

5.2.1. Electroless gold deposition

Electroless deposition was used to fabricate the $\text{Au}_{(\text{ext}+\text{pore})}\text{PC}$ and $\text{Au}_{(\text{pore})}\text{PC}$ membranes. The gold deposition procedure outlined in section 0 was carried out with

the following modifications. A gold deposition time of 20 h was used in this study which significantly reduces the pore size of the membrane without closing the pores. This gold deposition procedure produces the $\text{Au}_{(\text{ext+pore})}\text{PC}$ membrane in which the gold is deposited on all surfaces including those at the interface and within the pores of the membrane. In order to produce the $\text{Au}_{(\text{pore})}\text{PC}$ membrane one more step is carried out which involves removing the layers of gold on the membrane by wiping the surfaces with a cotton tip whilst the membrane is still wet.

5.2.2. Gold sputtering onto polycarbonate membranes

In order to fabricate the $\text{Au}_{(\text{ext})}\text{PC}$ membrane, polycarbonate membranes were sputtered with 12 nm of gold on the top interface of the membrane. A high vacuum turbo evaporation system, EMITECH K975X (Quorum technologies, UK), was used for the sputter coating of membranes with thin gold films. The thickness of deposited films was precisely controlled by the thickness monitor located inside the chamber.

5.2.3. Investigation of membrane transport properties

Transport experiments were carried out as stated in section 2.4.1. In this particular study ethanolic solutions of the hydrophobic dye, pinacyanol chloride (PCN), and the hydrophilic dye, rose bengal (RB), were used to probe the transport properties of the membranes. Their absorption spectra were monitored at 606.09 nm for PCN and 552.20 nm for RB.

5.3. RESULTS AND DISCUSSION

5.3.1. Fabrication and characterisation of gold - polycarbonate membranes

SEM was used to examine the surface morphology of the $\text{Au}_{(\text{ext+pore})}\text{PC}$, $\text{Au}_{(\text{pore})}\text{PC}$ and $\text{Au}_{(\text{ext})}\text{PC}$ membranes. Images of the various membranes are shown in Figure 5-2. The rough gold surface seen on the $\text{Au}_{(\text{ext+pore})}\text{PC}$ membrane is the typical morphology of gold films prepared by electroless deposition (Figure 5-2a). The

electroless deposition of gold provided a significant reduction in the pore diameter of the $\text{Au}_{(\text{ext+pore})}\text{PC}$ and $\text{Au}_{(\text{pore})}\text{PC}$ membranes (Figure 5-2 (a-b)) in comparison with the uncoated PC membranes (Figure 5-2c inset). For the $\text{Au}_{(\text{ext+pore})}\text{PC}$ and $\text{Au}_{(\text{pore})}\text{PC}$ membranes the pore size has been reduced to molecular dimensions and the pores are below the resolution of the SEM. Therefore samples were prepared using the same gold deposition procedure but with PC membranes with larger pore sizes (80 nm) in order to illustrate the reduction in the pore size achievable with electroless deposition (Figure 5-3). The pore diameter of the 80 nm PC membranes have been reduced to 29.4 ± 6.5 nm and 43.8 ± 13.3 nm for a $\text{Au}_{(\text{ext+pore})}\text{PC}$ and $\text{Au}_{(\text{pore})}\text{PC}$ membrane respectively. SEM images for the $\text{Au}_{(\text{pore})}\text{PC}$ membranes confirm that the gold layers on the interfaces of the membrane were removed successfully. The only gold present on the interface of the membrane is attributed to the tips of the gold nanotubes which have formed within the pores of the membrane (light rings, Figure 5-3b). The $\text{Au}_{(\text{ext})}\text{PC}$ membrane was formed through sputter coating one of the interfaces of the polycarbonate membrane with 12 nm of gold. From SEM images (Figure 5-2c) there has been a decrease in the pore size from 30 nm to 15 nm. The surface of the sputter coated membrane appears smoother and more homogeneous than the electroless deposition coated membranes.

Cross sections of the membranes were viewed under a TEM in order to confirm gold deposition within the pores of the $\text{Au}_{(\text{ext+pore})}\text{PC}$ and $\text{Au}_{(\text{pore})}\text{PC}$ membranes and the absence of gold within the pores of the $\text{Au}_{(\text{ext})}\text{PC}$ membrane (Figure 5-4). In the cross section for the $\text{Au}_{(\text{ext+pore})}\text{PC}$ membrane the gold is deposited on the top and bottom surfaces of the membrane and also within the pores (Figure 5-4a). For the $\text{Au}_{(\text{pore})}\text{PC}$ membrane gold is seen to be distributed only within the pores (Figure 5-4b). Due to the slightly tortuous nature of the pores in commercial polycarbonate membranes, it is not possible to form a cross section exactly along the grain of the pores which is why it appears in these images that the gold does not extend the entire length. However, gold is seen to be deposited in the centre of the membrane which indicates that gold deposition has extended through the entire thickness of the membrane. The TEM image for the $\text{Au}_{(\text{ext})}\text{PC}$ membrane (Figure 5-4c) confirms gold deposition has occurred on the top surface of the membrane and there is no evidence of gold within the pores.

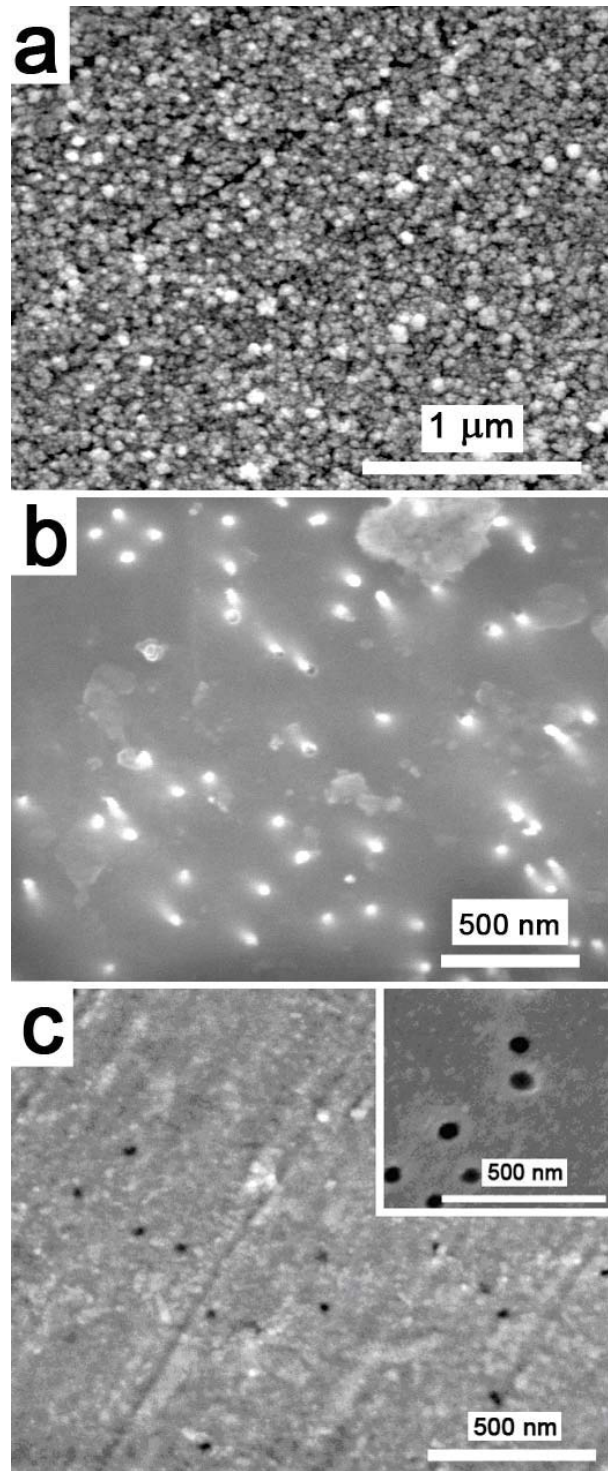


Figure 5-2 SEM images of the surface of the a) $\text{Au}_{(\text{ext+pore})}\text{PC}$, b) $\text{Au}_{(\text{pore})}\text{PC}$ and c) $\text{Au}_{(\text{ext})}\text{PC}$ membranes used in this study. Inset: 30 nm unmodified PC membrane.

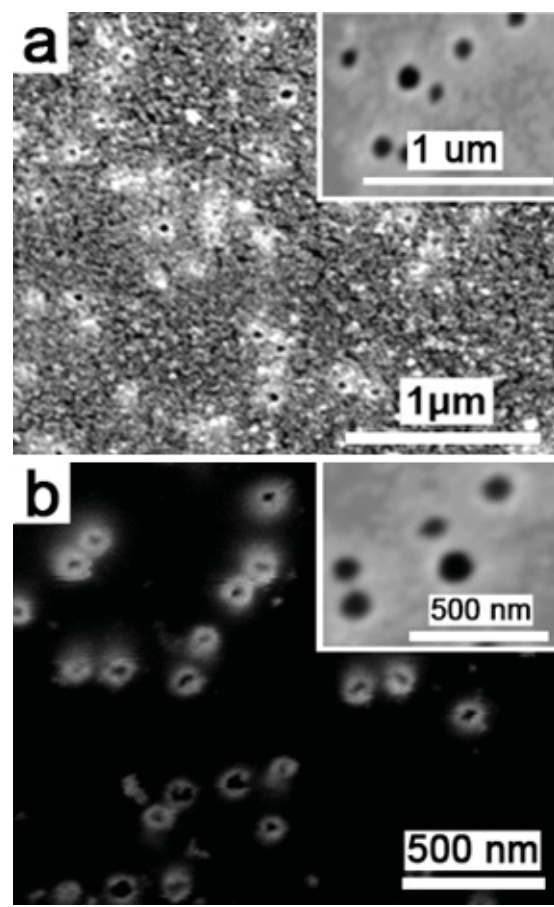


Figure 5-3 SEM images of (a) Au_(ext+pore)PC membrane and (b) Au_(pore)PC membrane based on 80 nm pore size polycarbonate membranes. Inset: uncoated polycarbonate membrane.

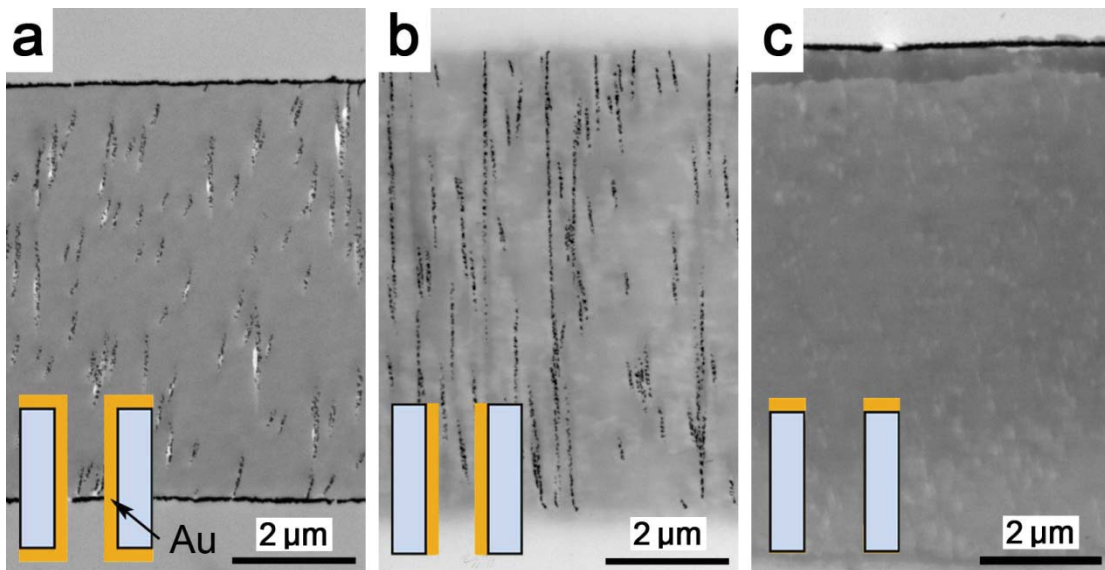


Figure 5-4 TEM images of the cross section of (a) $\text{Au}_{(\text{ext}+\text{pore})}\text{PC}$, (b) $\text{Au}_{(\text{pore})}\text{PC}$ and (c) $\text{Au}_{(\text{ext})}\text{PC}$ membranes. The dark regions are region of high gold concentrations. Insets: schematics of their corresponding membrane cross-section.

5.3.2. Surface functionalisation of gold - polycarbonate membranes

For the three Au-PC membranes fabricated, chemical specificity either on the entirety of the membrane, only within the pores of the membrane or only on one of the interface of the membrane can be produced. Chemical selectivity is imparted to the gold nanotube membranes by incorporating the highly hydrophobic and durable thiol, perfluorodecanethiol (PFDT). The SAM is formed wherever the gold is deposited therefore controlling the areas of the membrane that are functionalised with the hydrophobic thiol. Water droplet contact angle measurements were performed in order to verify attachment of the thiol to the gold surface and to determine the effects of hydrophobic surface functionalisation. Further evidence of PFDT attachment to gold membranes was ascertained in chapter 4 using cyclic voltammetry to determine the blocking of the gold surface by the thiols and the ability to remove the thiols.

Table 5-1 displays the water contact angle measurements on the surfaces of unfunctionalised and PFDT-functionalised membranes. For the $\text{Au}_{(\text{ext}+\text{pore})}\text{PC}$ membrane an increase in contact angle from 53° to 94° is observed after functionalisation which is expected as the face of the membrane is coated with gold

and hence subsequently covered with PFDT. For this same reason, a fairly large contact angle increase (from 76° to 103°) is also observed for the $\text{Au}_{(\text{ext})}\text{PC}$ membrane (Table 5-1). Both $\text{Au}_{(\text{ext+pore})}\text{PC}$ and $\text{Au}_{(\text{ext})}\text{PC}$ membranes have gold completely covering the face of the membrane and therefore the hydrophobic thiol will self assemble onto the face of these membranes. However, a larger increase in contact angle is observed for the electrolessly coated surface which is most likely attributed to the roughness of the electroless gold layer. Superhydrophobic surfaces are attained when the surfaces are made exceedingly rough [7]. Electroless deposition occurs as the nucleation and growth of gold nanoparticles [8] thus generating a slightly rougher surface than the sputter coating method.

In the case of the $\text{Au}_{(\text{pore})}\text{PC}$ membrane the contact angle remained relatively constant after PFDT modification (see Table 5-1). This is due to the removal of the layer of gold on the top surface of the membrane and so the thiol will attach only to the gold within the pores. This result confirms that the technique used for the removal of the gold layers on the faces of the membrane is effective.

While these contact angle results confirm the attachment of thiols onto the gold, they only describe the environment at the face of the membrane and not the chemical environment within the pores and hence do not represent the hydrophobic properties of the full membrane material. Therefore transport experiments with probe dyes are a much more suitable method to ascertain the full extent that thiol modification has on the properties of the membrane.

The contact angle experiments give insight into the solvent structuring of water in the vicinity of fluorocarbon layers. Whilst fluorocarbon layers are expected to have a greater affinity to water than their hydrocarbon counterparts, layers consisting of fluorocarbons are found to be hydrophobic. The enhanced hydrophobicity of fluorinated SAMs is due to the bulkiness of the thiols and hence larger thiol interspacing resulting in poorer van der Waals interactions with water [9]. The interactions of water with fluorinated layers are found to be primarily van der waals interactions and not dependent on electrostatic interactions [9]. The decreased van

der waals interactions with water are expected to influence the transport rates of the dyes through the functionalised membranes.

Table 5-1 Advancing contact angle measurements for the unfunctionalised and PFDT functionalised Au-PC membranes.

<i>Membrane structure</i>	<i>Contact angle (°) for unfunctionalised membrane</i>	<i>Contact angle (°) for PFDT-functionalised membrane</i>
Au_(ext+pore)PC	52.9 ± 6.2	93.5 ± 1.8
Au_(pore)PC	68.2 ± 6.3	70.5 ± 4.7
Au_(ext)PC	76.3 ± 2.9	102.7 ± 1.4

5.3.3. *Transport properties of gold – polycarbonate membranes*

To explore the transport and selectivity properties of hydrophobic (PFDT) modified hybrid Au-PC membranes, the flux of the dyes: PCN (hydrophobic) and RB (hydrophilic) were measured. The transport experiments carried out provide detailed information on the interactions between the dyes and the surface functional molecules allowing determination of the impact that the positioning of functional molecules has on the transport properties of the membrane. Figure 5-5 presents the transport of the probe dyes through the Au_(ext+pore)PC, Au_(pore)PC and Au_(ext)PC membranes before and after surface modification with PFDT. Straight-line plots are obtained indicating steady state (Fick's first law [10]) diffusion across the membrane. A summary of the permeation data of these dyes through functionalised and unfunctionalised Au-PC membranes is presented in Table 5-2. In this study it is important to note the transport results for the Au_(ext+pore)PC and Au_(pore)PC membranes can be directly compared, however the Au_(ext)PC membrane transport data cannot be directly compared to the Au_(ext+pore)PC and Au_(pore)PC membranes as the pore size is considerably larger for the Au_(ext)PC membrane (10-15 nm pore size). The transport rates of the dyes though the Au_(ext)PC membrane is almost a magnitude larger than that observed for the Au_(ext+pore)PC and Au_(pore)PC membranes (Table 5-2) due to the considerably larger pore size.

Table 5-2 Transport and selectivity properties of functionalised and bare gold membranes (errors obtained from three replicate measurements).

<i>Membrane</i>	<i>Treatment</i>	<i>PCN</i>	<i>RB</i>	<i>Flux Ratio</i> (<i>PCN:RB</i>)	<i>Increase in</i> <i>flux ratio</i>
Au_(ext+pore)PC	Bare	4.02 x 10 ⁻⁸	5.12 x 10 ⁻⁹	7.85	107%
		± 2.64 x 10 ⁻⁹	± 5.81 x 10 ⁻¹⁰		
	PFDT	3.76 x 10 ⁻⁸	2.31 x 10 ⁻⁹	16.28	
		± 1.47 x 10 ⁻⁹	± 2.03 x 10 ⁻¹⁰		
Au_(pore)PC	Bare	4.17 x 10 ⁻⁸	5.43 x 10 ⁻⁹	7.68	24%
		± 2.24 x 10 ⁻⁹	± 5.47 x 10 ⁻¹⁰		
	PFDT	3.95 x 10 ⁻⁸	4.12 x 10 ⁻⁹	9.59	
		± 2.24 x 10 ⁻⁹	± 1.68 x 10 ⁻¹⁰		
Au_(ext)PC	Bare	2.82 x 10 ⁻⁷	1.06 x 10 ⁻⁷	2.65	15%
		± 3.36 x 10 ⁻⁸	± 1.53 x 10 ⁻⁸		
	PFDT	2.52 x 10 ⁻⁷	8.08 x 10 ⁻⁸	3.12	
		± 1.42 x 10 ⁻⁸	± 3.68 x 10 ⁻⁹		

For each of the unfunctionalised Au-PC membranes, there is already a separation of the two dyes (Table 5-2, Figure 5-5). The observed difference in transport is due to the variation in the diffusion coefficients of the dyes which are attributed to factors such as the size, charge, shape and solubility of the molecules in the solvent. The unfunctionalised membrane transport data is primarily used as a basis to compare the functionalised membrane results to and hence ascertain the precise impact of functionalisation of the transport properties of the membrane. As the Au_(ext+pore)PC and Au_(pore)PC membranes have comparable structure dimensions, similar degrees of dye separation for these membranes are observed (the flux ratio of PCN:RB is 7.27 and 7.68 respectively). The dye transport rates through the unfunctionalised Au_(ext+pore)PC and Au_(pore)PC membranes are similar as the structures of these membranes and are identical with the exception of the absence of gold layers on the

interface of the $\text{Au}_{(\text{pore})}\text{PC}$ membrane. These membranes have the same pore size and their thicknesses are comparable regardless of the presence or absence of gold layers on the faces of the membrane. The thickness of the electroless gold layer on the interface of the $\text{Au}_{(\text{ext+pore})}\text{PC}$ membrane (Figure 5-4a) is negligible compared to the overall thickness of the membrane ($\sim 6 \mu\text{m}$). The unfunctionalised $\text{Au}_{(\text{ext})}\text{PC}$ membrane exhibits a smaller flux ratio of 2.65 as the pore size is significantly larger than the size of the probe dyes, thus offering less resistance to their transport. As properties such as shape and size have an impact on the diffusion properties of the dyes, any minute differences in these properties between the dyes will be less distinguishable at larger pore sizes due to less confinement and surface – molecule interactions.

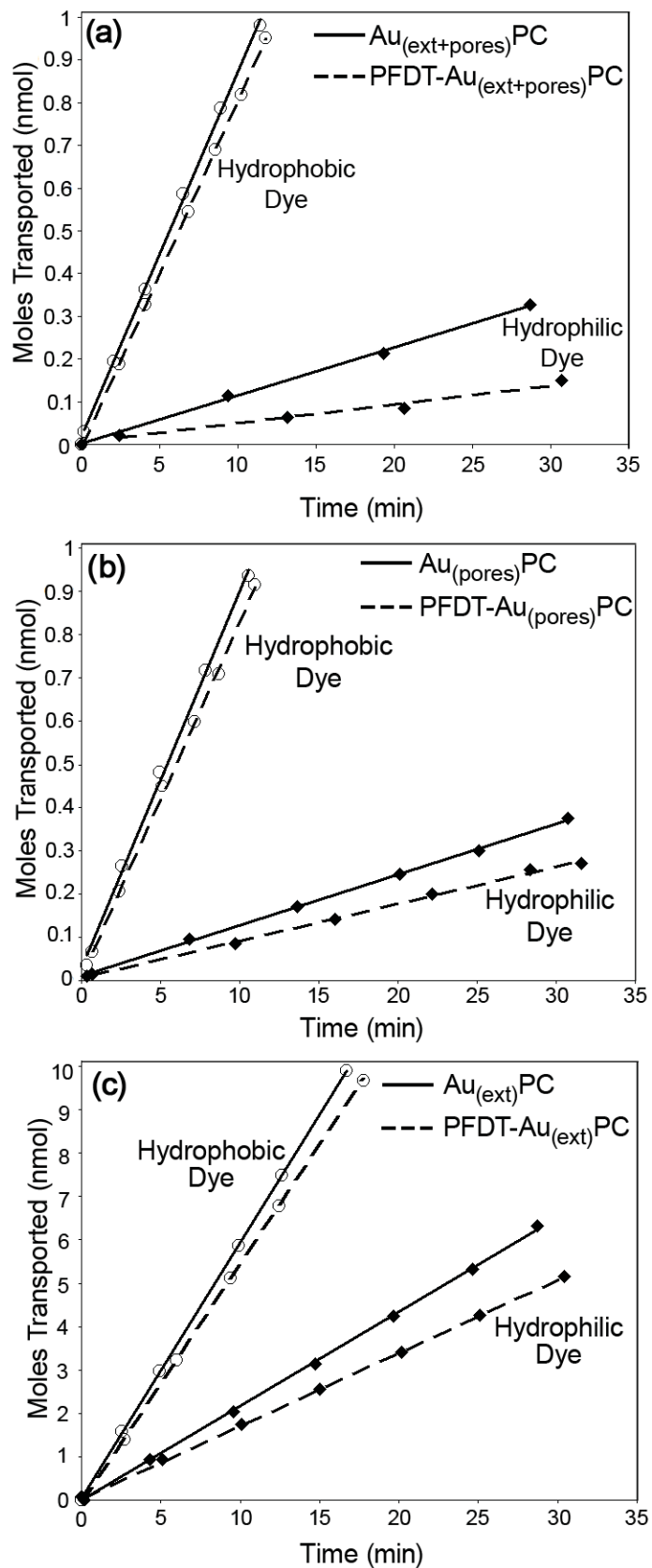


Figure 5-5 Transport of hydrophobic (PCN) and hydrophilic (RB) dye through unmodified and PFDT-modified (a) $\text{Au}_{(\text{ext+pores})}\text{PC}$ (b) $\text{Au}_{(\text{pore})}\text{PC}$ and (c) $\text{Au}_{(\text{ext})}\text{PC}$ membrane.

The overall effect of functionalising the Au-PC membranes with PFDT results in a hindrance in the transport of the hydrophilic dye leading to an increase in the flux ratio of the membrane (Table 5-2). Therefore through instilling a hydrophobic surface functionality to the membrane we have created a membrane with hydrophobic properties which can enhance the separation between hydrophilic and hydrophobic molecules. It is important to consider the partitioning of organic solutes into the SAM formed within the pores. The ability for molecules to partition into molecular layers such as SAMs and lipid bilayers and the impact this has on transport properties have been explored and reported in the recent literature [11-14]. In our case it is likely that PCN can partition into the thiol layers and thus diffusion across the membrane can occur through both the thiol layer and the solvent in the centre of the pore resulting in similar PCN transport rates through PFDT modified and unmodified membranes. The PFDT modified membranes exhibits a hydrophobic environment in which the hydrophilic dye would not enter into easily. Furthermore, it is unlikely that the RB will partition into the hydrophobic organic monolayer and hence the reduction of the transport rate can also be attributed to a reduction in the pore diameter from the adsorbed monolayer. These contributing factors lead to an overall decrease in the transport of RB through the PFDT modified membranes. Thus the PFDT modified membranes facilitate the transport of hydrophobic species through the membrane while hindering the transport of hydrophilic species. While the $\text{Au}_{(\text{ext})}\text{PC}$ membrane displays the smallest increase in flux ratio (15 %), this membrane facilitates transport of the dyes a magnitude faster than the $\text{Au}_{(\text{ext+pore})}\text{PC}$ and $\text{Au}_{(\text{pore})}\text{PC}$ membranes due to the considerably larger pore size. While the $\text{Au}_{(\text{ext+pore})}\text{PC}$ and $\text{Au}_{(\text{pore})}\text{PC}$ membranes present larger increases in the flux ratios after functionalisation (107 % and 24 % respectively), these membranes exhibit smaller rates of transport due to the small pore diameters.

$\text{Au}_{(\text{ext+pore})}\text{PC}$ membranes exhibit the greatest increase in selectivity of the hydrophobic dye over the hydrophilic dye after surface modification with PFDT (Table 5-2). After functionalisation the membrane exhibits an increase in flux ratio of 107 % which is due to the entire membrane being coated in the hydrophobic thiol layer. This membrane presents an environment into which the hydrophilic dye will

not partition into easily. The major influence on the permeability and flux of a particular molecule through the membrane will be due to the ability of the molecule to partition into the membrane. The partition coefficient is expected to differ for the different chemical environments introduced into the membranes by means of surface functionalisation. The partition coefficient K or “solubility” of the molecules between the membrane and the adjacent solution is defined by

$$K = \frac{C_{M0}}{C_{F0}} \quad (1)$$

where C_{M0} is the concentration immediately within the membrane and C_{F0} is the feed solution concentration adjacent to the face of the membrane. Figure 5-6a describes the concentration profile for RB as it approaches the PFDT-Au_(ext+pore)PC membrane, where C_F is the feed cell concentration, C_{F0} is the concentration of the feed solution immediately at the interface of the membrane, C_{M0} is the concentration immediately inside the membrane and C_P is the concentration of the permeate solution. The gradient of the concentration profile within the membrane describes the rate of transport across the membrane. The concentration profile of RB as it approaches the face of the membrane will diminish due to the hydrophobic layer positioned on the face of the membrane ($C_{F0} < C_F$, Figure 5-6a). A lower concentration at the interface of the membrane will result in a smaller concentration difference across the membrane and hence less driving force for the molecule to pass through the membrane. Furthermore, C_{M0} will be much smaller than C_{F0} due to the thiol layer present within the pores, thus resulting in a small partition coefficient (Eq. 1). Each of these factors contribute to a decreased concentration gradient across the membrane. The hydrophobic dye transport has not changed much with the addition of the hydrophobic thiol layer. Therefore, the inclusion of this SAM has not hindered the transport of the hydrophobic dye through the membrane.

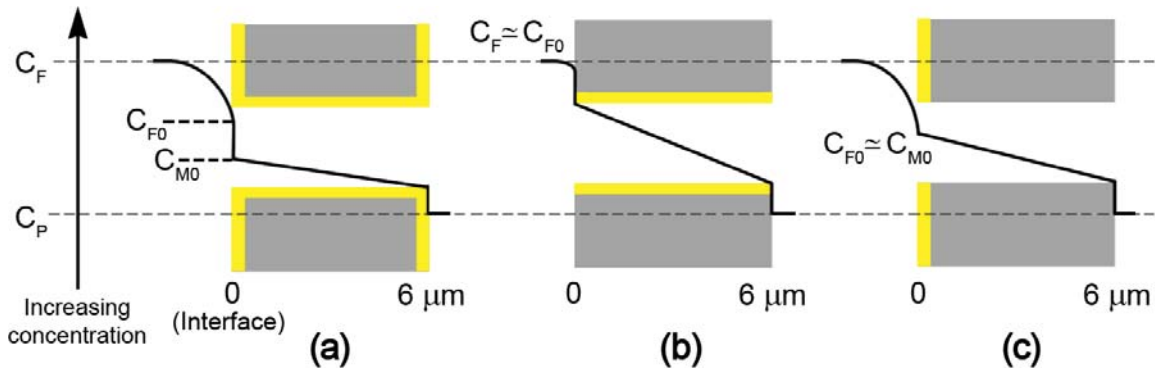


Figure 5-6 Concentration profiles for RB across PFDT modified a) $\text{Au}_{(\text{ext}+\text{pore})}\text{PC}$, b) $\text{Au}_{(\text{pore})}\text{PC}$ and c) $\text{Au}_{(\text{ext})}\text{PC}$ membranes.

The $\text{Au}_{(\text{pore})}\text{PC}$ membrane exhibits a slight increase in the flux ratio after the thiol is incorporated within the pores. Furthermore, the increase in flux ratio signifies that thiol deposition has occurred within the confines of the pore. Raman spectroscopy was used to confirm the presence of SAMs within the confined geometries of the pores as discussed in chapter 3. SAMs are shown to have disordered orientation and poor packing within narrow pores [15] which can partially explain the small increase in flux ratio of 24 %, considerably lower than the increase observed for the $\text{Au}_{(\text{ext}+\text{pore})}\text{PC}$ membrane (107 %). The small increase could be due to a disordered SAM layer within the pores and a lower density of thiols. However, the difference between the flux increase of the $\text{Au}_{(\text{ext}+\text{pore})}\text{PC}$ and $\text{Au}_{(\text{pore})}\text{PC}$ membranes is too large to only be attributed to the disorder of the thiol layer within the pores. The smaller increase in the flux ratio for the $\text{Au}_{(\text{pore})}\text{PC}$ membrane is most likely due to the absence of the thiol layer on the face of the membrane. Figure 5-6b represents the concentration profile of RB in the PFDT- $\text{Au}_{(\text{pore})}\text{PC}$ membrane. Due to the absence of the hydrophobic layer on the surface of the PFDT- $\text{Au}_{(\text{pore})}\text{PC}$ membrane, there will only be minor rejection of the hydrophilic dye away from the surface. Therefore the concentration immediately adjacent to the membrane face (C_{F0}) will only be slightly smaller than the concentration of the feed solution (C_F). There will be a slight decrease in the concentration of RB directly within the membrane (C_{M0}) due to the hydrophobic layer within the pores. The ability of RB to partition into the $\text{Au}_{(\text{pore})}\text{PC}$ membrane is low due to the thiols within the pores, however C_{F0} for $\text{Au}_{(\text{pore})}\text{PC}$ is larger than C_{F0} for $\text{Au}_{(\text{ext}+\text{pore})}\text{PC}$ and so there is a larger concentration difference of RB across the $\text{Au}_{(\text{pore})}\text{PC}$ membrane and hence a larger RB flux is observed. Due to the significant difference in RB transport rates between the $\text{Au}_{(\text{ext}+\text{pore})}\text{PC}$ and

$\text{Au}_{(\text{pore})}\text{PC}$ membranes it is evident that surface functionalisation plays a larger role than internal pore functionalisation in governing the transport properties of the membrane. As with the $\text{Au}_{(\text{ext+pore})}\text{PC}$ membrane, the transport of the hydrophobic dye has not been hindered due to the incorporation of the hydrophobic thiol.

The $\text{Au}_{(\text{ext})}\text{PC}$ membrane shows a slight increase in selectivity when functionalised with PFDT due to a decrease in the transport of the hydrophilic dye (Table 5-2). Given that the pore size is larger than the $\text{Au}_{(\text{ext+pore})}\text{PC}$ and $\text{Au}_{(\text{pore})}\text{PC}$ membranes, this increase in selectivity is therefore more profound. The increase in selectivity for the PFDT- $\text{Au}_{(\text{ext})}\text{PC}$ membrane is 15 % which is comparable to the $\text{Au}_{(\text{pore})}\text{PC}$ membrane while still obtaining fluxes a magnitude greater. The concentration profile of the $\text{Au}_{(\text{ext})}\text{PC}$ membrane (Figure 5-6c) is similar to the $\text{Au}_{(\text{ext+pore})}\text{PC}$ membrane. The concentration of the dye at the surface of the membrane will taper off due to the presence of PFDT. Although there is a lower RB concentration at the face of the $\text{Au}_{(\text{ext})}\text{PC}$ membrane, much like the $\text{Au}_{(\text{ext+pore})}\text{PC}$ membrane, the ability of the dye to permeate into the membrane is high due to no hindrance from thiols within the pores. With smaller pore sizes, the flux ratio of the PFDT- $\text{Au}_{(\text{ext})}\text{PC}$ membrane would be expected to improve greatly as more forced molecule-surface interactions will occur. These results support the conclusion that interface interactions have a larger contribution to the transport properties of the membrane than pore interactions.

5.4. CONCLUSION

The production of several hybrid gold-polycarbonate membrane structures has been demonstrated where the regions of gold deposition was controlled using sputtering and electroless deposition techniques. Modification of the surface properties of the membranes was carried out using a hydrophobic thiol (PFDT) in which PFDT only assembled on the gold coated regions of the membranes thus providing controlled positioning of functional areas. Overall, modification with PFDT resulted in a hindrance in the transport of the hydrophilic dye and an enhancement in the separation between hydrophilic and hydrophobic molecules. However, the $\text{Au}_{(\text{ext+pore})}\text{PC}$ membrane was found to exhibit the greatest increase in selectivity of the hydrophobic dye over the hydrophilic dye after PFDT modification (107 %),

while the $\text{Au}_{(\text{pore})}\text{PC}$ membrane exhibited a significantly lower flux ratio (24 %). The increase in flux ratio of the $\text{Au}_{(\text{ext})}\text{PC}$ membrane after PFDT modification (15 %) is comparable to the $\text{Au}_{(\text{pore})}\text{PC}$ membrane. However, given that the $\text{Au}_{(\text{ext})}\text{PC}$ pore size is larger than the $\text{Au}_{(\text{pore})}\text{PC}$ membrane and facilitates dye flux a magnitude higher, this increase in selectivity is more noteworthy. Therefore, it is apparent that membrane interface functionalisation contributes more to the transport properties of the membrane than pore functionalisation. The ability to repel molecules away from the interface appears to be the governing factor in the membrane's ability to control the transport properties.

5.5. REFERENCES

1. Hulteen, J.C., Jirage, K.B., and Martin, C.R., *Introducing Chemical Transport Selectivity into Gold Nanotubule Membranes*. Journal of the American Chemical Society, 1998. **120**: p. 6603-6604.
2. Majumder, M., Chopra, N., and Hinds, B.J., *Effect of tip functionalization on transport through vertically oriented carbon nanotube membranes*. Journal of the American Chemical Society, 2005. **127**(25): p. 9062-9070.
3. Ulbricht, M., Matuschewski, H., Oechel, A., and Hicke, H.G., *Photo-induced graft polymerization surface modifications for the preparation of hydrophilic and low-protein-adsorbing ultrafiltration membranes*. Journal of Membrane Science, 1996. **115**(1): p. 31-47.
4. Fleisher, R.L., Price, P.B., and Walker, R.M., *Nuclear tracks in solids: Principles and applications*. 1975, Berkeley, California: University of California Press. 626.
5. Schreiber, F., *Structure and growth of self-assembling monolayers*. Progress in Surface Science, 2000. **65**(5-8): p. 151-256.
6. Love, J.C., Estroff, L.A., Kriebel, J.K., Nuzzo, R.G., and Whitesides, G.M., *Self-assembled monolayers of thiolates on metals as a form of nanotechnology*. Chemical Reviews, 2005. **105**(4): p. 1103-1169.
7. Zhang, X., Shi, F., Niu, J., Jiang, Y.G., and Wang, Z.Q., *Superhydrophobic surfaces: from structural control to functional application*. Journal of Materials Chemistry, 2008. **18**(6): p. 621-633.
8. Gilliam, R.J., Thorpe, S.J., and Kirk, D.W., *A nucleation and growth study of gold nanowires and nanotubes in polymeric membranes*. Journal of Applied Electrochemistry, 2007. **37**(2): p. 233-239.
9. Dalvi, V.H. and Rossky, P.J., *Molecular origins of fluorocarbon hydrophobicity*. Proceedings of the National Academy of Sciences of the United States of America, 2010. **107**(31): p. 13603-13607.
10. Fick, A., *Poggendorff's Annal. Physik*, 1855. **94**: p. 59-86.
11. Bemporad, D., Essex, J.W., and Luttmann, C., *Permeation of small molecules through a lipid bilayer: A computer simulation study*. Journal of Physical Chemistry B, 2004. **108**(15): p. 4875-4884.

12. Paula, S., Volkov, A.G., VanHoek, A.N., Haines, T.H., and Deamer, D.W., *Permeation of protons, potassium ions, and small polar molecules through phospholipid bilayers as a function of membrane thickness*. Biophysical Journal, 1996. **70**(1): p. 339-348.
13. Janshoff, A. and Steinem, C., *Transport across artificial membranes - an analytical perspective*. Analytical and Bioanalytical Chemistry, 2006. **385**(3): p. 433-451.
14. Ulbricht, M., *Advanced functional polymer membranes*. Polymer, 2006. **47**: p. 2217–2262.
15. Jirage, K.B., Hulteen, J.C., and Martin, C.R., *Effect of thiol chemisorption on the transport properties of gold nanotubule membranes*. Analytical Chemistry, 1999. **71**(21): p. 4913-4918.

CHAPTER 6

STRUCTURAL AND CHEMICAL MODIFICATION OF POROUS ALUMINA MEMBRANES

Atomic layer deposition (ALD) of silica (SiO_2) was applied to porous alumina (PA) membranes with the aim of fine-tuning pore diameters and chemical selectivity. The chemical functionalisation of silica coated PA membranes with a perfluorodecyldimethylchlorosilane (PFDS) shows that the transport and selectivity properties of silica composite PA membranes can be varied by functionalisation using silane chemistry.

6.1. INTRODUCTION

Porous inorganic membranes with nanoscale pore diameters have attracted considerable interest in the last two decades for applications in various fields such as molecular separation, adsorption, catalysis, energy storage, biosensing, cell culture, template synthesis and drug delivery [1-5]. Among them, porous alumina (PA) membranes fabricated by electrochemical anodisation of aluminium are one of the most popular porous materials [1]. In regards to their controllable pore dimension and adjustable surface chemistry, these membranes have the potential to be used as an ideal model for fundamental and practical studies of molecular transport in membrane science and nanofluidics. PA membranes have recently become commercially available as filtration membranes, but are produced with a limited selection of pore diameters (20, 100 and 200 nm). The main disadvantage of these membranes is their relatively large minimum pore diameter (20 nm) which significantly limits their ability for molecular sieving and therefore restricts their application for separation of smaller molecules or gases. One of the fundamental issues is to manage both molecular diffusion and size selectivity properties as a function of pore size and their surface chemistry. To improve the size exclusion properties of PA membranes it is essential to reduce the pore diameter to a size that is comparable with molecular dimensions. In addition, through exploiting the chemical features of surface modifications of PA and the molecule to be selectively transported, the separation properties of the membranes can be tailored to suit specific applications.

A variety of surface modification techniques have been explored to improve the performance and properties of PA membranes including chemical vapour deposition (CVD), atomic layer deposition (ALD), thermal metal deposition, chemical and electrochemical metal deposition, plasma polymerisation, ion milling, sol-gel and layer by layer deposition [2-8]. Whilst the majority of the studies outlined in this thesis involve structurally modifying porous materials with gold via electroless deposition, this study explores ALD as an alternative technique for structural modification. ALD appears to be a promising strategy for the modification of PA as it provides conformal coatings with monolayer precision and permits the deposition of a broad range of materials including oxides, nitrides, sulphides and metals [9-15].

ALD of silica, titania and alumina to reduce the pore dimensions and therefore improve size selectivity properties of membranes has been successfully demonstrated by S.M. George and others [9-11, 14]. However, these studies did not include surface modification of ALD modified membranes which can impart chemical selectivity to the membrane and further improve separation properties. Hence, the aim of this work is to improve the separation properties of PA membranes by combining structural and chemical modification of their pores. We present a two step modification approach which includes ALD deposition of silica onto PA membranes (Si-PA membranes) and surface functionalisation by an ultra-thin organic film of silane. A schematic of the proposed approach is shown in Figure 6-1. In the first step, structural modification of PA membranes is achieved using ALD to perform the controlled reduction of the pore diameters to the desired dimensions. ALD deposition of silica has been chosen because of ease of functionalisation by silane chemistry, which provides a broad selection of silanes containing different functional groups, charge and interfacial properties [16]. The highly hydrophobic silane, perfluorodecyldimethylchlorosilane (PFDS) was employed in the second step of PA modification to impart chemical selectivity to the Si-PA membranes. The transport properties and selectivity of silane-Si-PA membranes towards hydrophobic and hydrophilic organic molecules are presented.

6.2. EXPERIMENTAL DETAILS

6.2.1. *Fabrication and functionalisation of silica modified porous alumina membranes via atomic layer deposition*

Details regarding the fabrication of Si-PA membranes can be found in section 2.1.3. The procedure used for functionalising the Si-PA membranes can be obtained from section 2.2.2.

6.2.2. Investigation of membrane transport properties

Transport experiments were carried out as stated in section 2.4.1. In this particular study aqueous solutions of the hydrophobic dye, tris(2,2'-bipyridyl)dichlororuthenium(II) hexahydrate (Rubpy), and the hydrophilic dye, rose

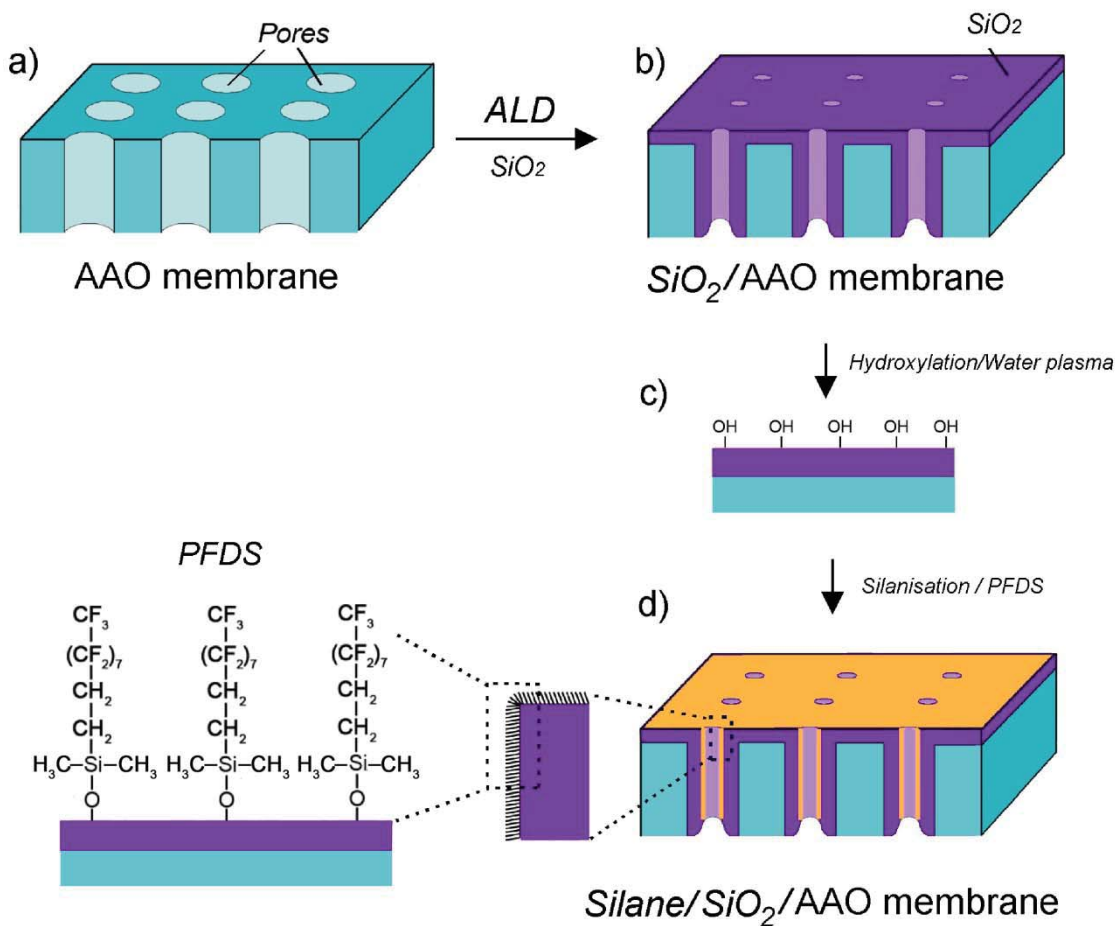


Figure 6-1 Schematic of the structural and chemical modification of PA membranes which includes (a) bare membrane, (b) atomic layer deposition (ALD) of silica, (c) hydroxylation step by water plasma and (d) functionalisation of silica modified PA membranes by perfluorodecyldimethylchlorosilane (PFDS). The top of the pores is presented.

bengal (RB), were used to probe the transport properties of the membranes. Their absorption spectra were monitored at 286.34 nm for Rubpy and 549.12 nm for RB. The PA membranes used for transport experiments were PA membranes coated with 5 cycles of Si deposition. These particular membranes were chosen for the transport experiments as they had the smallest pore size obtainable or greatest number of Si

deposition cycles before the pores were blocked. Partially blocked pores were obtained after 7 cycles. The membrane with the smallest pore size before becoming blocked was chosen to demonstrate the enhanced separation of molecular-sized species and also after PFDS functionalisation there would be maximum interaction of the solute with the functionalised pore walls of the membrane. To allow a direct comparison between unfunctionalised and functionalised membranes, transport experiments were first carried out with the unfunctionalised membrane then the same membrane was functionalised with PFDS and the transport experiment was repeated. Furthermore the transport experiments were taken for several modified and unmodified membranes to confirm the reproducibility of the membrane fabrication process.

6.3. RESULTS AND DISCUSSION

6.3.1. *Characterisation of modified porous alumina membranes*

The influence of ALD deposition cycles on the morphological changes of PA was investigated with particular focus on the reduction of the size of pore openings. A series of film deposition experiments were performed using PA membranes with different pore sizes (20, 100 and 200 nm). Figure 6-2 shows a series of typical SEM images of the top surface of PA membranes (20 nm pore diameters) before (Figure 6-2a) and after ALD deposition of silica (Figure 6-2b-d). Figure 6-2a presents the surface morphology of an unmodified commercial PA membrane which confirms non-uniform pore organisation, non-circular pore geometry and considerable variation of the pore size. Cross-sectional SEM images of the membrane profile structure confirm the asymmetric nature of PA membranes with a bulk pore structure comprised of straight channels with large diameters at the bottom and a very thin porous layer at the top with smaller pore openings (Figure 6-4f). These characteristics are expected from commercial PA membranes and are consistent with other reports [17].

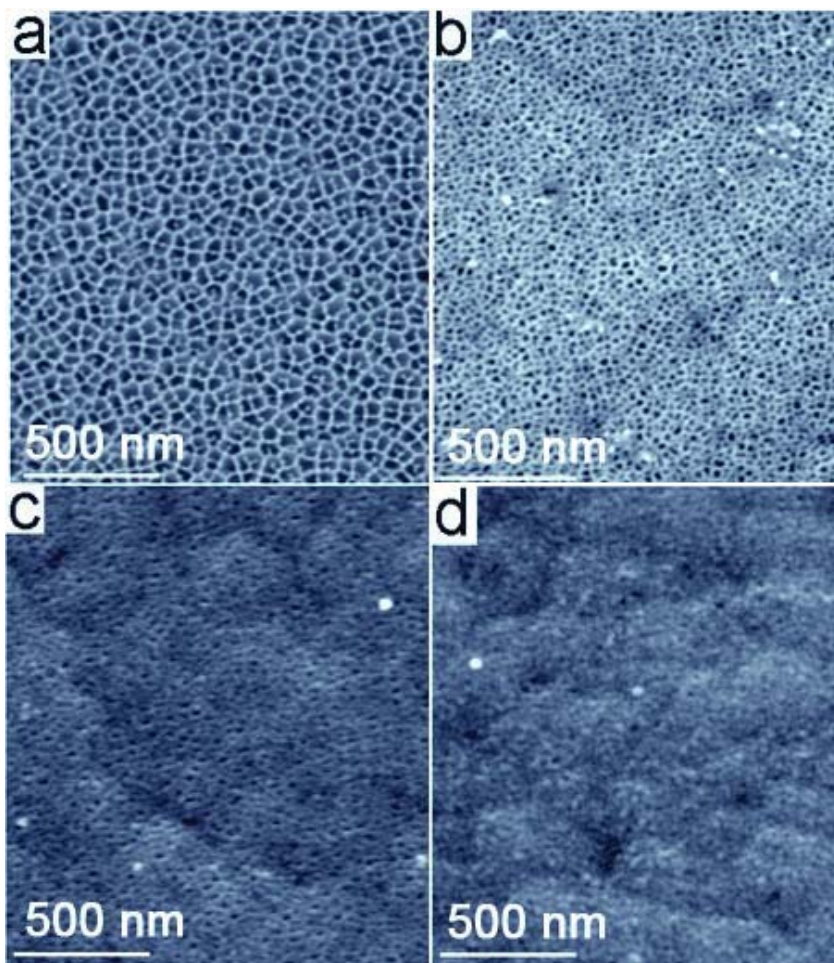


Figure 6-2 The reduction of pore diameters of PA membranes by ALD deposition of silica using different numbers of cycles. SEM images of PA membranes (20 nm pores) before (a) and after silica modification using (b) 3 ALD cycles, (c) 5 ALD cycles and (d) 7 ALD cycles.

Comparative SEM images of PA membranes (20 nm) after ALD deposition of silica using different numbers of cycles (3, 5 and 10) are shown in Figure 6-2b-d. In comparison with unmodified PA, these images clearly show the presence of the deposited film and the changes to the top surface topography of the membranes. SEM images and corresponding histograms of pore size distributions show that the pore size of modified PA membranes was reduced by increasing the number of cycles of SiO_2 deposition as a direct consequence of increasing film thickness. The correlation between the decrease in pore diameters and number of ALD cycles is shown in Figure 6-3. This graph shows that the pore diameters decrease monotonically with increasing number of ALD cycles up to 10 ALD cycles when the pores appear to be completely blocked (Figure 6-2d). The observed pore reduction

was in agreement with the film thickness measured on the control samples and calculated growth rate.

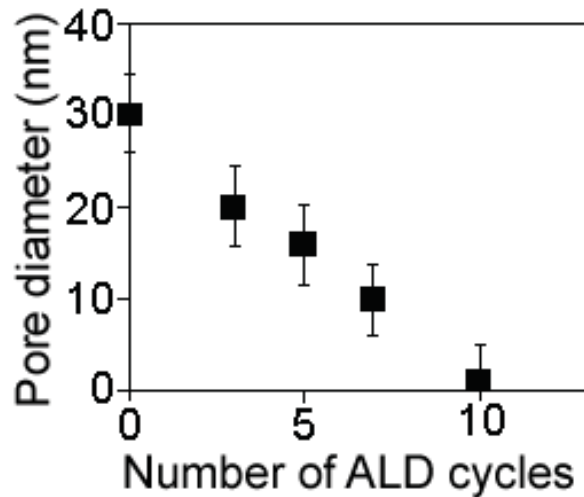


Figure 6-3 The correlation of the pore diameters and number of ALD cycles (PA membranes with 20 nm pores).

Therefore to reduce the pore diameter of PA membranes with larger pores (100 and 200 nm) it is essential to use a higher number of cycles (10 and 20). SEM images in Figure 6-4a–c illustrate the pore reduction of 100 nm PA membranes that have been modified with an increased number of ALD cycles. The mean diameter of pores was reduced to 40–50 nm and <10 nm using 10 and 20 ALD cycles respectively. Figure 6-4d–f shows SEM images of 200 nm PA membranes modified by 20 cycles where the diameter of pores were reduced to 80–100 nm. This confirms the importance of correlating the deposition conditions (number of cycles) or the film thickness with the pore dimensions. These results clearly show that with ALD it is possible to reduce larger pore diameters of PA to desired dimensions and proves that the ALD technique can be successfully used for controlled structural modification of membranes. The results are in agreement with previous studies of PA membranes where the reduction of pores to about 1–2 nm was achieved [12-13]. Furthermore, controlled reduction of pore structures has been demonstrated in our previous work using ALD of titania on diatoms and track-etched membranes [18-19]. Therefore ALD can be used for the structural modification of PA membranes with the capability to fabricate membranes with pore diameters comparable to molecular dimensions in order to achieve size selective separations.

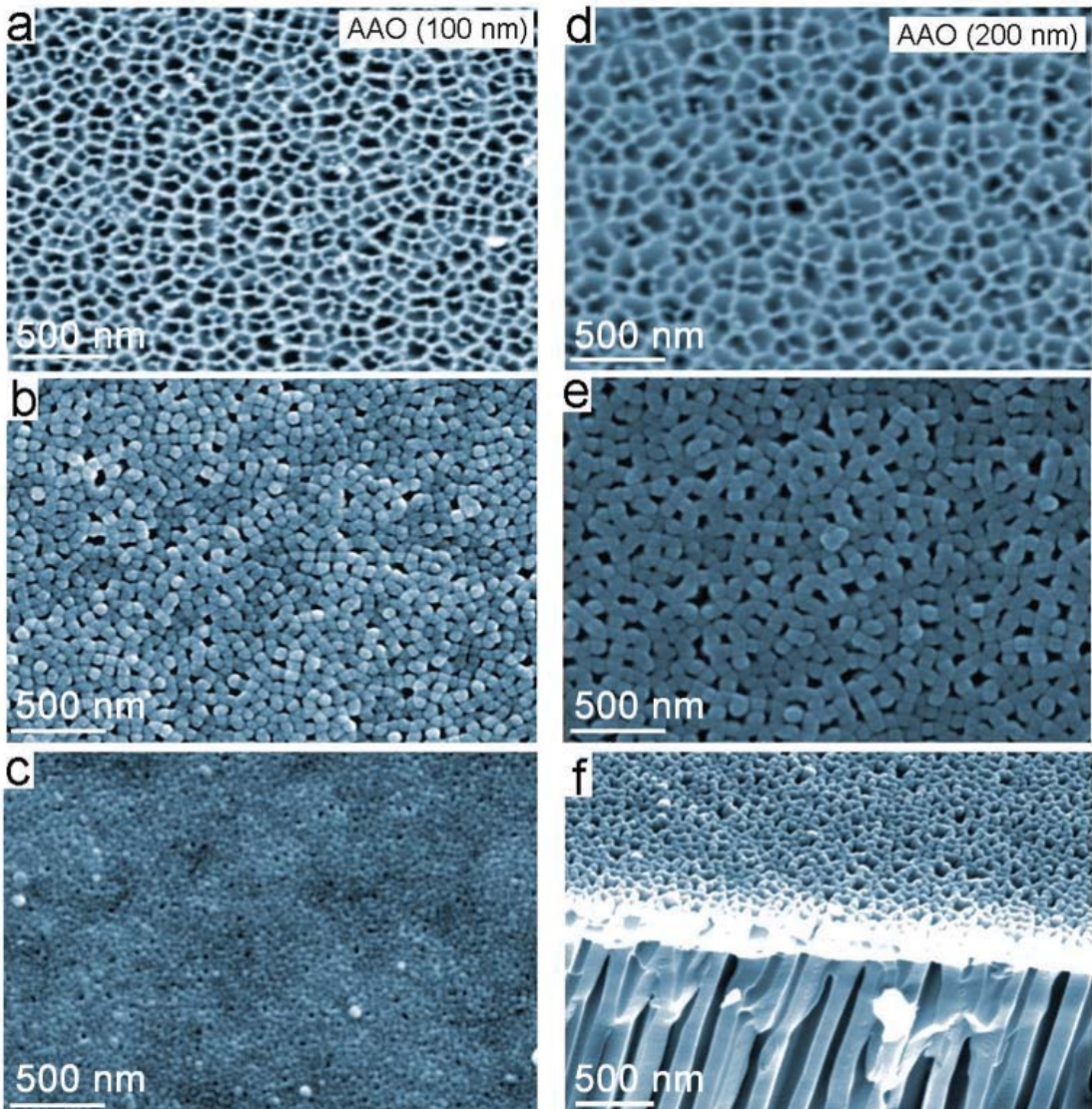


Figure 6-4 SEM images of PA membranes with larger pore diameters (100 and 200 nm) before and after ALD silica modifications. (a–c) PA membrane (100 nm pores) before (a) and after ALD deposition using (b) 10 ALD cycles and (c) 20 ALD cycles. (d–f) PA membrane (200 nm pores) before (d) and after ALD deposition using (e) 20 ALD cycles with (f) corresponding to a cross-section image.

Unfortunately, cross-sectional SEM images could not confirm the quality of ALD modification inside the pores (Figure 6-4f). Creating cross-sectional TEM and SEM samples is extremely difficult for PA, thus our investigational techniques are limited in the determination of the depth penetration of the silica into the channels. However, a recent study showed that the thickness of the silica layer slowly decreases inside of the pores as a result of limited diffusion through the nanopore's length [20]. This conclusion is based on modelling of ALD deposition inside cylindrical nanopores which demonstrates that the tapering of deposited layers inside pores is dependent on

experimental parameters in the ALD process and the dimensions of the nanopores [20]. However, in regards to the asymmetrical pore structure of commercial PA membranes and the presence of the top porous layer consisting of smaller diameter pores (about 1 μm in length), the existing model cannot predict in our case how the silica layer will decrease over the length of the pore. Dynamic SIMS analysis was performed to investigate the distribution of the Si element on and into the porous membrane structure as a result of ALD deposition of silica. A typical depth profile of Si and Al obtained from the top surface of a SiO_2 modified PA membrane is shown in Figure 6-5a. This profile clearly shows that SiO_2 was present on the membrane and that a significantly higher density was observed on the outer surface compared with the diminishing Si signal and increasing of Al as the profiling extends deeper in the pores. This result is in agreement with the model which predicts decrease in thickness of the ALD layer as a function of depth inside the pore. Further investigation using combined focused ion beam milling (FIB) and dynamic SIMS is underway to determine the depth and morphology of SiO_2 inside the pores. EDAX graphs of silica modified PA (Figure 6-5b and c) confirmed the existence of the Si peak and silica chemical composition of the top membrane surface. The intensity of Si peak increased with the number of ALD cycles applied during deposition verifying the increase in thickness of the SiO_2 layer on the top and the inside of pores.

Surface modification of Si-PA membranes with the highly hydrophobic fluorosilane, PFDS, was confirmed with contact angle measurements. A contact angle of 12° was observed on bare PA and unmodified Si-PA membranes (Figure 6-6a). Membrane functionalised with the hydrophobic silane showed a significant increase in the contact angle from 12° to 109° (Figure 6-6b) confirming that the surface of the Si-PA membrane was successfully functionalised with the highly hydrophobic silane. Based on other studies reported in literature and our recent work on modification of PA with 3-amino propyltriethoxysilane (APTES), we are certain that the silane layer is assembled inside the pores [21]. Even though the thickness of the SiO_2 coatings diminished slowly with their penetration into the pores, the silane will assemble onto both silica and alumina surfaces. Therefore after functionalisation the entire membrane will be coated in the silane. Furthermore as we have discussed in chapter

5, it is the external surface of the membrane that influences the transport properties of the membrane. Hence the modifications made to the surface Si layer will have the largest impact on the separation abilities.

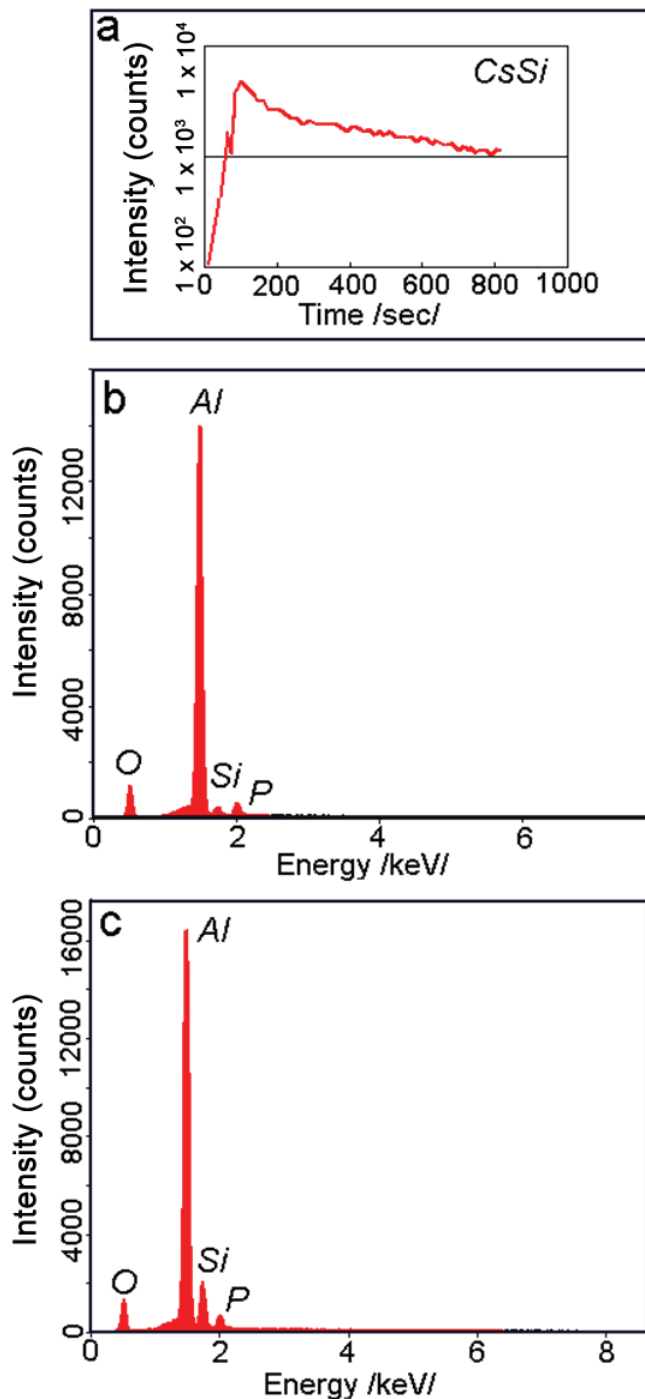


Figure 6-5 (a) The depth profile of an Si-PA membrane displaying the distribution of Si, obtained by dynamic SIMS analysis using a Cs^+ primary ion beam rastered from the top of the Si-PA membrane (20 nm pores, 3 cycles), (b) EDAX analysis graphs from Si-PA prepared by (b) 5 and (c) 10 ALD cycles.

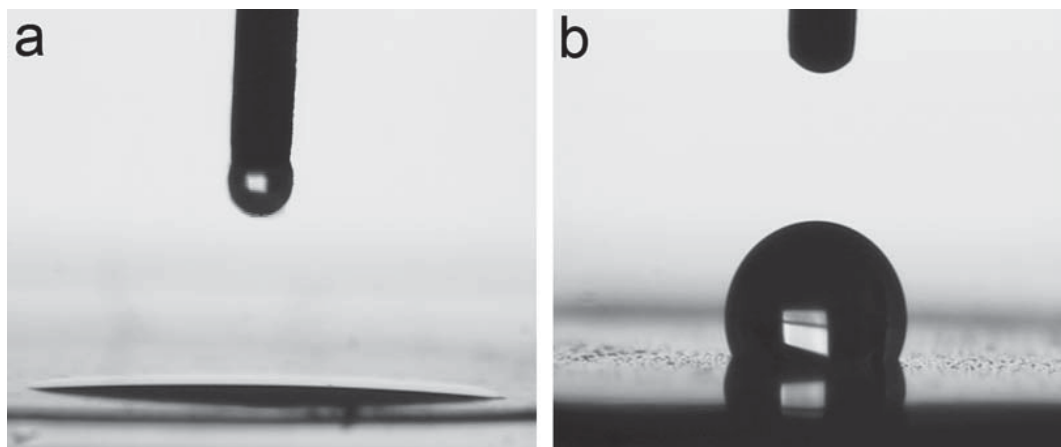


Figure 6-6 Images of a water droplet on (a) an unmodified Si-PA membrane (b) a PFDS modified Si-PA membrane (20 nm pores, 5 ALD cycles).

6.3.2. *Transport and selectivity of modified PA membranes*

The transport and selectivity properties of PFDS modified Si-PA membranes were explored using two dyes: tris(2,2'-bipyridyl) dichlororuthenium(II) hexahydrate (Rubpy) and rose bengal(RB), which have hydrophobic and hydrophilic properties, respectively. A summary of the permeation data of these dyes through functionalised and unfunctionalised membranes are shown in Table 6-1. The flux of the dyes through each of the membranes was recorded and the ratio of the flux for Rubpy to the flux for RB (flux ratio) was determined. Figure 6-7 represents the transport of both dyes through unfunctionalised Si-PA membranes and PFDS functionalised Si-PA membranes. In Figure 6-7a, it appears the flux of the hydrophobic dye (Rubpy) is larger than the hydrophilic dye (RB) even though the unmodified Si-PA membrane is hydrophilic, however this discrepancy is due to factors such as the solubility of the dyes in the solvent and their bulk diffusion rates and so the data for the unmodified membranes are used as a reference point for the transport rates through modified membranes. The data from Figure 6-7 confirms that the hydrophobic dye (Rubpy) is allowed to pass freely through both membranes (unfunctionalised and functionalised) while the transport of the hydrophilic dye is hindered when the membrane is functionalised. Thus through functionalizing the membrane with a hydrophobic silane it has become chemically selective, allowing the transport of hydrophobic species while the transport of hydrophilic species is hindered. From Table 6-1 it can be seen that the flux ratio of the membrane has increased from 2.46 when

unfunctionalised to 5.52 after functionalisation, leading to an increase in the flux ratio of 124 %.

Table 6-1 Summary of permeation data of hydrophobic (tris(2,2'-bipyridyl)dichlororuthenium(II) hexahydrate, Rubpy) and hydrophilic (rose bengal, RB) through perfluorodecyldimethylchlorosilane (PFDS) functionalised and unfunctionalised ALD silica modified PA membranes (Si-PA). PA membranes with 20 nm pores, modified by 5 ALD cycles were used.

Si-PA Membrane	Flux of permeate molecule (mol cm ⁻² h ⁻¹)		Flux Ratio Rubpy:RB
	Rubpy	RB	
Bare	5.42 x 10 ⁻⁷ ± 7.34 x 10 ⁻⁹	2.20 x 10 ⁻⁷ ± 1.24 x 10 ⁻⁸	2.46
PFDS functionalised	5.24 x 10 ⁻⁷ ± 4.55 x 10 ⁻⁸	9.49 x 10 ⁻⁸ ± 1.61 x 10 ⁻⁸	5.52

To interpret transport data of molecules through membranes, it is important to consider the driving force for the diffusion of molecules through the unmodified and silane modified channels of the membrane. As discussed in section 1.3, the diffusion of molecules through membranes due to concentration gradients is described by Fick's law of diffusion;

$$J = P(C_1 - C_2) \quad \text{Eq (1)}$$

where J is the flux across the membrane, P is the permeability coefficient, C_1 is the concentration in the feed cell and C_2 is the concentration in the permeate cell [19].

And,

$$P = \frac{DK}{L} \quad \text{Eq (2)}$$

where D is the diffusion coefficient, K is the partition coefficient and L is the thickness of the membrane. The permeability coefficient is dependent on the permeate, membrane material and the nature of the solvent [22]. The partition coefficient K is the ratio of the concentration of species at the membrane interface to the concentration of the species in the bulk solution. Thus the partition coefficient represents the affinity of the permeant for the membrane versus the solvent. The

diffusion coefficient D controls the rate of approach to concentration equilibrium [22].

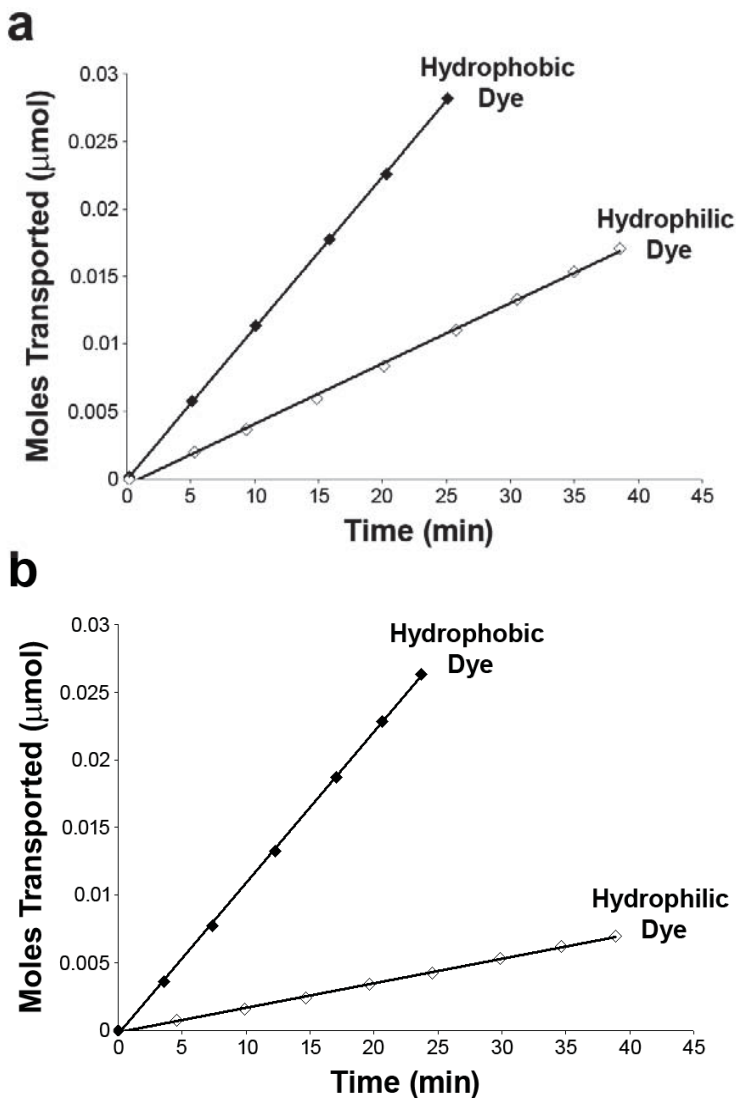


Figure 6-7 Transport of a hydrophobic (Rubpy) and a hydrophilic dye (RB) through (a) unmodified silica PA membranes (Si-PA) and (b) perfluorodecyldimethylchlorosilane (PFDS) modified Si-PA membranes (20 nm pores, 5 ALD cycles).

When comparing the flux of a particular dye through modified and unmodified membranes, the only change is the PFDS onto the membrane. The concentration difference, permeate, and solvent are kept constant during the experiments, which means from Eq. (1), the flux will be dependent on the permeability coefficient. As the permeability coefficient is dependent only on the permeant, membrane material and the nature of the solvent, this means that in our case variations in flux will only be due to the change in the nature of the membrane [23]. Modifications made to the

membrane will alter the ability of the dyes to partition within the membrane. The flux of the dyes through a particular membrane differ due to the nature of the dye, its permeability into the membrane phase, size of the molecules and solubility or diffusion in the solvent.

The transport of Rubpy through modified and unmodified membranes present similar transport rates (Table 6-1), which means the permeability coefficients must be comparable (Eq. (1)). Thus the ability of the hydrophobic dye to diffuse into the modified and PFDS-modified membranes is equivalent. This is perhaps a surprising result as the narrowing of the pores by the adsorbed monolayer would be expected to hinder the diffusion. However, the structure of PFDS within confined spaces such as pores is not well ordered and so the occlusion of the pores by the PFDS will be minimal [24-25]. Furthermore, with the incorporation of PFDS onto the membrane, the affinity for the hydrophobic dye to this hydrophobic membrane will increase. Even though the effective pore diameter has decreased with the adsorption of the silane layer, the partition coefficient, K , will become larger which in turn will increase the flux to compensate for the slightly smaller pore size. Consequently the affinity of Rubpy to the hydrophobic membrane offsets any effects from the decrease in pore diameter.

Figure 6-7 also compares the hindrance of the unmodified and PFDS modified membranes towards the transport of the hydrophilic dye, RB. The introduction of the hydrophobic silane decreases the rate of transport of the hydrophilic species through the pore in comparison with unmodified membranes (Table 6-1). This is expected as there is a reduction of the pore diameter due to the assembly of the silanes within the pore leading to a reduction of the diffusion coefficient. Furthermore as the functionalised membrane exhibits a hydrophobic environment the hydrophilic dye will not favour diffusion into the membrane. In our case the hydrophilic dye will be more soluble in the bulk solvent than in the hydrophobic environment within the membrane, thus the partition coefficient, K , will have decreased leading to a reduction in the flux of the dye (Eq. (1)). In contrast to the analysis of transport for the hydrophobic dye, the reduction of the transport rate is attributed to the decrease in affinity of the hydrophilic dye for the hydrophobic membrane in addition to the decreased pore size. The transport characteristics for the PFDS modified membranes

are similar to that of the PFDT-Au membranes as studied in chapters 4 and 5. This is due to the similarities between the PFDS and PFDT layers. Both SAMs contain a terminal fluorinated group which imparts hydrophobic properties to the membranes resulting in the hindrance of hydrophilic species and the free passage of hydrophobic species.

Furthermore, the silica and alumina surfaces will be slightly negatively charged in aqueous solution and this only reinforces the pronounced effect that PFDS functionalisation has on these membranes. Both unmodified Si-PA membranes and RB are negatively charged, therefore there is a hindrance of the transport of RB through the negatively charged membrane. However after functionalisation with the hydrophobic silane PFDS, a neutral surface is produced and so RB does not experience any hindrance due to the electrostatic effects and the flux would be expected to increase. However, RB will experience hindrance due to the hydrophobicity of this silane layer which reduces the flux of RB even further than the original negative membrane.

6.4. CONCLUSIONS

The structural and chemical modification of commercial PA porous membranes has been successfully implemented. Modification of PA membranes by ALD of silica has been employed to obtain controlled deposition of ultra-thin silica conformal films. The presented results show that the structural (pore size) properties of PA membranes can be altered systematically by adjusting the number of ALD cycles. The pore sizes of the PA membranes were reduced to allow molecular separations. The chemical functionalisation of silica coated PA membranes with a fluoro silane (PFDS) was demonstrated showing that the transport and selectivity properties of silica composite PA membranes can be varied by functionalisation using silane chemistry. The hydrophobic PFDS-modified membranes showed superior sensitivity to the transport of hydrophobic molecules over hydrophilic molecules. The resultant silica/PA membranes with specific surface chemistry and controlled pore size are desirable for molecular separation, cell culture, tissue engineering, bioreactors,

biosensing and drug delivery. The proposed processing scheme has potential to be extended to the development of composite membranes using other porous platforms.

6.5. REFERENCES

1. Diggle, J.W., Downie, T.C., and Goulding, C.W., *Anodic oxide films on Aluminium*. Chemical Reviews, 1969. **69**: p. 365.
2. Cameron, M.A., Gartland, I.P., Smith, J.A., Diaz, S.F., and George, S.M., *Atomic layer deposition of SiO₂ and TiO₂ in alumina tubular membranes: Pore reduction and effect of surface species on gas transport*. Langmuir, 2000. **16**(19): p. 7435-7444.
3. Alsyouri, H.M., Langheinrich, C., Lin, Y.S., Ye, Z.B., and Zhu, S.P., *Cyclic CVD modification of straight pore alumina membranes*. Langmuir, 2003. **19**(18): p. 7307-7314.
4. McCleskey, M., Ehler, D.S., Young, J.S., Pesiri, D.R., Jarvinen, G.D., Sauer, N.N. , *Asymmetric membranes with modified gold films as selective gates for metal ion separations*. Journal of Membrane Science, 2002. **210**: p. 273–278.
5. Popat, K.C., Mor, G., Grimes, C.A., and Desai, T.A., *Surface modification of nanoporous alumina surfaces with poly(ethylene glycol)*. Langmuir, 2004. **20**(19): p. 8035-8041.
6. Nagale, M., Kim, B.Y., and Bruening, M.L., *Ultrathin, hyperbranched poly(acrylic acid) membranes on porous alumina supports*. Journal of the American Chemical Society, 2000. **122**(47): p. 11670-11678.
7. Vajandar, S.K., Xu, D.Y., Markov, D.A., Wikswo, J.P., Hofmeister, W., and Li, D.Y., *SiO₂-coated porous anodic alumina membranes for high flow rate electroosmotic pumping*. Nanotechnology, 2007. **18**(27): p. 275705.
8. Winkler, B.H. and Baltus, R.E., *Modification of the surface characteristics of anodic alumina membranes using sol-gel precursor chemistry*. Journal of Membrane Science, 2003. **226**(1-2): p. 75-84.
9. Ott, A.W., Klaus, J.W., Johnson, J.M., George, S.M., McCarley, K.C., and Way, J.D., *Modification of porous alumina membranes using Al₂O₃ atomic layer controlled deposition*. Chemistry of Materials, 1997. **9**(3): p. 707-714.
10. Berland, B.S., Gartland, I.P., Ott, A.W., and George, S.M., *In situ monitoring of atomic layer controlled pore reduction in alumina tubular membranes using sequential surface reactions*. Chemistry of Materials, 1998. **10**(12): p. 3941-3950.

11. Chen, P., Mitsui, T., Farmer, D.B., Golovchenko, J., Gordon, R.G., and Branton, D., *Atomic layer deposition to fine-tune the surface properties and diameters of fabricated nanopores*. Nano Letters, 2004. **4**(7): p. 1333-1337.
12. Elam, J.W., Routkevitch, D., Mardilovich, P.P., and George, S.M., *Conformal coating on ultrahigh-aspect-ratio nanopores of anodic alumina by atomic layer deposition*. Chemistry of Materials, 2003. **15**(18): p. 3507-3517.
13. Pellin, M.J., Stair, P.C., Xiong, G., Elam, J.W., Birrell, J., Curtiss, L., George, S.M., Han, C.Y., Iton, L., Kung, H., Kung, M., and Wang, H.H., *Mesoporous catalytic membranes: Synthetic control of pore size and wall composition*. Catalysis Letters, 2005. **102**(3-4): p. 127-130.
14. Xiong, G., Elam, J.W., Feng, H., Han, C.Y., Wang, H.H., Iton, L.E., Curtiss, L.A., Pellin, M.J., Kung, M., Kung, H., and Stair, P.C., *Effect of atomic layer deposition coatings on the surface structure of anodic aluminum oxide membranes*. Journal of Physical Chemistry B, 2005. **109**(29): p. 14059-14063.
15. Miikkulainen, V., Rasilainen, T., Puukilainen, E., Suvanto, M., and Pakkanen, T.A., *Atomic layer deposition as pore diameter adjustment tool for nanoporous aluminum oxide injection molding masks*. Langmuir, 2008. **24**(9): p. 4473-4477.
16. Szczepanski, V., Vlassiouk, I., and Smirnov, S., *Stability of silane modifiers on alumina nanoporous membranes*. Journal of Membrane Science, 2006. **281**(1-2): p. 587-591.
17. Losic, D., Cole, M.A., Dollmann, B., Vasilev, K., and Griesser, H.J., *Surface modification of nanoporous alumina membranes by plasma polymerization*. Nanotechnology, 2008. **19**(24): p. 245704.
18. Losic, D., Triani, G., Evans, P.J., Atanacio, A., Mitchell, J.G., and Voelcker, N.H., *Controlled pore structure modification of diatoms by atomic layer deposition of TiO₂*. Journal of Materials Chemistry, 2006. **16**(41): p. 4029-4034.
19. Triani, G., Evans, P.J., Attard, D.J., Prince, K.E., Bartlett, J., Tan, S., and Burford, R.P., *Nanostructured TiO₂ membranes by atomic layer deposition*. Journal of Materials Chemistry, 2006. **16**(14): p. 1355-1359.
20. Perez, I., Robertson, E., Banerjee, P., Henn-Lecordier, L., Son, S.J., Lee, S.B., and Rubloff, G.W., *TEM-based metrology for HfO₂ layers and*

- nanotubes formed in anodic aluminium oxide nanopore structures.* Small, 2008. **4**(8): p. 1223-1232.
21. Jani, A.M.M., Anglin, E.J., McInnes, S.J.P., Losic, D., Shapter, J.G., and Voelcker, N.H., *Nanoporous anodic aluminium oxide membranes with layered surface chemistry.* Chemical Communications, 2009(21): p. 3062-3064.
 22. Lodish, H., Darnell, J., Matsudaira, P., Baltimore, D., and Berk, B., *Molecular cell biology.* 1995: W. H. Freeman Company.
 23. Wijmans, J.G. and Baker, R.W., *The solution-diffusion model - a review.* Journal of Membrane Science, 1995. **107**(1-2): p. 1-21.
 24. Hulteen, J.C., Jirage, K.B., and Martin, C.R., *Introducing Chemical Transport Selectivity into Gold Nanotubule Membranes.* Journal of the American Chemical Society, 1998. **120**: p. 6603-6604.
 25. Jirage, K.B., Hulteen, J.C., and Martin, C.R., *Effect of thiol chemisorption on the transport properties of gold nanotubule membranes.* Analytical Chemistry, 1999. **71**(21): p. 4913-4918.

CHAPTER 7

FORWARD OSMOSIS THROUGH SILICA MODIFIED POROUS ALUMINA MEMBRANES

The selective onset of forward osmosis across silica modified alumina membranes is examined. A set of dyes of differing size, charge and hydrophobicity were used as draw solutes to investigate the effects of draw solution solute on the water transport ability. The aim is to understand and hence later control the osmosis effect observed through silica modified alumina membranes.

7.1. INTRODUCTION

Forward osmosis (FO), an old technology, has seen renewed interest in numerous fields of science and engineering. While reverse osmosis (RO) is currently the most used membrane technology in water treatment and desalination, RO utilises hydraulic pressure which can be very costly [1]. Unlike RO, the FO process is not a pressure driven process and therefore can be very energy efficient. Forward osmosis generally uses a non-porous, semi permeable and dense membrane material which allows the transport of water while blocking solute molecules [2]. FO occurs due to the driving force from osmotic pressure. A highly concentrated solution (draw solution) will increase the osmotic pressure across the membrane and hence the water will permeate across the membrane into the draw solution (Figure 7-1). This process leaves a concentrated feed solution behind and the water in the draw solution is reclaimed through removal of the solute. Typically a draw solution containing high concentrations of ammonia-carbon dioxide is used to extract water from the feed solution [3]. After water extraction is complete the draw solution is heated at low temperatures to remove the dissolved gases which are then captured and reused, leaving fresh water behind.

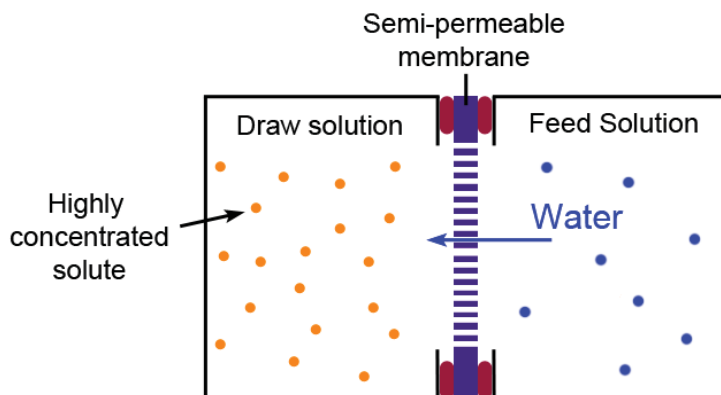


Figure 7-1 Schematic of the forward osmosis process. The feed cell is filled with water or contaminated water (e.g. seawater). The draw cell is filled with a highly concentrated solution. The water passes through the semi-permeable membrane due to the increased osmotic pressure across the membrane.

Common applications for forward osmosis include industrial wastewater treatment [2], liquid food processing [4], and the desalination of seawater [3, 5]. More recent areas of forward osmosis research include electric power generation [6-7], pharmaceutical processing [8] and controlled drug release [9-10]. Forward osmosis

implemented in drug delivery has the potential to provide targeted, extended and accurate release of drugs into the body. The application of FO membranes in the food and pharmaceutical industry can preserve the integrity of the feed solution as the process does not require high temperatures or pressures.

This work focuses on selective forward osmosis through silicon dioxide coated alumina membranes (Si-PA). These modified alumina membranes were described in chapter 6. During the studies carried out in chapter 6, an unusual FO effect was observed with some samples and the studies outlined in this chapter aim to explain this effect. Whilst conventional FO membranes provide no leakage of salts between the draw and the feed solution due to their dense construction [2], the membranes in this work contain pores ~ 15 nm in diameter and are thus not only permeable to water but also allow solutes to pass through. In this study we observe the onset of forward osmosis only when particular solutes are used in the draw solution. The main aim of this study is to determine why FO occurs for some solutes while not for others. A set of dyes of differing size, charge and hydrophobicity were used as draw solutes to investigate the effects of draw solution solute on the water transport ability. The possible mechanisms behind this discriminatory water transport are explored.

7.2. EXPERIMENTAL DETAILS

7.2.1. *Fabrication and functionalisation of silica modified porous alumina membranes via atomic layer deposition*

Details regarding the fabrication of Si-PA membranes can be found in section 2.1.3.

7.2.2. *Water transport experiments*

Transport experiments were performed using a U-tube permeation cell in which the membrane separates two half-cells; the draw solution and the feed cell. Permeation experiments were performed in which 3 mL of a 1 mM solution of the dye in water was used as the draw solution and 3 mL water was added to the feed cell. The exposed area of the membrane sample in the transport cell is 0.24 cm^2 . Dyes used in

this study include; rose bengal (RB), tris(2,2'-bipyridyl)ruthenium(II) (Rubpy), pinacyanol chloride (PCN), crystal violet (CV), methyl viologen (MV), bromocresol green (BG), rhodamine B (RhB), nickel sulphate (NS) and potassium ferricyanide (PF) (Table 7-1). The volume of water transported was determined by measuring the water level height in the cuvettes over time (Figure 7-2). Photographs of the permeation cell were taken with a digital camera at a fixed distance and height. The level of the meniscus for both feed and draw solutions was measured using Adobe Photoshop CS5. The change in the cell heights was determined as the height between the meniscus and the original meniscus position at the onset of the experiment. To determine the effect of salt concentration on water transport, aqueous solutions of KCl ranging from 1 μ M to 100 mM were used as the solvent in both the feed and draw solutions. 1 mM of either RB or CV (both of which facilitate water transport) was used as the draw solution. Control experiments were performed in which only water was added to both feed and draw solution cells and the water level height was measured to determine any loss of water due to evaporation. For determining the rate of dye diffusion across the membrane, the feed cell was continuously monitored with a UV-Vis fiber optic spectrophotometer (Ocean Optics, USA).

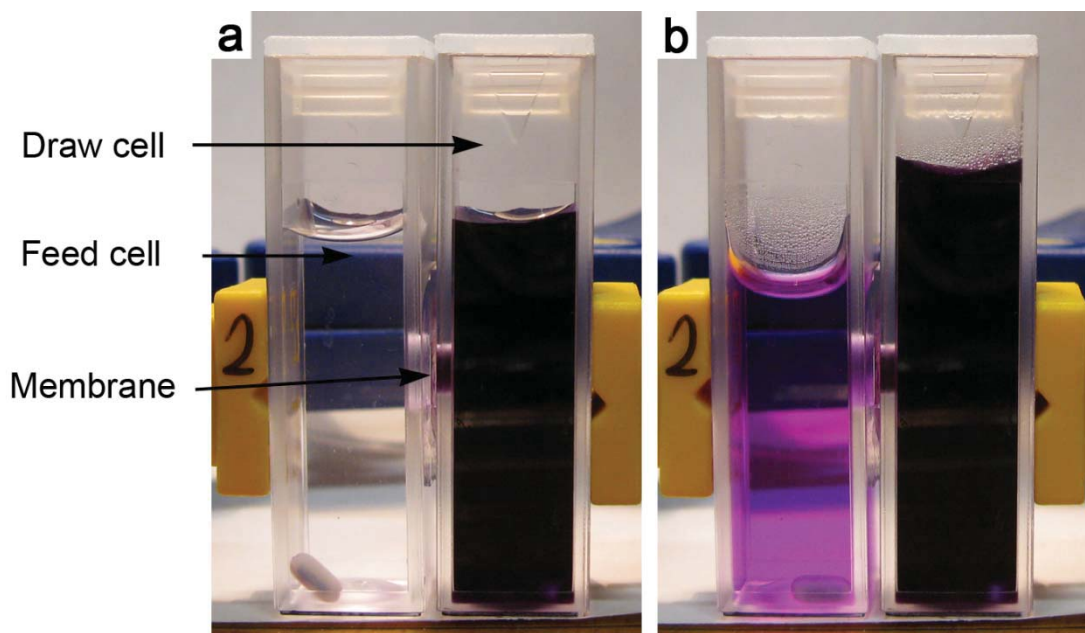


Figure 7-2 Photographs of a permeation cell with Si-PA, CV and 1 μ M KCl at (a) time = 0 and (b) time = 7 h.

7.3. RESULTS AND DISCUSSION

7.3.1. Dye dependence on the water transport through Si-PA membranes

Two transport effects are occurring simultaneously across these membranes. The concentration gradient causes the dyes to transport through the membrane from the draw to the feed cell while the osmotic pressure causes the water to transport in the opposite direction from the feed to the draw cell. Forward osmosis was found to occur through Si-PA membranes but only when particular dyes were used in the draw solution. The ability of the Si-PA membrane to facilitate water transport from the feed cell to the draw cell was determined using a set of different dyes (Table 7-1). This set includes dyes with varying size, shape, charge, hydrophilicity and molecular weight. It was found that some of the dyes facilitated water transport while the others did not. However, there does not appear to be an obvious trend between the properties of the dye, such as its size and charge, and the onset of water transport (Figure 7-3). Figure 7-4 presents the water transport through a Si-PA membrane caused by two dyes (CV and RB). Each of these dyes facilitates water transport at similar rates even though their sizes are quite different and they have opposing charge.

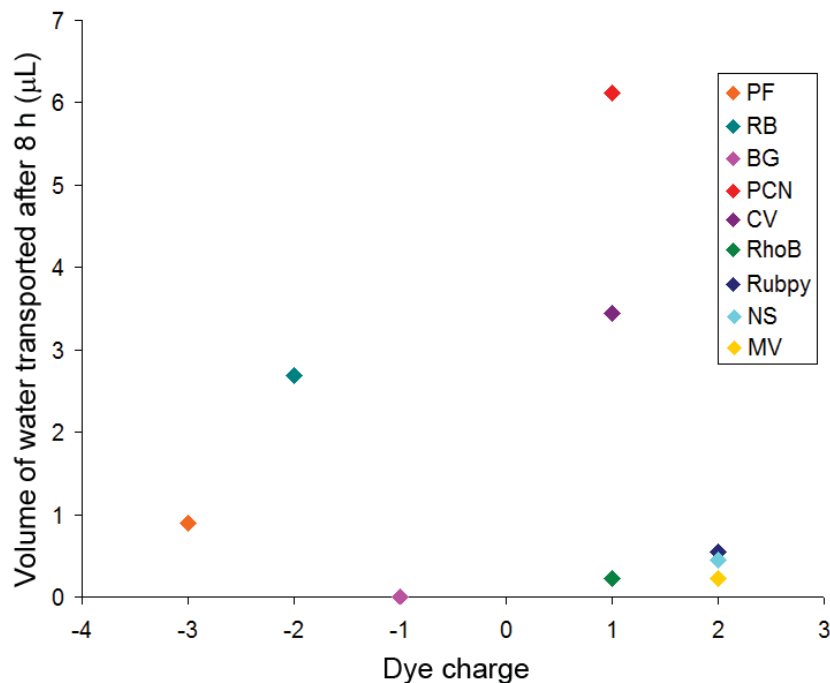


Figure 7-3 Amount of water transported through Si-PA membranes after 8h when various charged dyes are used as the permeant.

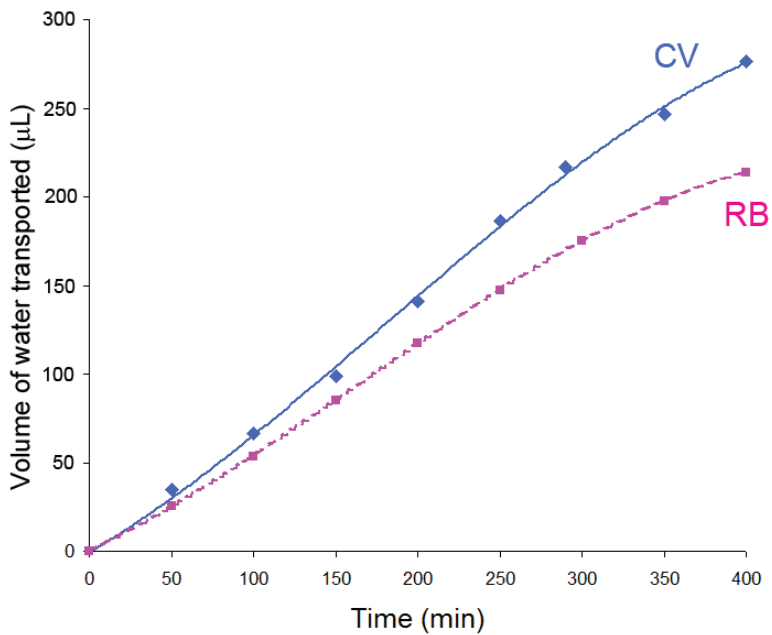
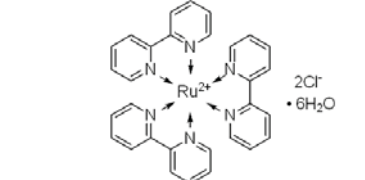
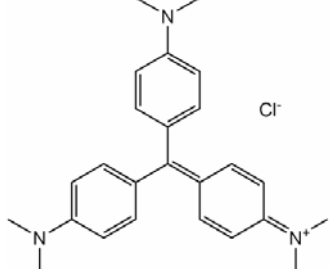
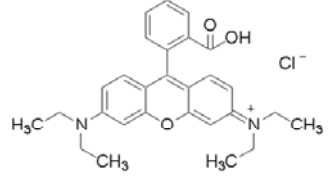
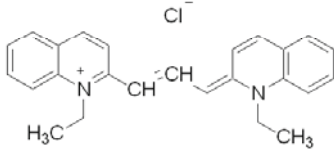
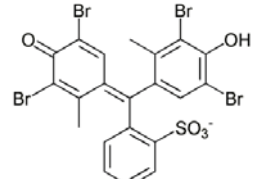
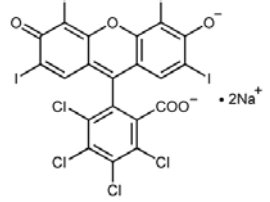
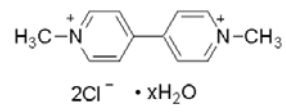
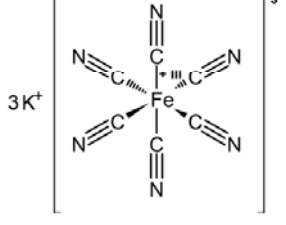
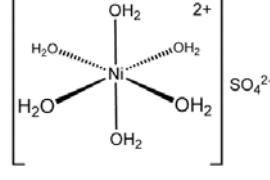
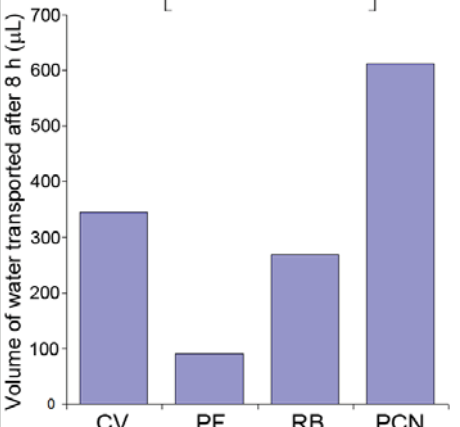


Figure 7-4 Water volume change in the feed cell due to water transport through Si-PA membranes containing crystal violet (CV) or rose bengal (RB) in the feed cell.

The main aim of this study is to determine why forward osmosis occurs for some dyes while not for others. It may depend on the degree of adsorption of the dye onto the surfaces of the Si-PA membranes. Some dyes will adsorb to the membrane while others will not. The dyes that adsorb onto the surface will contribute to the thickness of an electrical double layer thus reducing the effective pore size and causing forward osmosis to occur. As the surface of the membrane is hydrophilic, it is assumed that the adsorption of the dye onto the membrane will be related to the charge and hydrophilicity of the dye molecules and so it is very interesting that some hydrophobic dyes can also cause osmosis.

Perhaps the formation of a pore-occluding double layer only occurs for a percentage of the pores. If some pores are open to solute transport while others are only permeable to water this may give rise to the two transport mechanisms seen in this study (water transport in addition to permeant (dye) transport). Inhomogeneous ALD deposition may have given rise to open and partially blocked pores, the partially blocked pores will be susceptible to full blocking by the double layer while the larger sized pores will still remain open even in the presence of a large double layer. The effect of the double layer on the osmosis properties of these membranes will be investigated in section 7.3.3.

Table 7-1 List of dye molecules which facilitate and do not facilitate water transport through Si-PA membranes.

Does not facilitate water transport	Facilitates water transport
Tris(2,2'-bipyridyl)ruthenium(II) M=748.62 g/mol 	Crystal Violet M=407.98 g/mol 
Rhodamine B M=479.01 g/mol 	Pinacyanol Chloride M=388.93 g/mol 
Bromocresol Green M=698.01 g/mol 	Rose Bengal M=1017.64 g/mol 
Methyl Viologen M=257.16 g/mol 	Potassium Ferricyanide M=329.24 g/mol 
Nickel Sulfate M=154.76 g/mol 	

7.3.2. Comparison of water transport through bare PA and Si-PA

The water transport efficiency of the Si-PA membrane was compared against unmodified PA membranes using the dyes; CV and RB. For each of the dyes the Si-PA membrane produced larger water transport rates than the unmodified PA membrane (Figure 7-5). Therefore the addition of the Si layer on the top of the membrane contributes dramatically to the water transport rates. Decreased pore sizes (< 15 nm) must be an important factor in the ability of these membranes to facilitate water transport. The pore size of the unmodified PA membrane is ~ 30 nm while the surface pore size of the Si-PA membrane is ~ 15 nm (Figure 7-6). Furthermore, from the range of dyes used in this study there was found to be one discrepancy between Si-PA and PA membranes in which one of the probe molecules (potassium ferricyanide) facilitated water transport in the Si-PA case but not the bare PA case. However, potassium ferricyanide provided the lowest water transport rate of all the water-facilitating dyes through the Si-PA membrane and therefore the water transport rate across the PA membrane may occur but is too small to measure. Another major difference between PA and Si-PA membranes is that PA facilitates faster dye transport than Si-PA due to the larger pore size. As the dye concentration in the feed cell of the PA membrane increases relatively fast then the chemical potential across the membrane is equalised faster. As there is less drive for the water transport to equalise the chemical potential difference, lower water transport rates for the PA membrane are observed.

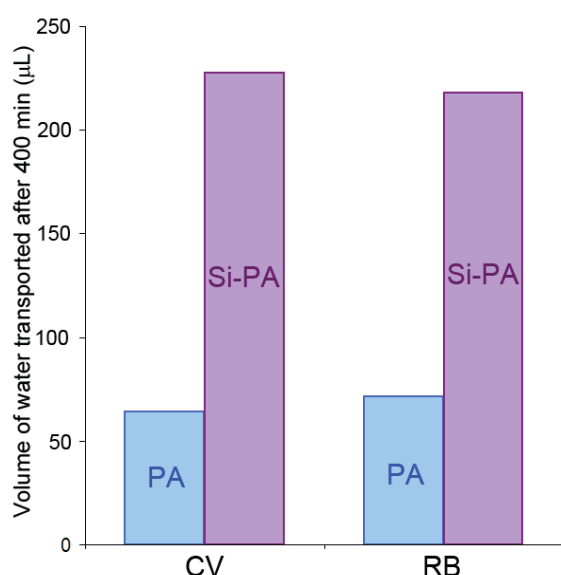


Figure 7-5 Amount of water transported for PA and Si modified PA after 400 min when CV or RB is used as the permeant.

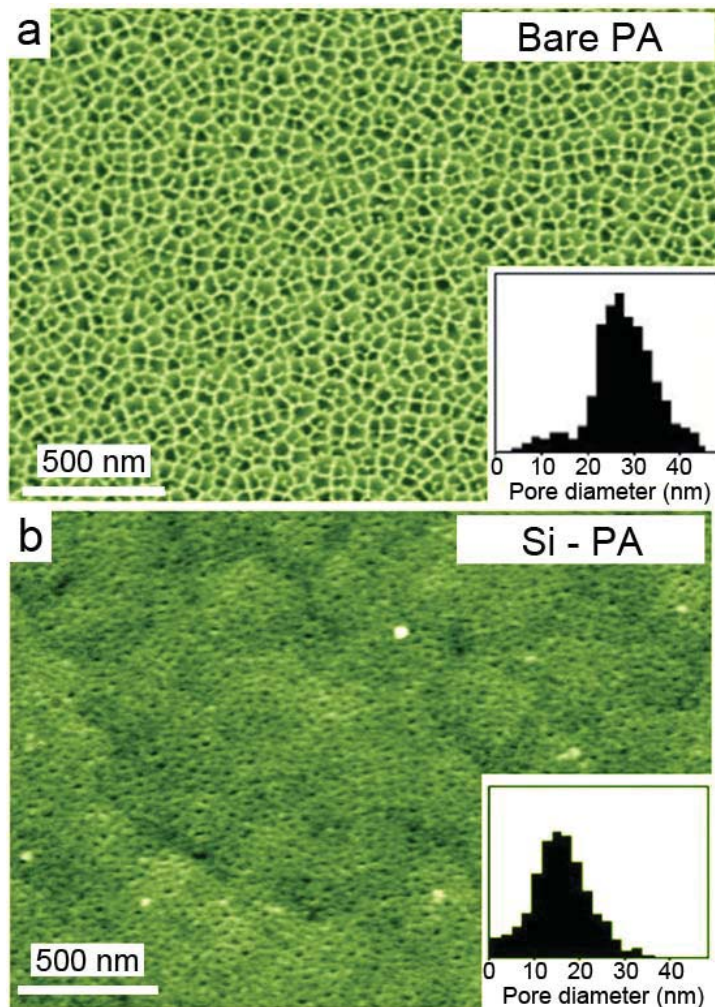


Figure 7-6 SEM images of (a) an unmodified PA membrane and (b) a Si-PA membrane.

7.3.3. Effect of salt concentration on the water transport properties

Increasing salt concentrations ranging from 0 – 100 mM were added to the feed and draw cells to determine whether the double layer on the membrane surfaces was responsible for the water transport. The best performing dyes (CV and RB) were used in this salt concentration study. Although PCN performed better than CV and RB it was not chosen due to its limited solubility in water and so the next two most suitable dyes (CV and RB) were used. Figure 7-7 and Figure 7-8 display the water transport through Si-PA membranes for CV (Figure 7-7) and RB (Figure 7-8) in different salt concentrations. The control data is for the cells which only contain water; this data was taken in order to determine how much water is lost due to evaporation. Generally the loss of water due to evaporation is under 0.5 mm. The

trend observed in Figure 7-7 and Figure 7-8 is summarised by Figure 7-9 which displays the amount of water transported after 300 min for various KCl concentrations. Overall an increase in the water transport is observed when the solvent contains 1 μ M - 10 μ M KCl. Followed by a decrease in water transport over the KCl concentration range of 100 μ M – 1 mM. In this range, the water transport is slower than the KCl-free scenario. KCl concentrations above 5 mM results in almost no water transport, which implies forward osmosis has ceased. For all KCl concentrations, the dye is still transported indicating that the pores are still open and the drop in the water transport is not due to blocked pores.

The Debye-Hückel theory explains that the Debye length increases with low salt concentrations and diminishes in high salt concentration [11]. The Debye length at 1 mM KCl is 10 nm which is of the same order as the pore diameter. For concentrations less than 1 mM KCl or without added KCl the Debye length in the pores is even larger thereby hindering the transport of the solutes and causing water transport to occur. The Debye length at 0.1 M KCl is 1 nm; in this case the double layer is compressed and the potential in the center of the pore will be substantially smaller than at the wall. When the double layer is compressed there is less hindrance in the transport of the dye molecules and thus water transport ceases. This is why there is a trend where the water transport increases at low KCl concentration and diminishes at higher KCl concentration (Figure 7-9).

When the dimensions of the pores approach the length of the double layer, overlap between the double layers from opposite sides of the pore occurs. Complete double layer overlap within the pore results in a channel that is virtually impermeable to ions with the same charge as the surface charge [12]. If the dye molecules are hindered in their diffusion across the membrane by the double layer then to offset the concentration difference between the feed and draw cell water will have to flow from the feed cell to the draw cell.

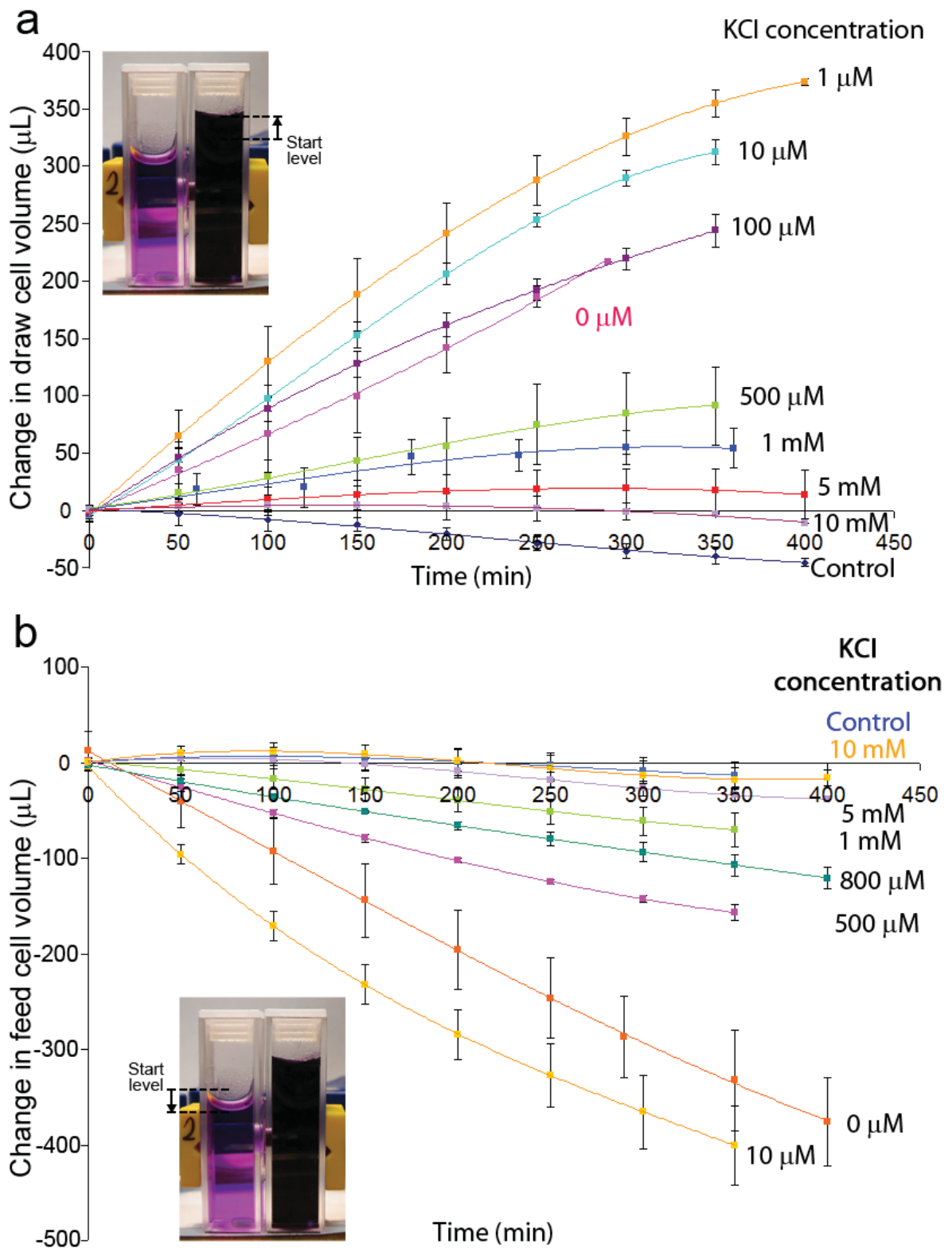


Figure 7-7 Volume change in the draw (a) and feed (b) cell due to water transport through Si-PA membranes containing crystal violet (CV) in the draw cell and varying KCl concentrations in the solvent.

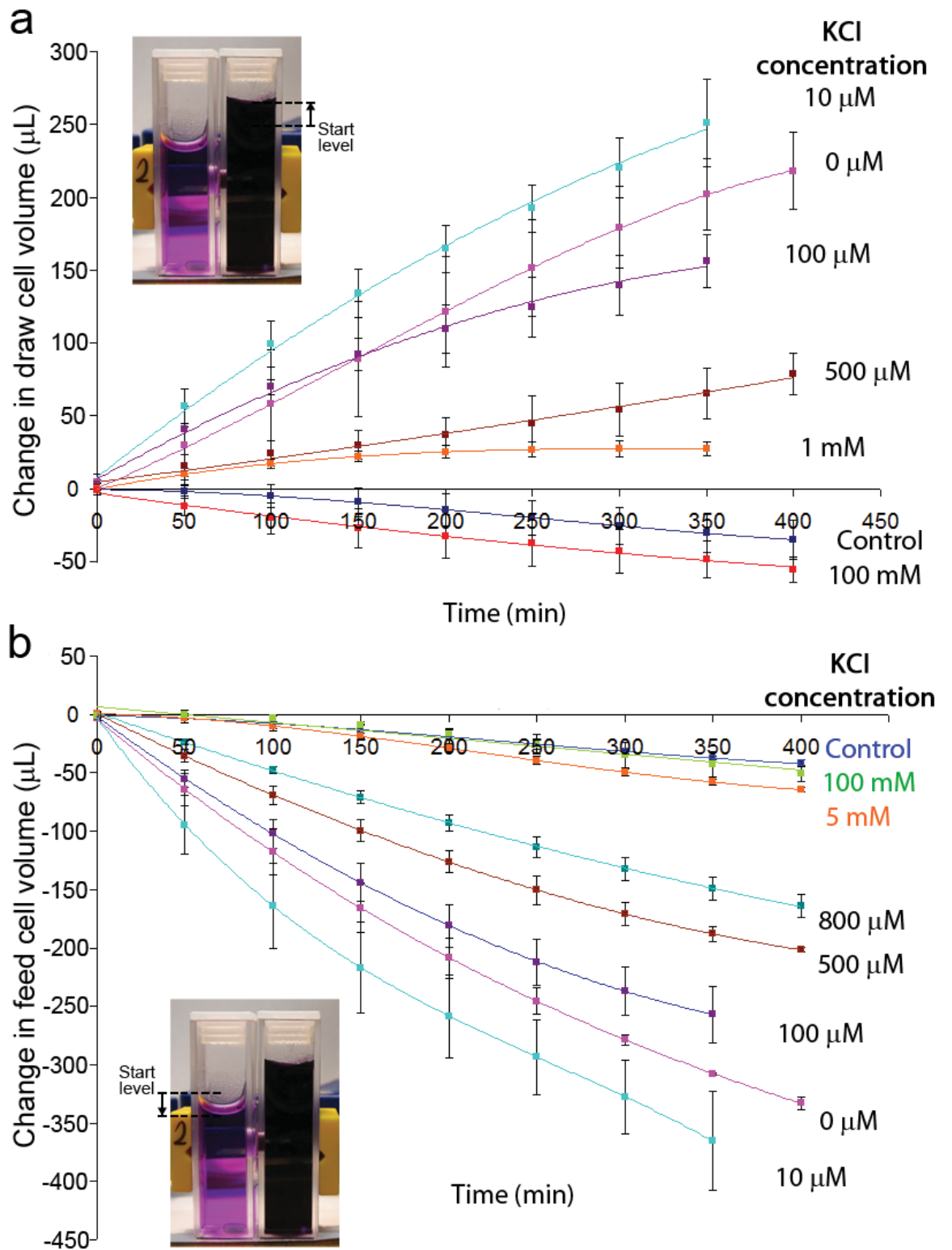


Figure 7-8 Volume change in the draw (a) and feed (b) cell due to water transport through Si-PA membranes containing rose bengal (RB) in the draw cell and varying KCl concentrations in the solvent.

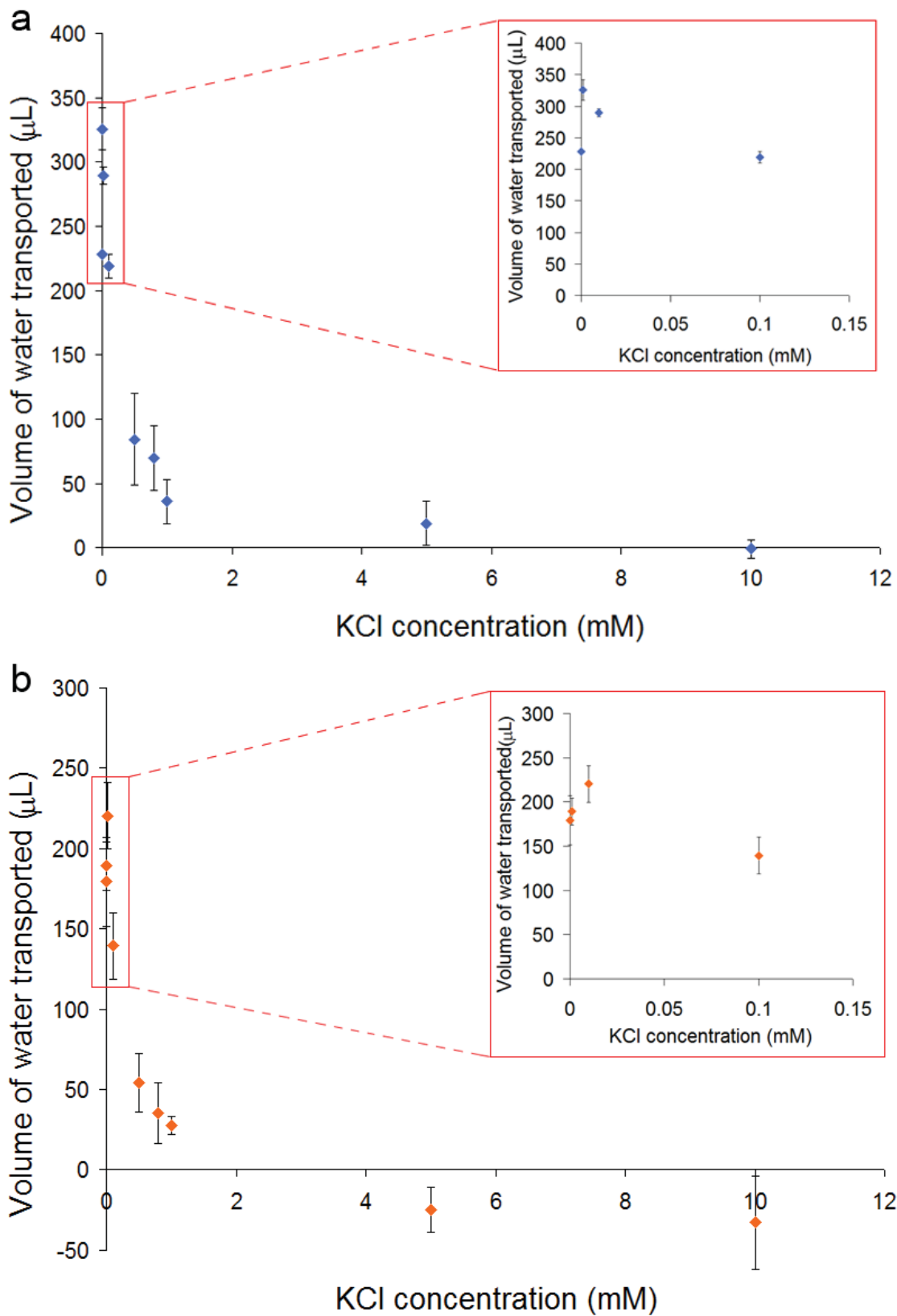


Figure 7-9 Volume of water transported through Si-PA membranes after 300 min for varying KCl concentrations when crystal violet (a) or rose bengal (b) is in the draw cell.

However, this theory does not appear to adequately explain the current observations. For example, dye transport does not seem to be hindered as two similar sized dyes, one which facilitates water transport and one which does not (RB and Rubpy respectively), present similar fluxes through the membrane (Table 7-2, Figure 7-10). The flux ratio (Rubpy:RB) is 2.46, which is typical for this pair of dyes. Forward osmosis generally occurs only when there is severe hindrance of the permeants ability to equalise the concentration difference across the membrane, however in this case the ability of the permeant to diffuse through the membrane seems unaffected. Currently work is continuing to gain a better understanding of this phenomenon.

Table 7-2 Summary of permeation data of RB (water transport facilitating dye) and Rubpy (non-water transport facilitating dye) through Si-PA membranes.

Flux of permeate molecule (mol cm ⁻² h ⁻¹)		Flux Ratio
Rubpy	RB	Rubpy:RB
$5.42 \pm 0.07 \times 10^{-7}$	$2.20 \pm 0.12 \times 10^{-7}$	2.46

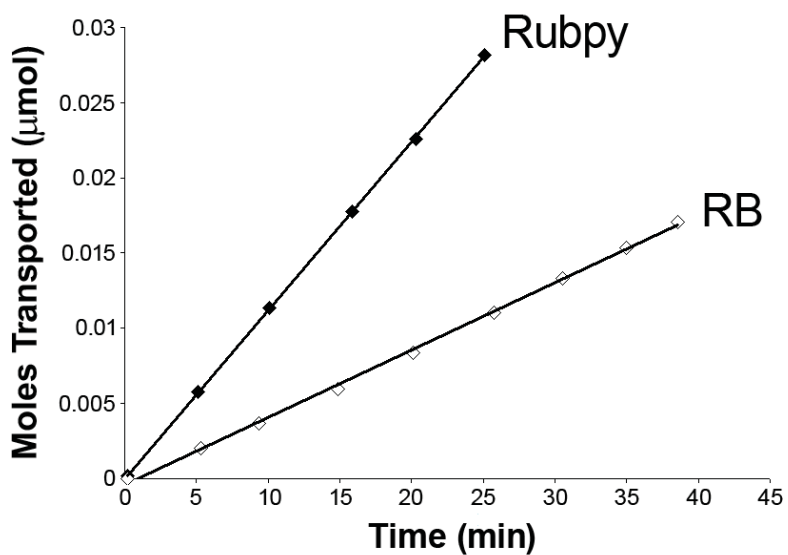


Figure 7-10 Transport of Rubpy and RB through a Si-PA membrane.

7.4. CONCLUSIONS AND FURTHER WORK

Forward osmosis was found to occur through Si-PA membranes but only when particular solutes were used in the draw solution. These solutes included dyes of differing size, charge, hydrophobicity and molecular weight. There did not appear to be an obvious trend between the properties of the dye and the onset of water transport. The water transport rates through Si-PA membranes and PA membranes were compared where larger water transport rates were observed for the Si-PA membrane. The larger water transport rate is most likely due to the occlusion of the pores by the silica layer which causes a hindrance in the solute diffusion. The forward osmosis observed in this study is likely due to a double layer effect. The double layer causes an occlusion of the pores and essentially decreases the pore size. Due to this occlusion, the dye transport is hindered and so water transport is required in order to offset the concentration difference between the feed and draw cell. As the electrical double layer thickness is increased with low salt concentrations and diminishes in high salt concentration an increase in water transport is observed at low KCl concentration and diminishes at higher KCl concentration.

Although the trend between solutes and forward osmosis was not elucidated, further experiments should be conducted to clarify this issue. The dye diffusion across the membrane for each of the dyes can be measured to determine any distinguishing trends between the dye transport rates and the water rates. Furthermore zeta-potential analysis would be useful in ascertaining the precise surface charge of the membrane in each of the solution environments. It would also be interesting to determine if any other properties of the dye could explain the occurrence. It is important to determine the trend behind the solutes and forward osmosis onset so as to provide control over the transport properties. It would be highly beneficial to predict the water transport rates for particular molecules or combinations of molecules. Through this information, highly sophisticated separations can be achieved.

The function of these membranes is analogous to a cell membrane, which are capable of the regulated transport of water, molecules and ions [13]. New areas of research into the fabrication of membrane materials strive to replicate what nature has already created [14]. Similar separations performed with cell membranes can potentially be

realised with these artificial membranes. These membrane materials can potentially be applied in dialysers as they are capable of the removal of excess fluid in the body in addition to metabolic waste and the replenishment of buffers. Fluid removal is one of the most important aspects of haemodialysis and as the pore size and surface chemistry of these membranes can be finely tuned, the selective removal of targeted proteins and waste can also be achieved.

7.5. REFERENCES

1. Drioli, E. and Giorno, L., *Membrane Operations: Innovative Separations and Transformations*. 2009: Wiley-VCH.
2. Cath, T.Y., Childress, A.E., and Elimelech, M., *Forward osmosis: Principles, applications, and recent developments*. Journal of Membrane Science, 2006. **281**(1-2): p. 70-87.
3. McCutcheon, J.R., McGinnis, R.L., and Elimelech, M., *A novel ammonia-carbon dioxide forward (direct) osmosis desalination process*. Desalination, 2005. **174**(1): p. 1-11.
4. Jiao, B., Cassano, A., and Drioli, E., *Recent advances on membrane processes for the concentration of fruit juices: a review*. Journal of Food Engineering, 2004. **63**(3): p. 303-324.
5. Kessler, J.O. and Moody, C.D., *Drinking water from sea-water by forward osmosis*. Desalination, 1976. **18**(3): p. 297-306.
6. Lee, K.L., Baker, R.W., and Lonsdale, H.K., *Membranes for power-generation by pressure-retarded osmosis*. Journal of Membrane Science, 1981. **8**(2): p. 141-171.
7. Loeb, S., *One hundred and thirty benign and renewable megawatts from Great Salt Lake? The possibilities of hydroelectric power by pressure-retarded osmosis*. Desalination, 2001. **141**(1): p. 85-91.
8. Yang, Q., Wang, K.Y., and Chung, T.S., *A novel dual-layer forward osmosis membrane for protein enrichment and concentration*. Separation and Purification Technology, 2009. **69**(3): p. 269-274.
9. Thombre, A.G., Cardinal, J.R., DeNoto, A.R., and Gibbes, D.C., *Asymmetric membrane capsules for osmotic drug delivery - II. In vitro and in vivo drug release performance*. Journal of Controlled Release, 1999. **57**(1): p. 65-73.
10. Herbig, S.M., Cardinal, J.R., Korsmeyer, R.W., and Smith, K.L., *Asymmetric-membrane tablet coatings for osmotic drug-delivery*. Journal of Controlled Release, 1995. **35**(2-3): p. 127-136.
11. Debye, P. and Huckel, E., *The theory of electrolytes. I. Lowering of freezing point and related phenomena*. Physikalische Zeitschrift, 1923. **24**: p. 185.

12. Schmuhl, R., Keizer, K., van den Berg, A., ten Elshof, J.E., and Blank, D.H.A., *Controlling the transport of cations through permselective mesoporous alumina layers by manipulation of electric field and ionic strength*. Journal of Colloid and Interface Science, 2004. **273**(1): p. 331-338.
13. Caplan, M., *Current Topics in Membranes*. Cell Biology and Membrane Transport Processes. Vol. 41. 1994: Academic Press, Inc.
14. Janshoff, A. and Steinem, C., *Transport across artificial membranes - an analytical perspective*. Analytical and Bioanalytical Chemistry, 2006. **385**(3): p. 433-451.

CHAPTER 8

LIGHT SWITCHABLE TRANSPORT THROUGH GOLD NANOTUBE MEMBRANES

The transport properties of the gold nanotube membranes were controlled through the reversible switching of adsorbed fluorinated azobenzene layers. The fluorinated, hydrophobic end group of the azobenzene chain produces a transition between hydrophobic and less hydrophobic surface properties when switching from the *trans* to the *cis* state.

8.1. INTRODUCTION

In recent years, there has been increased interest in the construction of stimuli responsive or gating membrane materials due to their ability to selectively mediate molecular transport [1-4]. Such membranes exhibit changes in permeability and selectivity due to a response to applied external stimuli. As the properties of the membrane can be controlled on demand, these responsive membranes have great potential in applications including switchable molecular separations [5], controlled drug delivery systems [6], chemical and bio-sensing [7]. Responsive membranes can be fabricated through modifying membrane surfaces with stimuli responsive SAMs. There are countless stimuli responsive SAMs which have been devised on planar surfaces which are yet to be applied in membrane technology.

There have been significant advancements in the development of stimuli responsive SAMs in order to provide a higher degree of control over surface properties [8-10]. The surface properties of the material are changed through the conformational transition of the adsorbed molecules in response to external stimuli. The external stimuli used to initiate switching in SAMs include light [8-10], temperature [11-13], electrical potential [15, 16], and surrounding media [14-15]. Depending on the nature of the switchable SAM employed, the external stimuli can instigate reversible attachment [16], changes in the structural conformation [17-19] or changes in oxidation states [2] of the assembled molecules. Amongst these switchable molecules, azobenzene and its derivatives display significant transformations in structure and dipole moments when irradiated with UV/visible light (Figure 8-1) [17]. For azobenzene containing SAMs, the conformation change in the azobenzene unit essentially buries the end functionality of the assembled molecule when switching from the *trans* state to the *cis* state. Depending on the end group functionality, the surface properties of the material can be significantly changed. Therefore, this opens up boundless potential for tailored switchable separations as the choices of end group functionalities are limitless. Recently, successful switching of surface properties have involved azobenzene SAMs containing a fluorinated, and thus highly hydrophobic, end group which results in changes in the wettability of the planar surface when switched between the *trans* and *cis* states [8, 20].

Herein, we demonstrate for the first time dynamically controlled interfacial properties of gold nanotube membranes through the reversible switching of adsorbed fluorinated azobenzene layers. The previous work involving fluorinated azobenzene SAMs on planar surfaces [8] have been adapted to our gold nanotube membranes in order to provide controlled reversibility of the transport properties. Gold nanotube membranes were fabricated through the electroless deposition of gold onto porous alumina templates (Figure 8-1). Azobenzene containing SAMs were assembled onto the gold membrane surface through the attachment of a thiol layer onto which the azobenzene moiety was attached via an amide linker. The fluorinated and hence highly hydrophobic end group of the azobenzene chain produces a transition between hydrophobic and less hydrophobic surface properties when photoisomerisation from the trans to the cis state occurs (Figure 8-1). The photoresponsive characteristics of these azobenzene modified membranes were examined through the switchable transport of a hydrophilic probe dye across the membrane.

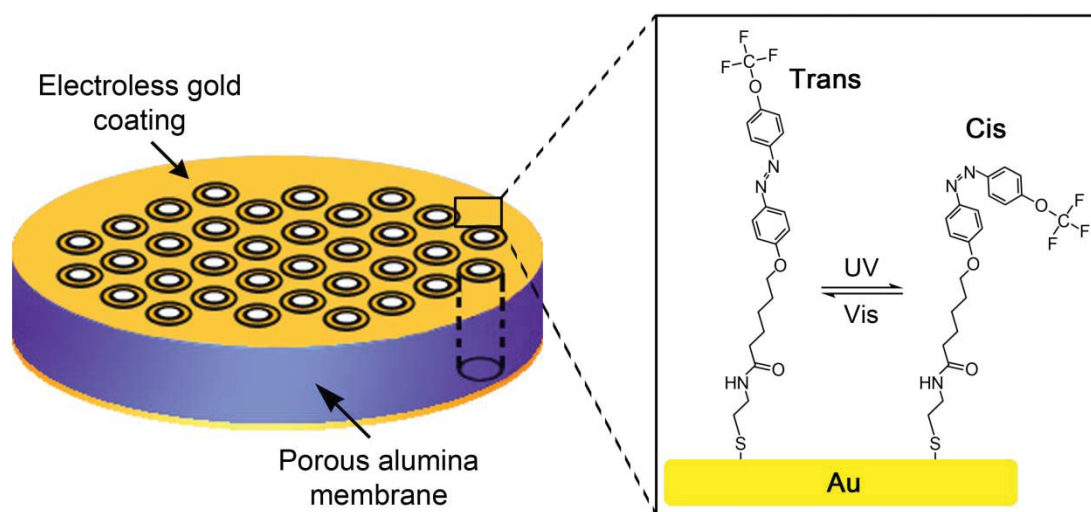


Figure 8-1 Schematic of gold coated alumina membrane with adsorbed azobenzene thiol layer and its reversible photoisomerisation between the trans and cis states.

8.2. EXPERIMENTAL DETAILS

8.2.1. *Fabrication of porous alumina membranes*

Porous alumina membranes were fabricated as outlined in section 2.1.1. The second anodisation was performed at 80 V for 15 min in 0.3 M oxalic acid resulting in porous alumina (PA) with thicknesses of 20 – 30 µm.

8.2.2. *Electroless gold deposition onto porous alumina membranes*

The electroless gold deposition was performed as stated in section 2.1.2.1. A gold deposition time of 16 h was used in this study.

8.2.3. *Synthesis of 7-[*(trifluoromethoxyphenylazo)phenoxy*]pentanoic acid*

The synthesis of the fluorinated azobenzene molecule was carried out as described in section 2.5.

8.2.4. *Azobenzene functionalisation of gold nanotube membranes*

The Au-PA membranes were first functionalised with cysteamine by immersion in a 3 mM solution in ethanol for 40 h, followed by rinsing in ethanol. The cysteamine modified membrane was then immersed in a solution containing 0.1 g of the azobenzene molecule, 15 mM EDC, 10 mM NHS in 100 mL ethanol for 72 h. The membrane was then rinsed copiously with ethanol and air dried. The *cis* state was achieved by irradiating with 370 nm light for 1 h at 100 W. *Trans* state was achieved through irradiating with Vis light (samples kept in glass containers in the sun).

8.2.5. *Investigation of membrane transport properties*

The hydrophilic dye, eosin yellow (EY), was used to probe the transport properties of the switchable membrane. EY was used instead of RB as it was found to be more hydrophilic than RB as shown in the appendix, Table A-1. Permeation experiments were performed in which a 1mM aqueous solution of EY was added to the feed cell while water was added to the permeate cell. The diffusion of the dye from the feed

cell to the permeate cell was continuously monitored with a UV-Vis fibre optic spectrophotometer (Ocean Optics, USA) at 517.24 nm. The flux of EY through the *trans* and *cis* states of the azobenzene modified membrane was documented.

8.3. RESULTS AND DISCUSSION

8.3.1. Characterisation of gold coated alumina membranes

The surface morphology of the Au-PA membranes were examined using SEM (Figure 8-2a). Significant reductions in the pore diameters occur after the membrane has been coated in gold. Measurements of the pore size of the PA templates and Au-PA membranes were extracted from the SEM images. The original pore diameter of the PA membrane (170.0 ± 21.1 nm) has been reduced to 66.8 ± 14.8 nm after electroless deposition (Figure 8-2a). From a cross sectional image of the Au-PA membrane (Figure 8-2b), the thickness of the membrane was found to be ~ 25 μm . Confirmation of gold deposition throughout the pores of PA membranes was outlined in chapter 3, where the alumina template was dissolved revealing the gold nanotube structures (chapter 3, Figure 3-3).

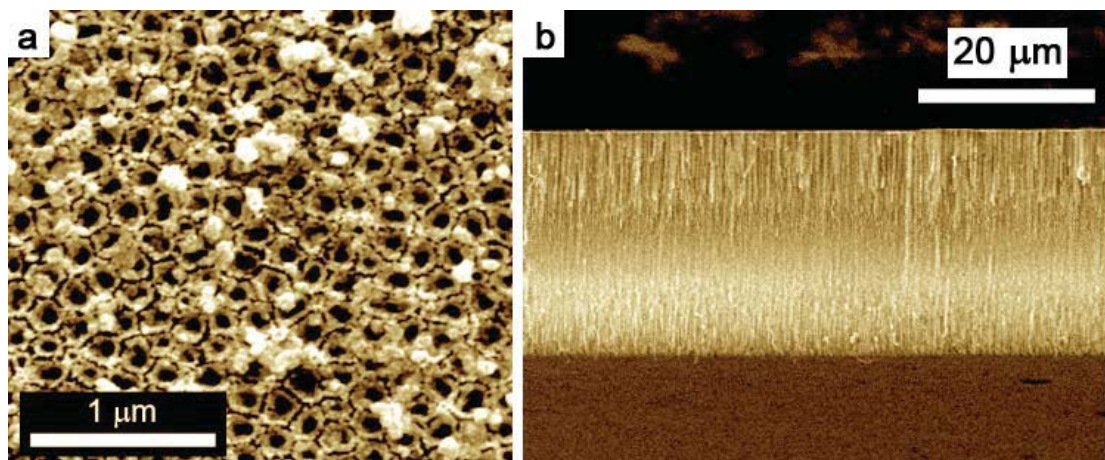


Figure 8-2 SEM images of the suface of a gold nanotube membrane after 16 h of gold deposition (a) and the cross sectional view of the gold nanotube membrane (b).

8.3.2. Characterisation of switchable azobenzene thiol on Au-PA membranes

The reversible wettability of azo-Au-PA membranes was investigated through measuring changes in the water droplet contact angle when switching between the *trans* and *cis* states (Table 8-1). On exposure to visible light the water contact angle increases as the azobenzene molecules convert to the *trans* state in which the fluorinated moiety is exhibited at the surface of the monolayer, producing a highly hydrophobic surface. The trans to cis isomerisation is initiated upon irradiation with UV light (365 nm) where the azobenzene unit undergoes a conformational change in which the fluorinated end group is no longer exhibited at the surface of the monolayer thus exhibiting a decreased contact angle. The contact angle difference between the *trans* and *cis* state is approximately 12°, which is comparable to the standard contact angle difference observed for azobenzene photoisomerisation on flat surfaces (~10°) [10, 21]. The *cis* state of the azobenzene SAM will expose the nitrogen groups in the azobenzene unit resulting in a more hydrophilic surface. However, the nitrogen groups are surrounded by carbon bonds and so the layer will retain some hydrophobic character. This is supported by comparing contact angle measurements with a long chain alkanethiol (decanethiol) modified Au-PA membrane which should be slightly more hydrophobic than the *cis* state azo-Au-PA membrane. As expected, the contact angle of the decanethiol modified membrane is slightly higher than the azo (*cis* state) modified membrane (Table 8-1). Furthermore, the contact angle measurement of the azo-Au-PA membrane in the *trans* state is larger than the decanethiol layer thus confirming enhanced hydrophobicity due to fluorinated terminal groups.

Table 8-1 1 µL water drop contact angle on azo and decanethiol modified Au-PA membranes.

Surface modification	Contact Angle (°)
Azo <i>trans</i> state	90.2 ± 2.9
Azo <i>cis</i> state	77.8 ± 4.9
Decanethiol	83.9 ± 1.9

8.3.3. Switchable transport properties of azobenzene modified Au-PA membranes

To explore the transport properties and switchability of the hydrophobic azo-Au-PA membranes, the flux of the hydrophilic dye (EY) across the membrane was measured. These transport experiments offer detailed information regarding the interactions between EY and the surface functional molecules allowing determination of the transport properties of the membrane when it is switched between the *cis* and *trans* state. Figure 8-3 presents the transport of EY through the azo-modified membrane in the *trans* and *cis* state. A summary of the permeation data of EY through the unmodified membrane and the *trans* and *cis* states of the azo-Au-PA membranes is presented in Table 8-2.

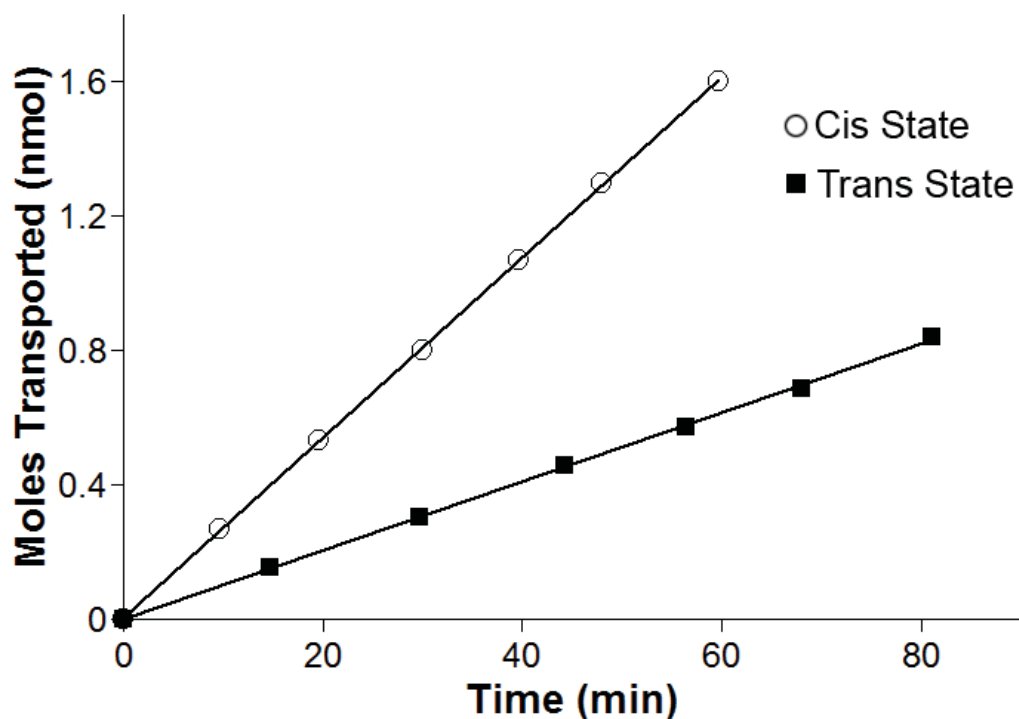


Figure 8-3 Transport of the hydrophilic dye (EY) across the azobenzene modified membrane when switched between the trans (highly hydrophobic) and cis (less hydrophobic) states.

The configuration of the azobenzene molecules when adsorbed in the pore is schematically represented in Figure 8-4. In the *trans* state the fluorinated end group of the chain is directed outwards into the pore, while in the *cis* state the fluorinated moiety points towards the surface of the pore. Each of these configurations will have a different impact on the transport of hydrophilic species due to the presence or absence of the fluorinated end group.

Table 8-2 Flux data for EY transport through unfunctionalised and azo-functionalised cis and trans state Au-PA membranes.

Surface modification	Flux of Eosin Yellow (mol cm ⁻² h ⁻¹)
Unfunctionalised	$8.19 \pm 0.78 \times 10^{-8}$
Azo-<i>cis</i> state (UV illuminated)	$6.36 \pm 0.37 \times 10^{-8}$
Azo-<i>trans</i> state (Vis illuminated)	$3.02 \pm 0.53 \times 10^{-8}$

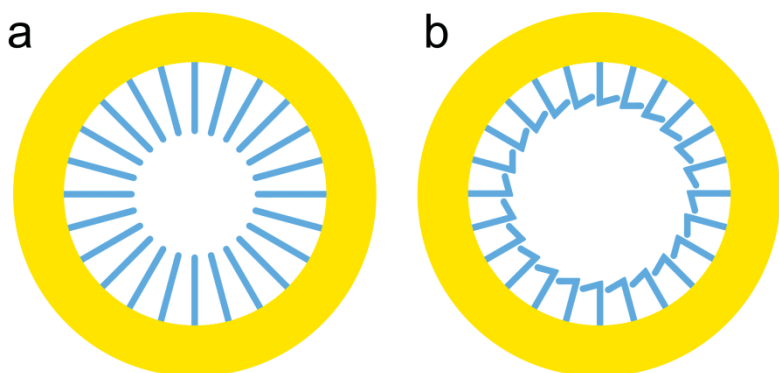


Figure 8-4 Schematic representation of the assembly of the azobenzene layer within a pore (top view) in the trans state (a) and the cis state (b).

An overall hindrance in the transport of the hydrophilic dye occurs after modifying the Au-PA membranes with the fluorinated azobenzene SAM (Table 8-2). Compared to the unmodified membrane a decrease of 63 % and 22 % occurs for the *trans* and *cis* states respectively. The decrease in the pore diameter due to the adsorbed azobenzene monolayer may contribute slightly to the decreases observed in the EY transport. However, the majority of the diminished EY flux is most likely due to the presence of fluorinated moieties in the SAM, for both *trans* and *cis* states.

When switching from the *cis* to the *trans* state of the azobenzene layer, a decrease of 53 % in the EY flux is observed (Table 8-2). This decrease is significant given that the contact angle measurements only reported a small decrease in wettability of the membrane when switching to the *trans* state, inferring that there was only a slight difference in the hydrophobicity of the membrane. When the azobenzene molecules convert to the *trans* state the fluorinated moiety is exhibited at the surface of the monolayer, producing a highly hydrophobic surface resulting in the hindrance of the transport of the hydrophilic dye. When the membrane is switched to the *cis* state, the azobenzene molecules undergoes a conformational change in which the fluorinated end group no longer protrudes at the surface of the monolayer thus exhibiting an increase in EY flux. Furthermore, in the *cis* state there is a breakdown of the chain packing in the azobenzene monolayer [22] which allows easier diffusion of the EY molecules along the walls of the pores.

The increase in pore size due to a transformation to the *cis* state will not be large enough to impact on the transport rates. Based on the height of a well ordered and packed C16 thiol layer (approx 2.6 nm) [23], the difference between the *trans* and *cis* layer heights will only be ~ 1 nm. In comparison to the pore size of the membrane (~ 67 nm), a change in pore diameter of 2 nm will not impact significantly on the transport rates. Therefore the decrease in transport observed when switching to the *cis* state is not due to a change in the pore size, but is attributed to the change in interfacial properties as a result of conformational changes in the azobenzene molecules.

8.4. CONCLUSIONS

A photoreversibly switchable azobenzene molecule was successfully synthesised and attached to a gold nanotube membrane via a cysteamine thiol layer. Due to the inclusion of a fluorinated moiety onto the end group of the azobenzene chain, the membrane surfaces are rendered photoswitchable from a highly hydrophobic state to a slightly less hydrophobic state. The transport of a hydrophilic probe dye through the azobenzene modified membrane demonstrated the potential of the switchable membrane, with transport rates decreased by 53 % when switching to the azo-*trans*

(highly hydrophobic) state. Therefore, through tailoring the end group functionality of the synthesised azobenzene molecule, a wide variety of switchable mechanisms could be achieved.

8.5. REFERENCES

1. Yang, B. and Yang, W.T., *Novel pore-covering membrane as a full open/close valve*. Journal of Membrane Science, 2005. **258**(1-2): p. 133-139.
2. Martin, C.R., Nishizawa, M., Jirage, K., Kang, M.S., and Lee, S.B., *Controlling ion-transport selectivity in gold nanotubule membranes*. Advanced Materials, 2001. **13**(18): p. 1351-1362.
3. Nishizawa, M., Menon, V.P., and Martin, C.R., *Metal Nanotubule Membranes with Electrochemically Switchable Ion-Transport Selectivity*. Science, 1995. **268**: p. 700-702.
4. Casasus, R., Marcos, M.D., Martinez-Manez, R., Ros-Lis, J.V., Soto, J., Villaescusa, L.A., Amoros, P., Beltran, D., Guillem, C., and Latorre, J., *Toward the development of ionically controlled nanoscopic molecular gates*. Journal of the American Chemical Society, 2004. **126**(28): p. 8612-8613.
5. Ulbricht, M., Ozdemir, S., and Geissmann, C., *Functionalized track-etched membranes as versatile tool to investigate stimuli-responsive polymers for "smart" nano- and microsystems*. Desalination, 2006. **199**(1-3): p. 150-152.
6. Jeon, G., Yang, S.Y., Byun, J., and Kim, J.K., *Electrically Actuated Smart Nanoporous Membrane for Pulsatile Drug Release*. Nanoletters, 2011.
7. Tokarev, I., Gopishetty, V., Zhou, J., Pita, M., Motornov, M., Katz, E., and Minko, S., *Stimuli-Responsive Hydrogel Membranes Coupled with Biocatalytic Processes*. Acs Applied Materials & Interfaces, 2009. **1**(3): p. 532-536.
8. Lim, H.S., Han, J.T., Kwak, D., Jin, M.H., and Cho, K., *Photoreversibly switchable superhydrophobic surface with erasable and rewritable pattern*. Journal of the American Chemical Society, 2006. **128**(45): p. 14458-14459.
9. Browne, W.R. and Feringa, B.L., *Light Switching of Molecules on Surfaces*. Annual Review of Physical Chemistry, 2009. **60**: p. 407-428.
10. Jiang, W.H., Wang, G.J., He, Y.N., Wang, X.G., An, Y.L., Song, Y.L., and Jiang, L., *Photo-switched wettability on an electrostatic self-assembly azobenzene monolayer*. Chemical Communications, 2005(28): p. 3550-3552.

11. Zareie, H.M., Boyer, C., Bulmus, V., Nateghi, E., and Davis, T.P., *Temperature-responsive self-assembled monolayers of oligo(ethylene glycol): Control of biomolecular recognition*. Acs Nano, 2008. **2**(4): p. 757-765.
12. Fletcher, B.L., Retterer, S.T., McKnight, T.E., Melechko, A.V., Fowlkes, J.D., Simpson, M.L., and Doktycz, M.J., *Actuatable membranes based on polypyrrole-coated vertically aligned carbon nanofibers*. Acs Nano, 2008. **2**(2): p. 247-254.
13. Wang, W.C., Tian, X.D., Feng, Y.P., Cao, B., Yang, W.T., and Zhang, L.Q., *Thermally On-Off Switching Membranes Prepared by Pore-Filling Poly(N-isopropylacrylamide) Hydrogels*. Industrial & Engineering Chemistry Research, 2010. **49**(4): p. 1684-1690.
14. Liu, Y.L., Zhao, M.Q., Bergbreiter, D.E., and Crooks, R.M., *pH-switchable, ultrathin permselective membranes prepared from multilayer polymer composites*. Journal of the American Chemical Society, 1997. **119**(37): p. 8720-8721.
15. Ku, J.R., Lai, S.M., Ilieri, N., Ramirez, P., Mafe, S., and Stroeve, P., *pH and ionic strength effects on amino acid transport through Au-nanotubule membranes charged with self-assembled monolayers*. Journal of Physical Chemistry C, 2007. **111**(7): p. 2965-2973.
16. Walczak, M.M., Popenoe, D.D., Deinhammer, R.S., Lamp, B.D., Chung, C.K., and Porter, M.D., *Reductive desorption of alkanethiolate monolayeres at gold - a measure of surface coverage*. Langmuir, 1991. **7**(11): p. 2687-2693.
17. Jung, U., Filinova, O., Kuhn, S., Zargarani, D., Bornholdt, C., Herges, R., and Magnussen, O., *Photoswitching Behavior of Azobenzene-Containing Alkanethiol Self-Assembled Monolayers on Au Surfaces*. Langmuir, 2010. **26**(17): p. 13913-13923.
18. Mu, L., Liu, Y., Cai, S.Y., and Kong, J.L., *A smart surface in a microfluidic chip for controlled protein separation*. Chemistry-a European Journal, 2007. **13**(18): p. 5113-5120.
19. Peng, K., Yu, S.T., Alberts, D.J., and Lahann, J., *Switching the electrochemical impedance of low-density self-assembled monolayers*. Langmuir, 2007. **23**(1): p. 297-304.

20. Paik, M.Y., Krishnan, S., You, F.X., Li, X.F., Hexemer, A., Ando, Y., Kang, S.H., Fischer, D.A., Kramer, E.J., and Ober, C.K., *Surface organization, light-driven surface changes, and stability of semifluorinated azobenzene polymers*. Langmuir, 2007. **23**(9): p. 5110-5119.
21. Hamelmamm, F., Heinzmann, U., Siemling, U., Bretthauer, F., and der Bruggen, J.V., *Light-stimulated switching of azobenzene-containing self-assembled monolayers*. Applied Surface Science, 2004. **222**(1-4): p. 1-5.
22. Kuiper, J.M., Stuart, M.C.A., and Engberts, J., *Photochemically induced disturbance of the alkyl chain packing in vesicular membranes*. Langmuir, 2008. **24**(2): p. 426-432.
23. Porter, M.D., Bright, T.B., Allara, D.L., and Chidsey, C.E.D., *Spontaneously Organized Molecular Assemblies .4. Structural Characterization of Normal-Alkyl Thiol Monolayers on Gold by Optical Ellipsometry, Infrared-Spectroscopy, and Electrochemistry*. Journal of the American Chemical Society, 1987. **109**(12): p. 3559-3568.

CHAPTER 9

CONCLUDING REMARKS

This thesis outlined the development of membrane materials capable of performing controlled molecular separations. This was achieved by fabricating porous membranes with controllable structural, physical and chemical properties. Membranes such as polycarbonate and porous alumina membranes were used in these studies due to their ordered pore architectures. Further structural modification of the membranes was carried out in order to reduce the pore diameter of the membranes. Pore size reduction was achieved using two methods; electroless deposition of gold and atomic layer deposition (ALD) of silica. The pore size of the membranes was altered systematically by adjusting the number of ALD cycles or by adjusting gold deposition time.

The surface properties of the membranes were tailored in order to provide controlled molecular transport. Desired chemical properties were imparted to the membranes by modifying the membrane surfaces with SAMs. The surface properties of gold nanotube membranes were varied using thiol chemistry while the silica-alumina membranes were functionalised with silanes. The chemical functionality applied to the membranes generally involved hydrophobic SAMs as it presented a simple

technique to demonstrate changes to the transport properties of membranes due to introduced surface functionalities.

Electroless deposition was utilised to coat PA membranes with gold. The gold surfaces were functionalised with 3-mercaptopbenzoic acid and the layer was subsequently characterised with Raman spectroscopy. To our knowledge, this was the first attempt to characterise SAMs within pores and probe their spatial distribution using scanning cross-sectional Raman spectroscopy. This study confirmed the deposition of the thiol SAM throughout the length of the pore. Due to the curvature of the gold within the pores, there was an increased SERS effect when viewing the cross section of mMBA-Au-PA membranes. Higher peak intensities in the Raman spectra were observed for mMBA assembled in the middle of the membrane and towards the bottom of the membrane. We postulated that this effect was due to the formation of bottle necked pores which resulted in a smaller pore diameter at the top of the membrane and hence less surface area available for thiol assembly. Furthermore, inhomogeneous gold deposition at $> 5 \mu\text{m}$ depth into the membrane caused structural pinhole defects in the gold nanotubes to occur thus increasing the roughness and surface area of the gold in these sections which can contribute to the increased SERS signal.

The functionalisation of gold nanotube membranes with SAMs of fluorinated thiols (PFDT) was demonstrated showing that the transport and selectivity properties of gold nanotube membranes can be varied by functionalisation using thiol chemistry. PFDT functionalised membranes showed excellent sensitivity for the transport of hydrophobic molecules over hydrophilic molecules. Their transport, selectivity and stability properties were superior in comparison to membranes functionalised with an analogous alkanethiol monolayer (decanethiol).

The effects of the controlled positioning of functional groups on the transport properties of the membrane were investigated. Gold was deposited on different areas on the membrane; on one of the membrane interfaces, within the pores of the membrane and completely coating all surfaces of the membrane. Gold-thiol chemistry was exploited in which the thiols only assembled on the gold coated

regions of the membrane thus providing controlled positioning of functional regions. Modification of the surface properties of the membranes was carried out using PFDT in which PFDT only assembled on the gold coated regions of the membranes thus providing controlled positioning of functional areas. Overall, modification with PFDT resulted in a hindrance in the transport of the hydrophilic dye and an enhancement in the separation between hydrophilic and hydrophobic dyes. From this study it became apparent that membrane interface functionalisation contributes more to the transport properties of the membrane than pore functionalisation. The ability to repel molecules away from the interface appears to be the governing factor in the membrane's ability to control the transport properties.

PA membranes were structurally modified by the atomic layer deposition of silica onto the face of the membrane. The chemical functionalisation of silica coated PA membranes with a fluoro silane (PFDS) was demonstrated showing that the transport and selectivity properties of silica composite PA membranes can be varied by functionalisation using silane chemistry. The hydrophobic PFDS-modified membranes showed superior sensitivity to the transport of hydrophobic molecules over hydrophilic molecules.

Forward osmosis was found to occur through Si-PA membranes but only when particular solutes were used in the draw solution. These solutes included dyes of differing size, charge, hydrophobicity and molecular weight. There did not appear to be an obvious trend between the properties of the dye and the onset of water transport. The forward osmosis observed in this study is likely due to a double layer effect. The double layer causes an occlusion of the pores and essentially decreases the pore size. Due to this occlusion, the dye transport is hindered and so water transport is required in order to offset the concentration difference between the feed and draw cell. As the electrical double layer thickness is increased with low salt concentrations and diminishes in high salt concentration an increase in water transport is observed at low KCl concentration and diminishes at higher KCl concentration.

Stimuli responsive membranes based on gold coated PA membranes were produced. The transport properties of the gold nanotube membranes were controlled through

the reversible switching of adsorbed fluorinated azobenzene layers. The fluorinated, hydrophobic end group of the azobenzene chain produced a transition between hydrophobic and less hydrophobic surface properties when switching from the *trans* to the *cis* state. The transport of a hydrophilic probe dye through the azobenzene modified membrane demonstrated the potential of the switchable membrane, with transport rates decreasing when switching to the azo-*trans* (highly hydrophobic) state. Therefore, through tailoring the end group functionality of the synthesised azobenzene molecule, a wide variety of switchable mechanisms could be achieved.

9.1. FUTURE DIRECTIONS

Current membrane research strives to construct membranes with higher flux, greater transport selectivity and sufficient long-term stability. Advances in membrane design require the capability to finely control the pore architecture of the membrane. While the gold nanotube membranes were based on ideal model membranes the electroless deposition method must be further improved to minimise imperfections and increase reproducibility. For example it is essential to thoroughly investigate the effects of the gold plating bath components. In addition more efficient pre-bath sample preparation strategies can be devised to ensure good initial gold deposition. In particular the initial surface preparation for tin chelation is a critical step to obtain homogeneous gold deposition. This can be improved by correct preparation of the surface prior to tin deposition such as applying surface coatings with a greater density of sites available for tin chelation.

Improvements in membrane design should also include tuning of the transport properties of gold nanotube membranes using surface modifications. The research outlined in this thesis has only presented enhanced separation abilities due to surface functionalisation and has not demonstrated the ability to completely block the passage of a particular target molecule. This can be achieved by reducing the pore diameters to dimensions where the surface functional layers occlude a large percentage of the pore. However, with this strategy flux will be sacrificed and therefore innovative membrane structure design will need to compensate for the reduced flux. For example a conventional membrane design can be adopted which

involves an ultrathin membrane attached to a microporous support. In addition, porous alumina can be fabricated with periodic asymmetric variations in its pore diameter otherwise known as Brownian ratchets. In systems with periodic barriers to movement directed or rectified motion can arise and so higher transport rates can be realised with Brownian ratchet membranes.

Surface functionalisation strategies should also be developed in order to perform specific and more complicated functions and separations. This can be demonstrated by employing more advanced functional layers or by coating various areas of the membrane with different SAMs, therefore producing multi-functional surfaces. For example porous materials can be coated with a functional layer within the pores which is capable of retaining or preserving drugs or bioactive molecules while the outer surface of the membrane can be coated with a functional layer which allows membrane compatibility within the environment it is introduced.

Further developments into advanced surface functionalisations also include the development of stimuli responsive membranes. The azobenzene surface modifications outlined in this thesis can be adapted to perform any desired separation through tailoring the end group functionality of the synthesized azobenzene molecule. This can be achieved by substituting various aniline derivatives during the synthesis of the azobenzene compound. Other stimuli responsive surface modifications can also be explored. For instance, advancements have been made with various stimuli responsive polymers capable of responding to temperature, surrounding environment and electrical potential.

The use of thiol modified gold nanotube membranes in commercial applications is limited by the stability of alkanethiol SAMs on gold. There is evidence of dramatic changes in the structure and integrity of thiol containing SAMs over a period of several months. To overcome these issues the development of more stable and versatile surface functionalisation systems is required. For instance covalent attachment of diazonium salts to gold via electrochemical reduction is a promising strategy. Alternatively other membranes and surface modification techniques can be used which are capable of providing a robust bond such as silane modification of silica membranes.

Membrane characterisation is a major research area in the membrane industry and involves the characterisation of membrane structures and surface functional layers. Valuable information about the membrane structures including pore size, length, orientation, spacing and porosity was obtained using scanning electron microscopy (SEM). To obtain images of membrane structures with better resolution innovative imaging techniques must be used. High resolution nano-computed X-ray tomography (Nano-CT) and focussed ion beam (FIB) milling coupled with SEM will allow for three dimensional imaging of membrane structures. The three dimensional imaging of membrane structures using these new techniques is an important step in membrane development. It is also imperative to confirm the nature of SAMs within pores in order to clarify their full impact on the transport phenomena through membranes. Analysis of the thiol layers on gold nanotube membranes can be further investigated with Raman spectroscopy. Many current Raman systems are coupled with atomic force microscopy (AFM) and are capable of spatially resolved techniques such as mapping and depth profiling and can therefore be used to create three dimensional images of thiol distribution throughout the membrane.

The application of electroless gold deposition onto porous materials other than polycarbonate and porous alumina has currently not been investigated. Electroless gold deposition is a technique that can be easily adapted to other materials. While templated nanotubes and nanorods have been fabricated by electroless gold deposition onto porous membranes, various other nanomaterials can be coated to create countless gold nanostructures. Through expanding the range of gold coated nanostructures, new and unique material properties may be conceived.

There were several unresolved questions from the forward osmosis effect we observed with Si-PA membranes (chapter 7). The trend between solutes and forward osmosis could not be explained. Further experiments must be conducted to clarify this issue and to understand the underlying mechanisms of this system. The dye diffusion across the membrane for each of the dyes can be measured to determine any distinguishing trends between the dye transport rates and the water rates. Furthermore zeta-potential analysis would be useful to confirm the precise surface charge of the membrane in each of the solution environments. It would also be

interesting to determine if any other properties of the dye could explain the occurrence. Highly complicated separations could be performed if the water transport rates for particular molecules or combinations of molecules could be predicted.

The studies outlined in this thesis illustrate the fundamental transport of probe dyes through modified membrane. Ongoing studies should extend into more commercially focused studies such as biomedical separations and biosensing applications. The development of biosensors can be achieved through functionalising the membrane surfaces with tailored recognition chemistry which is specific to target molecules or ions. The conductivity of gold nanotube membranes also presents a convenient method for molecule detection via electroanalytical techniques. Biomedical applications often require molecules to be recovered and refined from highly complex media. Consequently for biomedical separation applications, such as protein purification and artificial organs, it is imperative to continue advancements in membrane design and surface modification.

APPENDIX

The oil/water partition coefficients for the dyes used in these studies is presented in Table A-1. The procedure for obtaining the oil/water partition coefficients was outlined in section 2.4.2.

Table A-1 Transport and selectivity properties of functionalised and bare gold membranes (errors obtained from three replicate measurements).

Dye	Partition coefficient (K)	Log K
Eosin yellow	0.344088 ± 0.058864	-0.46333 ± 0.07154
Crystal violet	194.261 ± 13.13586	2.288386 ± 0.029585
Pinacyanol chloride	185.8598 ± 42.53566	2.25997 ± 0.095348
Rose bengal	26.70105 ± 2.22004	1.426528 ± 0.035293
Rhodamine B	161.7279 ± 7.54154	2.208785 ± 0.019966
Tris(2,2'-bipyridyl)ruthenium(II)*	0.000679 ± 1.46 x 10 ⁻⁵	-3.16783 ± 0.009369

* In the literature tris(2,2'-bipyridyl)ruthenium(II) is classed as a hydrophobic molecule [1-4].

1. Choi, H.N., Cho, S.H., Park, Y.J., Lee, D.W., and Lee, W.Y., *Sol-gel-immobilized Tris(2,2'-bipyridyl)ruthenium(II) electrogenerated chemiluminescence sensor for high-performance liquid chromatography*. Analytica Chimica Acta, 2005. **541**(1-2): p. 49-56.
2. Klotzbach, T., Watt, M., Ansari, Y., and Minteer, S.D., *Effects of hydrophobic modification of chitosan and Nafion on transport properties, ion-exchange capacities, and enzyme immobilization*. Journal of Membrane Science, 2006. **282**(1-2): p. 276-283.
3. Maeda, S., Hara, Y., Nakamaru, S., and Hashimoto, S., *Design of Autonomous Gel Actuators*. Polymers, 2011. **3**: p. 299.
4. Takato, K., Gokan, N., and Kaneko, M., *Effect of humidity on photoluminescence from Ru(bpy)(3)(2+) incorporated into a polysaccharide solid film and its application to optical humidity sensor*. Journal of Photochemistry and Photobiology a-Chemistry, 2005. **169**(1): p. 109-114.